Chair of Petroleum and Geothermal Energy Recovery

Master's Thesis

Application of existing marine pipelines in terms of carbon dioxide transportation

Askar Davletbaev

May 2023

MONTANUNIVERSITÄT LEOBEN
www.unileoben.ac.at

AFFIDAVIT

I declare on oath that I wrote this thesis independently, did not use other than the specified sources and aids, and did not otherwise use any unauthorized aids.

I declare that I have read, understood, and complied with the guidelines of the senate of the Montanuniversität Leoben for "Good Scientific Practice".

Furthermore, I declare that the electronic and printed version of the submitted thesis are identical, both, formally and with regard to content.

Date 12.05.2023

Signature Author
Askar Davletbaev

Davletbaev Askar
Master Thesis 2023
Petroleum Engineering

Application of existing marine pipelines in terms of carbon dioxide transportation

Supervisor: Ameneh Sobhani
Supervisor: Marina Ilyaeva

Chair of Petroleum and Geothermal Energy Recovery

Acknowledgements

I wish to convey my sincere appreciation to my supervisor from Ufa State Petroleum Technological University Ilyaeva Marina Aleksandrovna and my supervisor from University of Leoben Ameneh Sobhani for their assistance in scientific inquiries on the proposed research topic.

I would also like to acknowledge the contribution of the staff of the Oil and Gas Transport and Storage and Gas Chemistry and Chemical Process Modelling Departments of Ufa State Petroleum Technological University for their training in the use of specialized software in the field of hydrocarbon pipeline transport.

Abstract

The thesis examines the problem of using retired offshore gas and oil pipelines for further use in the carbon dioxide utilization program. The relevance lies in the general direction of energy industry development associated with the transition to ecologically clean fuels. The aim of the work is to determine if it is possible to convert pipelines for feedstock re-injection under given infrastructure parameters.

The assessment was carried out by numerical modelling using industry software and solving analytical solid mechanics equations. A comprehensive analysis of the component composition of the separated carbon dioxide from the hydrogen production unit was carried out using three separation technologies as examples. The behavior of the fluid along the pipeline route with the determination of the required pressure and temperature for supercritical pumping was studied using different software packages. Various schemes are considered for the analysis of the stability of a pipeline structure when laid in a trench with backfill, taking into account the worst variant of loss of stability due to a load-bearing capacity failure of the soil. The analysis of corrosion deterioration in emergency situations, together with the environmental impact assessment, made it possible to verify the safety of the project.

The results suggest the feasibility of such projects and complement existing industry guidelines on transition procedures. Based on existing recommendations and normative documents, together with calculations and modeling, a new detailed algorithm was developed to assess the possibility of reorienting pipelines. This algorithm can be applied to develop future projects.

Zusammenfassung

Die Studie untersucht das Problem der Nutzung stillgelegter Offshore-Gas- und Ölpipelines zur Weiterverwendung im Rahmen des Kohlendioxid-Nutzungsprogramms. Die Relevanz liegt in der allgemeinen Entwicklungsrichtung der Energiewirtschaft im Zusammenhang mit dem Übergang zu ökologisch sauberen Kraftstoffen. Ziel dieser Untersuchung ist es, die Machbarkeit von Nachrüstungen von Pipelines zur Erleichterung der Wiedereinführung von Rohstoffen unter Berücksichtigung der vorherrschenden Infrastrukturparameter zu ermitteln.

Die Bewertung erfolgte durch numerische Simulationen mit branchenspezifischer Software und die Lösung analytischer Abhängigkeiten der Festkörpermechanik. Eine detaillierte Analyse der Komponentenzusammensetzung des abgeschiedenen Kohlendioxids aus der Wasserstoffproduktionsanlage wurde am Beispiel von drei Abscheidungstechnologien durchgeführt. Das Verhalten des Fluids entlang der Pipelinestrecke mit der Bestimmung des erforderlichen Drucks und der Temperatur für überkritisches Pumpen wurde mit verschiedenen Softwarepaketen untersucht. Es wurden verschiedene Schemata zur Analyse der Stabilität einer Pipelinestruktur bei der Verlegung in einem Graben mit Verfüllung betrachtet, wobei die schlimmstmögliche Variante des Stabilitätsverlustes aufgrund einer Verletzung der Tragfähigkeit des Bodens berücksichtigt wurde. Die Analyse der Korrosionsverschlechterung in Notfallsituationen sowie die Umweltverträglichkeitsprüfung ermöglichten es, die Sicherheit des Projekts zu überprüfen.

Die Ergebnisse lassen Rückschlüsse auf die Durchführbarkeit solcher Projekte zu und ergänzen die bestehenden Empfehlungen der Industrie für das Übergangsverfahren. Auf der Grundlage bestehender Empfehlungen und normativer Dokumente sowie von Berechnungen und Modellierungen wurde ein neuer detaillierter Algorithmus entwickelt, um die Möglichkeit einer Neuausrichtung von Pipelines zu bewerten. Dieser Algorithmus kann bei der Entwicklung künftiger Projekte angewendet werden.

Table of Contents

Chapter 1

Introduction

1.1 Background and Context

In oppose to the traditional scheme of carbon capture and storage, Gazprom International and Wintershall Noordzee B.V. suggested the idea of usage the existing marine gas pipelines in order to burry CO_2 in empty reservoirs of the North Sea (Wintershall, 2021). There are many stranded pools and more than 4,800 kilometres of pipelines in the southern North Sea, of which 1,200 kilometres are maintained by Wintershall Noordzee. Part of this system is available for carrying CO_2.

This solution provides both significant economic effect of equipment turnover and compliance with the politics of decarbonization of the energy sector. However, not only gas pipelines can be repurposed, but also offshore oil pipelines.

The concept can be implemented equally effectively in the conditions of the Russian oil and gas industry. Following the idea of the regulatory documents related to hydrogen energy transition, Gazprom and Rosatom announced blue hydrogen project for Sakhalin island (Afanasiev, V., 2021). As it is discovered previously, the production of blue hydrogen is closely conducted with the CO_2 emissions, so potentially depleted reservoirs of Sakhalin-1 and Sakhalin-2 projects may fulfill the need of storing (Davletbaev, A., et al., 2021).

Hence, the primary proposition of this dissertation is to examine and assess the appropriateness of the named conversion of the current offshore oil and gas infrastructure in terms of decarbonisation and carbon dioxide transportation.

1.2 Scope and Objectives

The main goals of the investigation are:

1. Analysis and collection of information about the existing offshore pipeline infrastructure in the Sakhalin region. Estimation of actual carbon dioxide releases from hydrogen generation by methane steam reforming. Determination of the probable composition of the resulting fluid. Determination of permissible and optimal parameters for pumping liquid carbon dioxide providing a single-phase flow.

2. Comparative analysis of pipeline stress and stability parameters during transportation of natural gas, oil and liquid carbon dioxide. Analysis of possible scenarios of loss of stability.

3. Determination of the expected corrosion rate of the pipeline system using software systems at various operating conditions.

4. Assessment of possible risks and environmental impacts during the project implementation. Strategic analysis of the project and re-qualification process assessment. Final assessment of the feasibility of repurposing the existing offshore pipeline infrastructure. Update the existing algorithm for assessing the feasibility of re-routing the pipelines based on the calculations made.

1.3 Achievements

Regarding the study's framework, a list of calculations was drawn up to analyze the technical side of the project. An extended analytical dependence for calculating the stability of the pipeline, taking into account the weight of the ground under local loss of ground stability, is derived. This allowed a comparative evaluation of the pipelines before and after conversion, as well as an intermediate verdict on the feasibility of the idea.

1.4 Technical Issues

The technical difficulties in the design analysis include the ambiguity of selecting a design model for supercritical flow in a complex system geometry.

1.5 Overview of Dissertation

The thesis contains a detailed analysis of the conversion, from selection of the pipeline infrastructure and determination of the component composition to the performance of the process calculation with an assessment of the strength properties of the system. It concludes

with an environmental risk assessment, strategic planning and consideration of a unified transition algorithm.

Chapter 1 contains general information about the work, its structure, relevance, and the topic summary with results and conclusions.

Chapter 2 is devoted to a review of previous research and development towards CO_2 transport and utilization.

Chapter 3 focuses specifically on the selected infrastructure using the Sakhalin Island example. The source of the carbon dioxide and the composition of the resulting fluid is identified. The use of pumping equipment in pumping corrosive media, namely CO_2, is also considered.

The fourth chapter describes all the theoretical principles on which all the calculations are based. These include the process calculation, strength analysis and stability assessment for the two schemes, as well as the calculation of the corrosion rate.

The fifth chapter contains two different facets of project development: an environmental impact assessment of potential leakage, and an overall strategic analysis to identify the strengths and weaknesses of the project.

The sixth chapter is devoted to the regulatory framework and a synthesis of the previous theoretical chapters in the form of an elaborated feasibility assessment algorithm.

The seventh chapter contains concrete results of calculations based on the theoretical dependencies given in chapter 4, as well as a discussion of the findings with interpretation.

The eighth chapter closes the paper by summarizing the research, assessing whether the objectives have been achieved and focusing on prospective areas of research related to the thesis topic.

Chapter 2

State of the Art

Carbon dioxide is a well-known basic constituent of the carbon cycle. Unlike natural resources, it is produced by the combustion of either fossil or plant-based substances, as well as other chemical reactions. Carbon dioxide plays a major role in causing alterations in the Earth's climate. because of its capability to absorb numerous wavelengths of infrared radiation, and because it remains in the atmosphere of the planet for extended periods of time.

Between 1959 and 2006, the average rate of CO_2 accumulation in the atmosphere was 1,4 ppm per year, while from 2006 to 2018 it increased to approximately 2,0 ppm per year. Overall, this rate has been linear. Still, some existing absorbers, like the oceans, have the potential to provide future springs. As a result, the carbon dioxide content increases exponentially.

Based on preliminary analysis represented in the Bulletin of the American Meteorological Society (Dunn, R.J. et al., 2021*)*, The worldwide mean value of global atmospheric carbon dioxide in 2020 was 412,5 ppm, establishing a newly set record high, notwithstanding the recession induced by the pandemic. The agency's observations show an increase of more than 2,5 ppm, one of the largest in the history of measurement.

The main source of dioxide emissions is direct and indirect fusion in energy processes. These include the use of hydrocarbon feedstocks for heat production. According to State of the Climate in 2019 from NOAA and the American Meteorological Society (NCEI, 2019).

Being concerned about the possible prognosis about the future level of emissions the global energy society decided to change the direction of development to an eco-friendly one. One of the possible solutions is to base on a hydrogen energy. In 2021 The Administration of the Russian Federation has instituted a document called "The concept of hydrogen energy development in the Russian Federation". It was preceded by the European “Roadmap for moving to a competitive low carbon economy in 2050”. According to the named documents, the most perspective and efficient hydrogen technologies should be used soon as well as strategic and economic analysis should be considered (The Government of the Russian

Federation, 2021, the European Parliament, 2021). In other words, it results in an attempt to converse the fuel demand from the comprehensive resources to hydrogen.

Hydrogen has a good ability to burn with the release of excess energy. Despite its notable advantages as a fuel in green energy, its successful integration into the process requires many challenges to be met, from synthesis to storage to application. There are similarities as well as contrasts to conventional fuels, such as liquefied petroleum gases and liquid fuels like gasoline. The industrial and commercial aspects of deploying hydrogen necessitate a tackling of the underlying challenge of generating green energy. In order for hydrogen to fully realize its capabilities as versatile energy carrier, numerous hurdles must be overcome, including production, transmission, storing and dispensing of the gas. The named issues were studied by Neha Singh Chauhan and Vineet Kumar Singh (Chauhan, N. et. al., 1970).

Various types of H_2 can be generated using different sources: the grey one is obtained from natural gas using methane conversion (reforming) without capturing flue gases, if carbon dioxide capture technology is applied, the hydrogen is called the blue one. The yellow one is a product of nuclear technologies and the purest one is green. The name of the last one defines the usage of natural renewable resources, like wind, sun and water. Despite the desired clarity, green hydrogen methods proceed with the lowest energy efficiency, so blue and yellow ones are widely used. Nuclear plants strongly depend on the location they can be constructed at, so it drastically lessens the acceptability and omnitude. Therefore, the most efficient way is to provide steam methane reforming (SMR) and obtain hydrogen, especially considering the number of natural gas reservoirs in the world and current state of the fuel industry, primarily based on hydrocarbons. The detailed process of SMR and hydrogen production technologies was studied by various authors (Barbir, F. et al., 2016).

Despite the merits of smooth transition from gas energy to hydrogen, providing fewer carbon emissions, some serious drawbacks may occur. According to the research done by Robert Howarth and Mark Jacobson (Howarth, R.W., et al., 2021), the process of production of H_2 is closely conducted with extra emissions of CO_2: steam methane reforming (SMR) technology itself, the energy needed to drive SMR, indirect emissions. If carbon capture facilities are presented, they also yield carbon dioxide exhaust. So, the best result is 135 g CO_2eq/MJ for the best available technology. The excessive amount of carbon rich flue gases may be filtered, captured and stored.

All capture methods are based on a comprehensive technique of concentrating and then purifying a process stream which contains CO_2. The differences among the various practices lie in the choice of flow path and certain upstream concentrating phases before purification. The purification process before transport are often similar across a range of methods. The

largest energy consuming phase of carbon sequestration is the initial step of carbon capture and The cleanliness of the CO_2 in the flow prior to sequestration level is the main determinant of the cost involved.

Constituents are greater for charcoal than for natural gas. Further elevated values can be detected in the midstream flows in a treatment plant. At a hydrogen production unit using steam reforming of methane, the carbon dioxide content can be well above 30-45%, while the additional cost of carbon dioxide capture is lower. Many techniques exist for the segregation of CO_2, and these are an important area of investigation. Some methods are better suited rather than others, according to flow properties such as temperature, CO_2 content and impurities, e.g. water. A widespread technique for separating and cleaning CO_2 from a gas stream, which is extensively applied in the industry, is solvent extraction and recovery with an amine solution. The amine partitioning process is made up of two phases with an absorber tower and a reclaimer. The power consumption is mainly from heat from the reboiler in the regeneration unit, some energy for cooling in the condenser and the stripped amine chiller and re-circulation pumps. Many natural gas plants utilize this method with a comparable goal of eliminating SO_x. The other CO_2 separation technique, which is more compressible ('electric operation'), is the use of membranes. (Hickem, T., et al., 2021).

During post-combustion the fuel is combusted with an N_2/O_2 blend of air and the CO_2 is stripped from the flue gases. The cost of both gas and coalfired units using post-combustion is in a comparable range and is stated to be \$60/tCO_2eq. Post-combustion is also reported to be lower cost for new build versus upgrading of current plants.

Pre-combustion converts the combustion feedstock to a non-carbon-containing formation, like hydrogen out of syngas, with the subsequent stripping of the carbon dioxide out of the midstream. The hydrogen is then burned as a carbon free-fuel substitute. The common method of pre-combustion carbon sequestration may be used for any operation in which a syngas blend is produced.

Oxy-fuel capture is based on the combustion of fuel using pure oxygen instead of air as the main oxidizer. Accordingly, the first step is to separate air required for combustion into oxygen and nitrogen. Fuel combusted with oxygen gives a higher CO_2 concentration in the flue gas. Then ash, SO_2, SO_3 oxides and various other contaminants are extracted out of the combustion gases, and the gas is chilled to a temperature so cold that the contained water precipitates, retaining a minor quantity that can be recovered and re-liquefied for future transportation, storage or utilization.

Different schemes of carbon capture studied by KSB (KSB CO_2 capture report, 2021). Three options are described: capture before burning, oxy-fuel capture and capture while burning.

The containment and transport of compressed carbon dioxide requires a logistical framework that facilitates the movement of the captured CO_2 from its point of origin to its designated storage location. The dissemination and commercialization of carbon dioxide to beverage producers entail technologies that have already been established, prima facie attesting to the pivotal role of liquid natural gas (LNG) transportation as a significant benchmark in larger-scale industrial applications. The lowest cost method of transportation at moderate ranges less than 500 km is by pipeline. CO_2 exists as a gas under normal atmospheric conditions and temperatures; therefore, it may be cost-effective to cool and pressurize the flow for transportation over extended distances. Maximizing proximity between the storage and the capturing point is the key to optimizing the overall efficiency of the process.

Various scenarios of transportation cases were studied by Korean researchers (Kang, K. *et al.*, 2014). The routes included various number of capture plants, different structure and various obstacles. The total costs were analyzed and predicted using Parker Model, although different cost models may be applied (Knoope, M. et al., 2013, McCollum, D. et al., 2010, Parker, N., 1970). Several mathematical equations have been proposed to accurately determine the diameter of a pipeline, as it plays a crucial role in the overall design and cost considerations. Pipeline transportation costs were calculated using standard pipe diameters within the Nominal Pipe Size (NPS) range, instead of being reliant on user-specified pressure differentials. The capital expenditures (CAPEX) associated with CO_2 pipeline can be classified into four distinct categories, namely materials, labor, right-of-way expenses, and miscellaneous expenditures. The determination of the material costs was based on a straightforward calculation whereby the weight of the pipeline was derived from the thickness of the pipe and then multiplied by the prevailing price per ton.

According to the results, the best variant was the scenario where CO_2 is additionally supplied on the route. The additional capture plant yielded in positive economic effect, even though the total distance remained the same.

As previously stated, the transportation of gaseous carbon dioxide through pipelines is not deemed economically feasible due to the significant volume of the gas, its low density, and the occurrence of significant pressure losses. Under certain circumstances, it may still be more economical to transport carbon dioxide in its gaseous form, as opposed to its liquid or supercritical states. The study conducted by Knoope et al. The model exhibits the ability to assess the comparative cost-effectiveness of gaseous and liquid CO_2 transportation. (Knoope, M. et al., 2013).

This study incorporated optimization of both gaseous and dense liquid transport. For liquid cases, the inlet pressures ranged from 9 to 24 MPa, in steps of 1 MPa, and with 0 to 10 booster stations. For gaseous CO_2 transport, inlet pressures ranged from 1,6 to 3 MPa, in steps of 0,1 MPa, and the outlet pressure was fixed on 1,5 MPa. The omission of recompression as a potential solution for gaseous transportation was determined based on its excessive energy consumption and associated costs. Overall, 191 cases were analyzed.

In order to validate the viability of the conjunction of inlet pressure, diameter, and quantity of booster stations, the velocity is subjected to calculation. In accordance with the pipeline design provided (P-001 Process Design, 2006), a maximum velocity threshold of 6 m/s has been established for liquid CO_2 in order to prevent damaging pipeline erosion and associated vibrations. Additionally, a minimum velocity requirement of 0.5 m/s has been determined to ensure proper flow of the CO_2. A velocity spectrum of 5-20 m/s is assumed for gaseous CO_2 transport. If a specific case resulted in a velocity outside the identified range, the case was ignored. The energy expenses are computed for every possible matchup of booster station, pipeline diameter, and inlet pressure. Subsequently, the levelized costs of CO_2 transport were calculated. The ideal synthesis of booster station quantity, inlet pressure, and diameter was determined based on the lowest levelized costs.1

After an analysis, it was determined that when traveling 100 km over agricultural terrain, a CO_2 mass flow rate of 16.5 Mt/y and a CO_2 mass flow rate of 15.5 Mt/y for offshore pipelines, it is more economical to transport CO_2 in its gaseous form instead of its liquid form. Transporting gaseous CO_2 through pipelines offers the benefit of utilizing thinner pipes (equivalent to only 1% of the outer diameter), which leads to decreased expenditure on pipeline materials.

Pipeline transportation is entailed by possible issues. Related studies are provided below. It is known that high-pressure pumps in a special design are necessary for the transportation of liquid carbon dioxide, since the fluid is extremely aggressive under certain conditions. The most suitable pumps for these purposes, as well as their parameters are listed in KSB paper. Another serious issue is impurities of the flow.

The effect of impurities on pipeline performance was studied by Suoton and Iqbal in 2017 (Peletiri, P.S. et al., 2017). It is necessary to identify the critical pressure and temperature because pipelines are used to transport CO_2 in its supercritical state. It is worth noting that a high proportion of carbon dioxide in the mixture contributes to greater stability, in which case the external components change the critical point parameters only slightly. However, when designing the process infrastructure and performing state calculations, accurate determination of pressure and temperature is a necessity. The Peng-Robinson equation of state (EOS) demonstrated the lowest absolute average deviation (AAD) compared to the other cubic EOS

models for the estimation of density in binary mixtures containing carbon dioxide. (Cal, E. et al., 1970) and the best in calculating critical temperature and pressure of CO_2 was used (Zhao, Q. et al., 2014).

According to the results, the lighter components than CO_2 cause an increase in pressure losses. The presence of H_2 entails the greatest escalation in pressure drop, whereby CO, N_2, and CH_4 follow in diminishing order of effect. The elements N_O, O_2, and H_2S exhibit varying effects on pressure loss, while H_2O and SO_2 are known to result in reduced pressure loss. An elevation in both pressure and temperature has been observed as an established phenomenon when foreign substances are present in a mixture concomitant with CO_2. The singular pipeline that exhibited a decrease in critical pressure was the Weyburn pipeline, and it is plausible that this occurrence was attributed to the existence of C_2H_6, which is a representation of C_{2+}. Even small increases in pressure at the critical point require more use of steel pipes with increased wall thickness and high energy requirements to compress the fluid in the pumping units. Only then will the safe transport of single-phase supercritical carbon dioxide through field pipeline networks be assured.

All pipelines demonstrated critical temperatures that were lower than the critical temperature of pure CO_2, thereby indicating a reduction in the ability of CO_2 to exist as a supercritical fluid within these transport channels. At pressures exceeding the critical pressure, the influence of temperature is negligible unless the temperature descends to a point where solidification occurs. When the pressure exceeds the critical threshold, it has been observed that fluids possessing elevated critical temperatures transition into the liquid state prior to fluids with less significant critical temperatures. To reduce the influence of impurities, special cleaning methods are used. Thus, the experience of using three options by Air Products was studied: sour compression, auto-refrigeration and membrane recovery of CO_2 and O2 from the vent stream (White, V. *et al.*, 2013). A simplified scheme of the processes is shown in Figure 1. The theory of sour compression is that during compression to 30 bar most of the SO_x and NO_x in the raw CO_2 will react to form acids. The flow of air traveling alongside a vehicle, commonly referred to as slipstream, is directed into a specialized component known as a flue gas cooler condenser (FGCC) with the purpose of decreasing the temperature of flue gas and facilitating the condensation of water vapor from the stream. A two-stage diaphragm compressor, equipped with an interstage cooler and a condensate separator, is employed to elevate the flue gas pressure to 15 bar before its introduction into the initial column. The column in question has a capacity of 15 bars and is of the packed type. The process involves cooling and recirculating the condensate from the bottom of the column to the top, thereby facilitating sufficient contact between vapor and liquid to ensure sufficient dwelling time for the sour compression reactions to manifest. Moreover, there exists a minor inflow of freshwater flowing into the upper end of

the column. The flue gas stream discharged from the upper section of the column undergoes compression using a one-stage diaphragm compressor to reach a pressure level of 30 bar, prior to its introduction into the subsequent column, which is equipped with condensate recirculation and makeup water injection. After departing from the summit of the 30-bar column, the stream undergoes a desiccation process within a Temperature Swing Adsorption unit (TSA) and

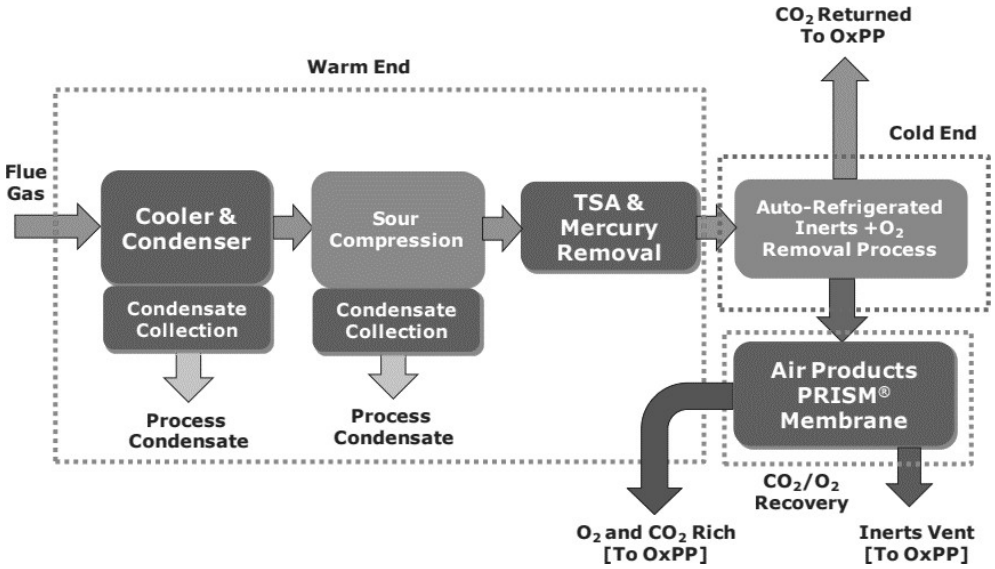

subsequently proceeds towards the low-temperature section of the operation.

Figure 1 – Overall scheme of CO_2 purification unit by Air Products (White, V. et al., 2013)

The auto-refrigeration process aims to eliminate nitrogen, oxygen, and argon from the atmosphere by means of partial condensation. While undergoing partial condensation, the majority of argon, nitrogen, and oxygen within the incoming stream will remain in their gaseous form and be segregated as an unreactive drainage feed. Some though will remain dissolved in the CO_2, The inclusion of a distillation column in the partial condensation process can effectively eliminate impurities, resulting in a CO2 product stream of over 99% purity. The final step is the PRISM membrane recovery of carbon dioxide from the vent stream which would otherwise be lost in the process. Thus, such technology is able to produce almost pure CO_2 with the minimal level of losses. In that case the flow is almost pure, however usually it contains some water and other substances. Thereof, the known risk of damage by corrosion arises. Mesa corrosion remains another negative factor while transporting carbon dioxide.

The influence of various parameters was studied by Frédéric Vitse, Srdjan Nesic Yves Gunaltun (Vitse, F. et al., 2003). Temperature ranged from 40°C to 100°C. As the temperature increases, there is a concurrent augmentation in the rate of corrosion. The maximum corrosion rate is reported at 70°C. The correlation is then reversed, leading to a drop in the corrosion process intensity until it reaches 90 °C. As the temperature rises, the rate of condensation also sees a

corresponding rise. No matter the CO_2 levels in the system, a consistent pattern indicating the highest corrosion rate at temperatures between 70-80°C is observed.

These results can be interpreted as follows: at lower temperatures (below 70°C), the corrosion rate increases with temperature according to Arrhenius' law applied to the endothermic reaction of corrosion by CO_2. At temperatures exceeding 80°C, there is a decline in the corrosion rate, signifying the manifestation. of an additional phenomenon associated with such high temperatures. There are at least three possible explanations for this. The thickness of the liquid film that condenses on the wall becomes more significant at elevated The rise in condensation rate has resulted in elevated temperatures. The direct transfer of corrosive agents through the condensed liquid to the steel inner surface may therefore be limited, which may explain the reduced corrosion rate. One possible interpretation is that at elevated temperatures, the formation of an iron carbonate layer from the corroded materials could potentially shield the metal from subsequent corrosion to some extent. One possible reason for this phenomenon is that increased temperatures result in more corrosion and consequently more iron ions in the condensed water, leading to an elevation in the water's pH levels. A modification in pH may alter the mode in which the electrochemical reaction is carried out at the wall. The associated corrosion rate might therefore become slower over time.

The aforementioned two assumptions align with the empirical observation that the corrosion speed tends to be considerably lower when the condensation rates are low. Under severe misting conditions, the corrosion speed is observed to be four times higher than under minimal condensation when exposed to a temperature of 70°C and a CO2 partial pressure of 0,4 MPa.

The corrosion rate may be calculated with various models. De Waard, NORSOK M506, KSC and Tulusa models are used to evaluate corrosion rate when a stable turbulent single-phase flow is presented, while Ohio, IFE, Cassandra and Oddo and Tompson are suitable for multiphase flow as well (Zinnatullin, A. et al., 2007).

The model described in (Vitse, F. et al., 2003) predicts of the corrosion rate by CO_2 under dewing conditions. Top-Of-The Line corrosion phenomena are analyzed by considering the areas of expertise encompassed by this field include fluid dynamics, energy transfer, chemical reactions, and electrical reactions. It provides a more thorough understanding of how primary factors, namely temperature, total pressure, and CO_2 partial pressure, contribute to the overall process, the gas velocity, and the condensation rate. Once the issue of safe transport has been resolved, the next step is to organize the rational storage of the captured raw materials.

Related technology of storing carbon dioxide in underground reservoirs was suggested in 1990s and later developed by various researchers. The most notable documents within this field are (Busch, A. et al., 2008, Aminu, M.D. et al., 2017, Van Der Meer, B., 2005). The process of

further storing of carbon dioxide as well suitable conditions were studied in (Hendriks, C., et al., 2004). Various types of underground reservoirs may be effectively used to burry CO_2: the aforesaid consists of idle natural gas reserves, abandoned crude oil reserves, extant oil reserves suitable for exploration utilizing enhanced oil recovery (EOR) techniques, impenetrable coal seams amenable to enhanced coal bed methane recovery (ECBM), and subterranean strata containing water.

According to the provided calculations and estimation, the total estimated underground storage potential is estimated to range from 500 to 6000 Pg. Natural gas fields offer the highest storage potential. The capacity for groundwater reservoirs is evaluated in the span from 30 to 1100 Pg. But when the conditions for a gated system are less stringent, the horizon's capacity can be many folds beyond that of the aquifers.

Hydrocarbon repositories are likely to present the most economical storage solutions. It has been observed that onshore storage facilities typically incur lower costs in comparison to their offshore counterparts. The expenses fluctuate considerably across various projects and are contingent on the specific oil and gas prices. At current times, coal bed methane storage combined with advanced recovery is often more costly because of the high number of bores needed.

Enhanced oil recovery may prove to be commercially advantageous in several instances. The application of enhanced oil recovery through carbon dioxide injection (EOR-CO_2) has been a longstanding practice in the oil industry. Despite ongoing efforts, there is a severe lack of publicly accessible information regarding the injection and cycling of CO2 in exhausted oil and gas reserves. (Stevens, S., et al., 1998). As of now, there hasn't been any direct or indirect evaluations conducted specifically to gauge CO2 sequestration in any CO2-EOR project. Consequently, the outcomes of these processes are generally demonstrated with respect to the production levels that are stated in terms of "target initial oil in position" (OIIP). Method of EOR-CO_2 can be applied as a transitional step in terms of burying in prospectively depleted oil and gas reservoirs.

Carbon dioxide can be also used to partially or completely replace the buffer gas in the underground storage of natural gas. Using CO_2 as a solvent for high-boiling hydrocarbons can lead to a considerable augmentation in the beneficial storage capacity and residual condensate production. Various papers are devoted to the study of this issue (Khan, S., et al., 2016). Gaz De France was the first company to successfully replace 20% of buffer volume with a mixture of 90% of nitrogen and 10% of carbon dioxide (Khan, S., et al., 2016).

Dorokhin V. reviewed most of the worldwide projects dedicated to CO_2 storage in terms of geological properties of reservoirs.

Previously the consequences of injecting CO_2 into an oil field in order to increase oil recovery were analyzed (Riding, J. et al., 2009, Shogenova, A. et al., 2007). Hydrodynamic modeling has shown that the spread of CO_2 occurs under the influence of regional groundwater flow. Research conducted on the ramifications of carbonate acid produced from the reaction between dioxide and reservoir water demonstrated a rise in porosity and permeability as the outcome of the breakup of calcite and dolomite. The strength of cement stone was found to remain unchanged in an experiment that examined the impact of carbon dioxide.

The question of choosing the optimal state of injected CO_2 remains relevant. An example of carbon dioxide storage in ocean depths and in geological strata located under the ocean floor is given by Safonov, M. et al. Huang H.P., Chang S.G. mention the storage of CO_2 in supercritical and liquid states at the bottom of the oceans (Safonov, M. et al., 1970). Bachu, S. and Shaw,J. discovered the possibility of burying the dioxide in depleted oil and gas reservoirs (Bachu, S. and Shaw, J., 2005). In other papers the possibility of CO_2 burial in salt caverns is considered (Bachu, S., 1970). The article by Andre, L. et al. discusses the burial of CO_2 in the Dogger aquifer structure of the Paris basin in a supercritical aggregate state (Andre, L. et al., 2007). The method for pumping CO_2 trap of water-bearing formation with thermo-baric parameters promoting prolonged burial of CO_2 in liquid state was suggested by Khan S.A., Dorokhin V.G. and Khvostova V.J (Khan, S. et a., 2016).

When injected carbon dioxide is accompanied by non-isothermal effects due to heat exchange and equilibrating processes. They can be used for monitoring the plume propagation in the subsurface. Bielinski, A. et al. investigated the application of numerical multi-phase simulation program processing the data obtained by temperature sensors (Bielinski, A. et al., 2008). For these purposes distributed temperature sensing (DTS) cables were proposed. Their edge is that they provide information to complement classic geophysical methods such as seismic and electrical methods. In a further aspect, the wires can be positioned fixedly beside the casing of the well, where they provide near-continuous temperature data, both in time and depth.

According to the experiments, the time dependent temperature signal was measured at an observation well at 50 m distance from the injection point is simulated for various model setups and CO_2 injection temperatures. Various simulation cases were setup varying rock permeabilities from 30 to 1000 mD and CO_2 injection temperatures from 40 to 60°C. Influences of grid size, permeability ratio and boundary conditions were investigated. Measurements at various depths gave information about the shape of the CO_2 plume and thus about the permeability distribution in the formation. Therefore, this study suggested that temperature measurements at observation wells can be an intelligent way of monitoring a CO_2 plume.

The infrastructure for injection of dioxide into the reservoir requires capital investments, since it is necessary to purchase pumping equipment and construct technological pipelines. In the study related to economic analysis of geological sequestration Kosowski P. and Kuk M. discovered that the total cost of injection depends on variable factors: location of the well, depth of injection, average temperature in reservoir rock, injection rate, the permeability of the rock and the amount of CO_2 (Kosowski P. et al., 2016). Taking into consideration the last factor, the maximum price is around 20 \$/tCO_2 and the minimal one tends to zero for 0 and 30 million of captured carbon dioxide respectively.

Chapter 3

Carbon utilization prerequisites

3.1 Project infrastructure

The main companies engaged in the production and transportation of hydrocarbons in the Sakhalin region are Rosneft, Gazprom and Sakhalin Energy. The main production facilities include the following (Sakhalin Energy, 2023).

1. The PA-A/Molikpaq, PA-B, and Lun-A platforms used for oil and gas extraction.
2. Onshore processing facility (OPF).
3. The pipeline network on the southern area of Sakhalin Island is known as Transsakhalin.
4. Booster Station (BS) №2.
5. The Prigorodnoye production complex comprises of both a liquefied natural gas (LNG) plant and an oil export terminal.

Information on the current oil and gas production volumes of the operated platforms, plants and pumping stations is given in Table 1 (Nadein, V. et al., 2010).

Table 1 – Production rate at existing production units (Nadein, V. et al., 2010)

Facility	Production data
Platform PA-A	oil: 14308,86 m^3/day; gas: 1,699 mil. m^3/day.
Platform PA-B	oil: 11129,11 m^3/day; gas: 2,605 mil. m^3/day.
Gas metering and reduction station	gas: 3,398 mil. m^3/day.
Platform LUN-A	multiphase: 1189,38 m^3/day.
Onshore processing facility	oil: 31002,52 m^3/day; gas: 52,896 mil. m^3/day. glycol: 335,94 m^3/day.
Booster station №2	oil: 31002,52 m^3/day;

	gas: 49,696 mil. m^3/day.
Production complex	condensate: 794,84 m^3/day; LNG: 9,6 mil. t/year; oil: 7948,4 m^3/h.

The actual scheme of existing pipelines with inner diameters and lengths is depicted at Figure 2. The full scheme is attached in Appendix A, Figure 40. Summary data about all the operated pipelines is presented in Table 2 (Markin, A. et al., 2011).

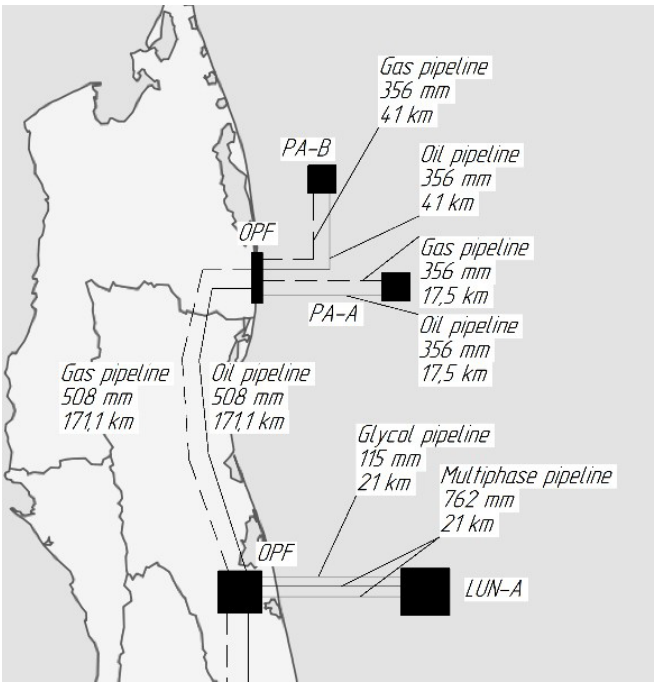

Figure 2 – Oil and gas production infrastructure of Sakhalin (Sakhalin Energy, 2023)

Table 2 – Pipeline network summary (Markin, A. et al., 2011)

Pipeline	Construction type	Length, km	Inner diameter, mm	Maximum operating pressure, MPa
PA-A – OPF(Piltun-Astokhskoye) oil pipeline	marine	17,5	327	9,1
PA-A – OPF(Piltun-Astokhskoye) gas pipeline	marine	17,5	327	9,8
PA-B – OPF(Piltun-Astokhskoye) oil pipeline	marine	41	327	9,1
PA-B – OPF(Piltun-Astokhskoye) gas pipeline	marine	41	327	9,8
OPF(Piltun-Astokhskoye) – OPF(Lunskoye) oil pipeline	onshore	171,1	508	5,2

OPF(Piltun-Astokhskoye) – OPF(Lunskoye) gas pipeline	onshore	171,1	508	9,25
LUN-A – OPF(Lunskoye) multiphase pipeline №1	marine	21	762	9,8
LUN-A – OPF(Lunskoye) multiphase pipeline №2	marine	21	762	9,8
LUN-A – OPF(Lunskoye) glycol pipeline	marine	21	115	12
OPF(Lunskoye) – BS №2 gas pipeline	onshore	283,1	1220	9,25
OPF(Lunskoye) – BS №2 oil pipeline	onshore	284,1	610	5,2
BS №2 – Production complex gas pipeline	onshore	332,4	1220	9,25
BS №2 – Production complex oil pipeline	onshore	333,5	610	5,2

Hence, the combined length of the pipeline system surpasses 1,700 kilometers, while nearly 180 km are laid in the sea.

As noted earlier, one of the main directions of the development of the energy industry is general decarbonization, reduction of harmful emissions in the atmosphere and, as a consequence, reduction of the impact on the climate. In this case, the traditional oil and gas industry is gradually being modified by creating developments in the field of hydrogen energy and integrating them into technological processes. In terms of the government strategy, the territory of the Sakhalin Region is considered as a potential site for the development of hydrogen technologies. Based on the available documents and reports, KPMG audit company has compiled preliminary options for the implementation of projects (Savin, V. et al., 2021).

The energy sources for hydrogen production are the existing power plant, as well as new renewable sources. Two variants of hydrogen generation are considered: steam methane reforming and electrolysis. The raw materials in the first case are natural gas and water, in the second – water. The largest power plants and facilities are the Central and the Northern energy districts resulting in 631,7 MW and 86,6 MW of generated energy. The available amounts are 33,7 MW and 4,6 MW respectively. The Central one also has the highest average power capacity factor – 0,461.

The summary about two possible projects is presented in Table 3 and Figures 3,4.

Table 3 – Comparative analysis of hydrogen energy projects (KPMG, 2021)

Option	Technology	Expected initial generated volume of H_2, t/year	Energy consumption, mil. kWh/year	Natural gas consumption, mil. m^3/year
№1	SMR	25000	136	150
№2	Electrolysis	3000	136	41

The average levelized cost of hydrogen (LCOH) for SMR is within the range of 1,4-3,3 $/kg, while the same index for electrolysis is between 2,5 and 4,5 $/kg. The named cost difference, production rate and developed gas production infrastructure make SMR the most efficient option in terms of hydrogen production and distribution (Savin, V. et al., 2021).

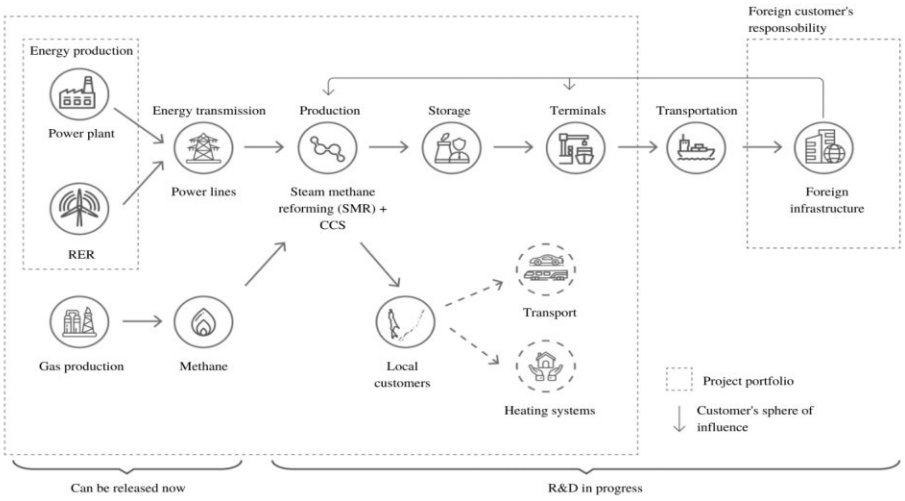

Figure 3 – SMR project realization (KPMG,2021)

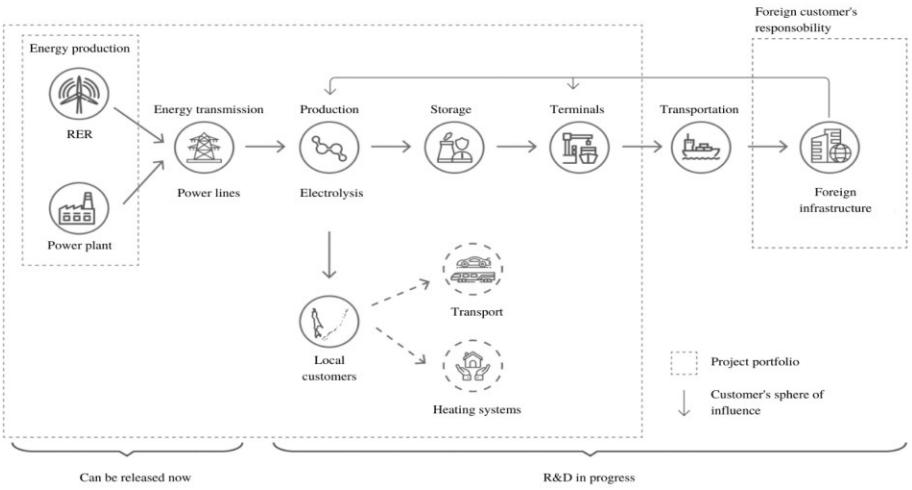

Figure 4 – Electrolysis project realization (KPMG,2021)

The expected timeline of the project is the following:

1. 1st – 3rd quarters of 2021 – signing of a cooperation agreement by the project partners;
2. December 2021 – designing of the concept, feasibility study;
3. 2023 year – documents draft; establishing the special economic zone for Sakhalin; the beginning of construction operations;
4. 2025 year –the launching of the plant producing 30000 t/year;
5. 2030 year – the intensifying of production up to 100000 t/year.

The technological chain of the SMR by Rosatom is depicted at Figure 5.

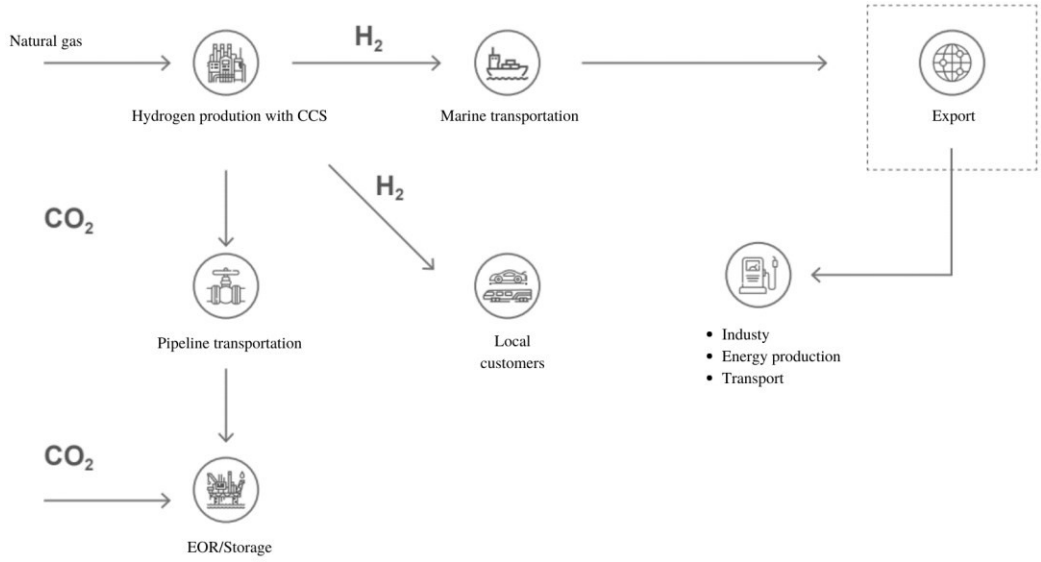

Figure 5 – Technological chain of hydrogen production by Rosatom (KPMG,2021)

3.2 Flow composition

The important problem is to properly estimate the expected emission level of the hydrogen plant. During the SMR procedure, each unit of methane used leads to the creation of a single mole of carbon dioxide and a quartet of hydrogen gas particles.:

$$CH_4 + 2H_2O \rightarrow CO_2 + 4H_2 \tag{3.1}$$

Hydrogen exhibits a gross calorific heat content of 0,286 MJ per mole, which is equivalent to 3,5 moles of H2 per MJ. The carbon dioxide generated in the SMR procedure is expressed as:

$$(3{,}5\ moles\ H_2/MJ) \cdot (1\ mole\ CO_2/4\ moles\ H_2) = 0{,}875\ moles\ CO_2\ per\ MJ.$$

The production plan results in a certain quantity of hydrogen moles (Harrison S., et al., 2016):

$$\nu = \frac{m}{M}, \tag{3.2}$$

where m – total mass of generated H_2, g;

M – molar mass of H_2, g/mol.

Substituting the data in equation 3.2:

$$\nu = \frac{10^5 \cdot 10^6}{2{,}014} = 4{,}965 \cdot 10^{10}\ moles.$$

Considering the calorific heat content, obtained number of moles can be transferred into $1{,}42 \cdot 10^{10}$ MJ or $1{,}242 \cdot 10^{10}$ moles of CO_2. When the CCS technology is applied along with treating the emissions from exhaust flue gases, the total amount results in 500-600 Mt of CO_2 with impurities per year.

The above-mentioned strategies for the production of hydrogen do not specify the exact technologies, and therefore we will consider carbon dioxide capture technologies. The composition of the gas, which is subsequently compressed and buried, largely depends on the chosen technology. Separately, three options are studied: post-combustion, oxy-fuel combustion and pre-combustion. In order to define the composition of the fluid the initial composition of the natural gas should be studied. However, the main purpose of this study is not the flue gas purification process, but pipeline transportation cases. Therefore, the mean composition of CO_2 streams applying best technologies is defined in the Table 4 (Onyebuchi, V.E. et al., 2018).

Table 4 – Expected mean composition of CO_2 streams

Component	Post-combustion, % mol.	Oxy-fuel combustion, % mol.	Pre-combustion, % mol.
CO_2	99,8	99,6989	98,54
O_2	0,015	0,3	0
H_2O	0,00064	0,001	0,0006
H_2	0	0	0,34
H_2S	0	0	0,034
CH4	0	0	0,028

N_2	0,1833	0,00000001	1,02
SO_x	0,00067	0,000043	0,037
NO_x	0,00039	0,00005	0,0004

Based on the data obtained, the initial fluids are created in the thermodynamic analysis software. Since carbon dioxide and other impurities are present in addition to methane, the standard calculation model for hydrocarbons of Peng-Robinson (PR) is not suitable, so the PR EOS with corrected binary interaction coefficients (BIPs) has been chosen (Li, H. et al., 2009). High-accuracy CO_2 or CERG-2008 models cannot be applied due to the presence of certain impurities (Davletbaev, A. et al., 2022). The resulting phase envelops are presented at Figure 6,7,8. The equilibrium state curves were plotted using Multiflash software. The integrated critical point tool allows to find the exact values of pressure and temperature from the solution of the selected equations of state. Two curves for water and vapor-liquid equilibrium (VLE) are presented. Resulting parameters of critical points of mixtures are presented at Table 5.

Table 5 – Critical points of fluids

Capture type	Pressure, MPa	Temperature, °C
Post-combustion	7,403	30,857
Oxy-fuel combustion	7,407	30,807
Pre-combustion	7,618	30,310

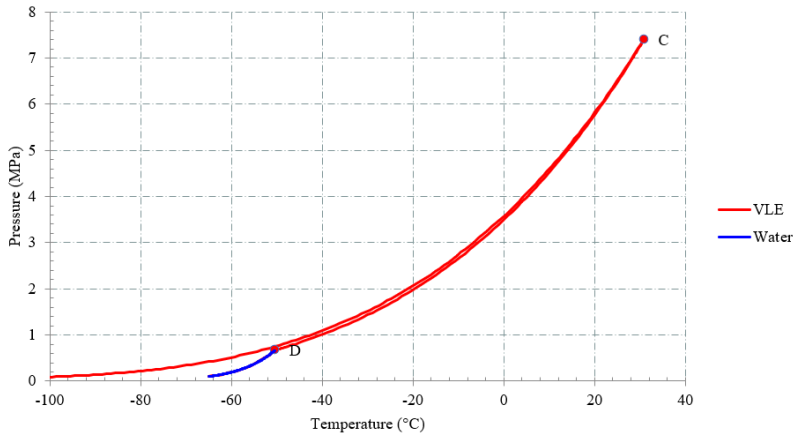

Figure 6 – Oxyfuel combustion phase envelope

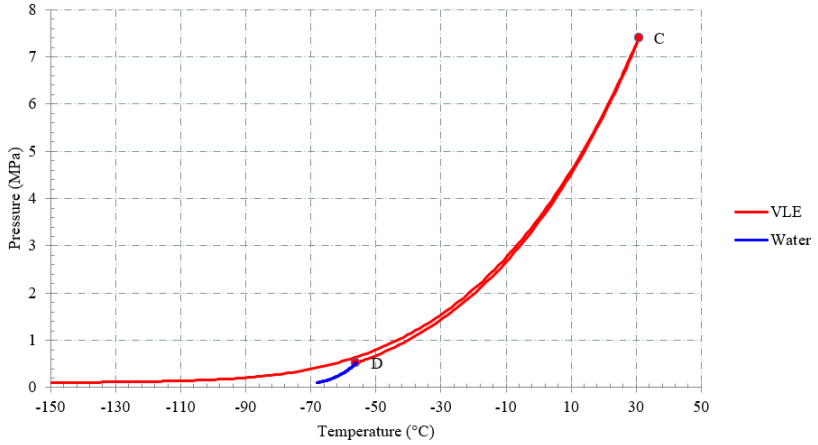

Figure 7 – Post-combustion phase envelope

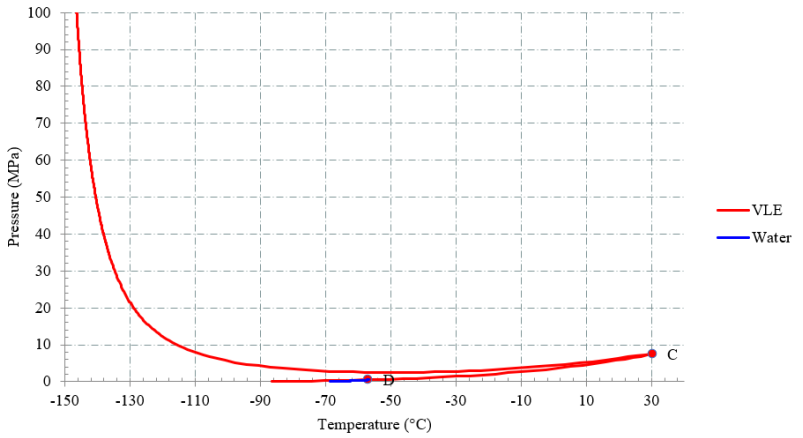

Figure 8 – Pre-combustion phase envelope

Therefore, average critical parameters are 7,476 MPa and 30,658 °C. To implement transportation in supercritical phase the existing pipelines must be adapted to work in these conditions. According to the Table 2 all 6 marine pipelines may be used, the glycol pipeline is not taken into consideration due to relatively small diameter.

The possible annual capacity of CO_2 can be evaluated using initial data about the amount of captured substance and component composition. Assuming the number of operating days equal to 350, the mass flow can also be calculated (Table 6).

Table 6 – Capacity evaluation

Capture type	Total mass per year, kg	Mass flow (N=350), kg/s
Post-combustion	547311967,29	18,099
Oxy-fuel combustion	547802621,11	18,115
Pre-combustion	550797291,47	18,214

3.3 Pumping equipment

This study does not consider the details of the operation of centrifugal and injection pumps when pumping carbon dioxide in various states as well as choosing the proper equations of state. However, the main requirements and recommendations are the following.

Due to low lubricity the attention should be paid to rotor construction, the number of stages on inline stack should as less as possible. Liquid or gas seals with track record and special O-ring materials are recommended to resist explosive decompression due to entrapped CO_2. Due to the presence of water in a mixture carbonic acid may be occurred while operating, so stainless steel eliminates the problem.

Unlike oil pumps, it is deemed unnecessary to consider the net positive suction head. (NPSH) for systems that operate above critical pressure because cavitation cannot occur. The utilization of extremely powerful SCO_2 could result in challenges related to the strength of materials, particularly as the size of compressors and turbines decreases.

The standard procedure to choose the pump and predict the gas behavior at operating conditions is the following (Adams, R. et al., 2014):

1. Comparison of experimental PVT data with standard equations of state (EOS) models.
2. Evaluating how well experimental data at different locations matches with EOS models.
3. A mutually agreed upon EOS model is chosen by both the vendor and client.
4. Phase maps are created for each operating conditions, considering presence of liquids or hydrates.
5. Blow down scenarios for Emergency Shutdown are defined.

6. Gas seal inlet conditions are studied.

Nowadays a huge variety of equipment adopted for pumping acidic fluids and corrosion aggressive substances is presented. All of them meet the requirements of ANSI B73.1 and ISO 5199. Most of them use SS304, SS316 or SS904 materials. Different API 610 Type BB3 pumps are widely used at CO_2 injection projects. Common performance graphs are presented at Figures 9,10. They indicate the recommended operating zones of the pumping equipment depending on the generated head and volume flow. In the event that the working position lies beyond the limits of the designated model, it is probable that the impeller blades will undergo the condition of stalling.

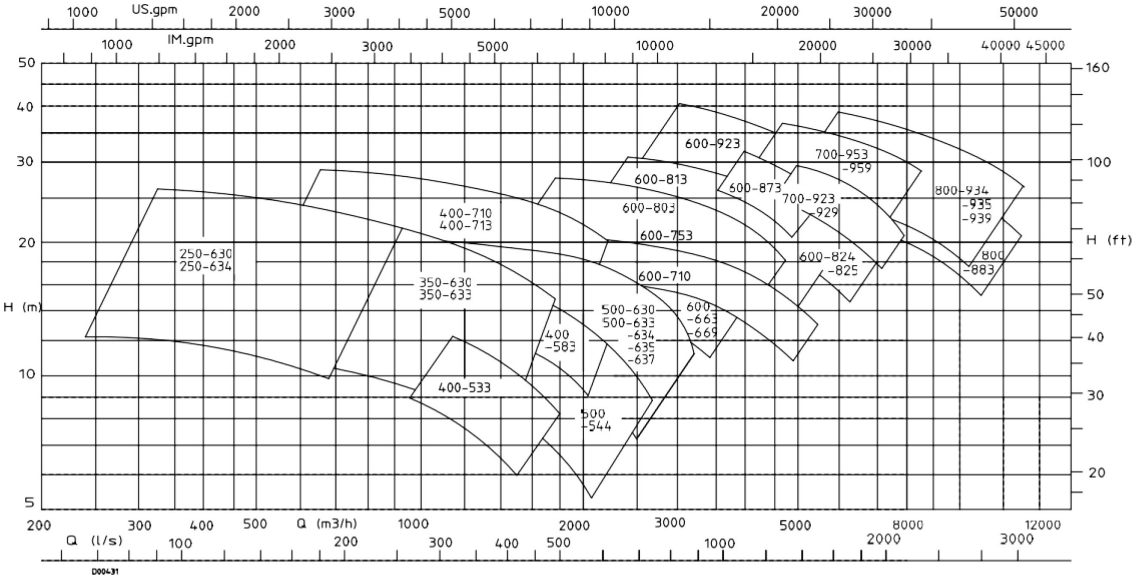

Figure 9 – H/Q graph of KSB KWP-K ATEX (n=580 rpm) (KSB,2022)

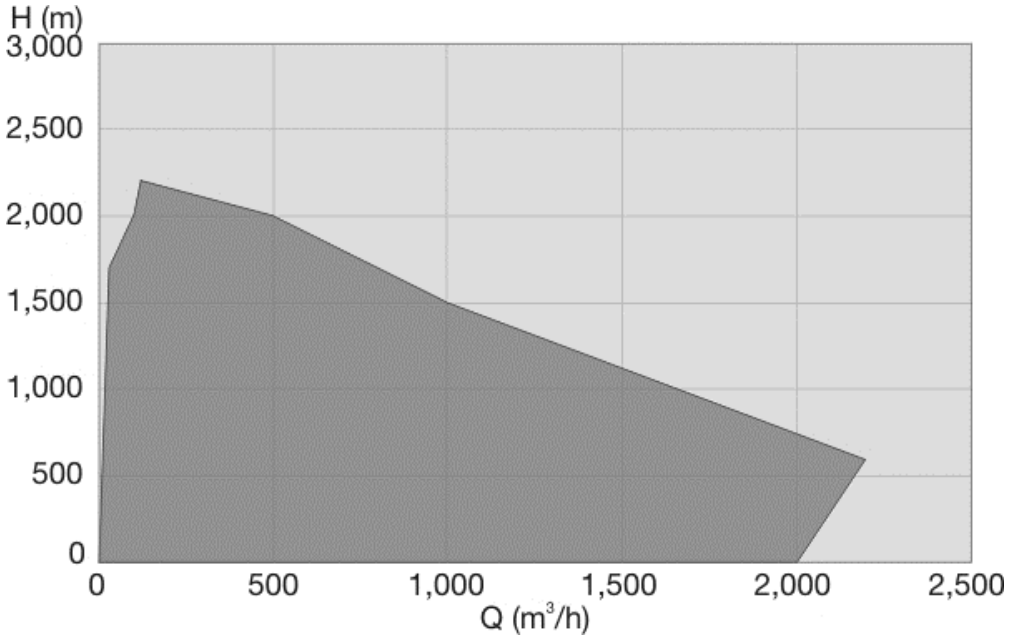

Figure 10 – H/Q graph of Sulzer MSD/MSD2 (50 Hz) (Sulzer,2022)

Chapter 4

Calculation methodology

4.1 Technological calculation

Since already constructed pipelines are used in this case, the diameter, materials and route have already been set. The only parameters that need to be determined are pressure and temperature. It is necessary to calculate the thermobaric conditions during fluid injection in the pipeline from the condition of providing supercritical flow along the entire route and at the entrance to the platform riser. Therefore, the pressure and temperature drop should be calculated.

Numerous scholars have delved into the issue of the accuracy of pressure loss calculations in pipelines that are subjected to the presence of multiple phases and supercritical conditions, particularly when the terrain is rough (Fang, X. et al., 2012, Anderson, M., 2011). In summary, the deduction can be drawn that the determination of pressure drop is accomplished through implementation of the ensuing formula (Fang, X. et al., 2012):

$$\Delta P = \Delta P_{fr} + \Delta P_{ac} + \Delta P_{g}, \tag{4.1}$$

where ΔP_{fr} – friction pressure drop, ΔP_{ac} – acceleration pressure drop and ΔP_{g} – pressure drop due to the gravity.

The named components are calculated by the following formulas (Fang, X. et al., 2012):

$$\Delta P_{fr} = \frac{G^2}{2\rho} \cdot \frac{L}{D} \cdot f, \tag{4.2}$$

$$\Delta P_{ac} = \frac{G^2}{2\rho} \cdot \frac{L}{D} \cdot f_{ac}, \tag{4.3}$$

$$\Delta P_{g} = \pm g \left(\frac{\rho_{out} + \rho_{in}}{2}\right) \cdot L \cdot sin\theta, \tag{4.4}$$

where G – mass flux, kg/(m^2· s);

ρ – fluid density, kg/m^3;

L – tube length, m;

D – inner diameter, m;

f – friction factor;

f_{ac} – acceleration factor;

θ – pipe inclination angle.

The symbol "+" represents upward flow while the symbol "-" represents its opposite, which is the downward flow.

The f factor, which pertains to supercritical friction, should not be misconstrued with the friction coefficient, also referred to as the Fanning friction factor (Fang, X. et al., 2012):

$$f = f_{iso,b} \left(\frac{\mu_w}{\mu_b}\right)^{0,49\left(\frac{\rho_f}{\rho_{pc}}\right)^{1,31}}, \tag{4.5}$$

where $f_{iso,b}$ – isothermal single-phase friction factor at fluid bulk temperature;

μ_w, μ_b – dynamic viscosity at inner wall temperature and fluid bulk temperature respectively, Pa· s;

ρ_f, ρ_{pc} – fluid density at film temperature and pseudo-critical temperature respectively, kg/m^3.

For cooling processes, f_{ac}can be approximated with the one-dimensional approximation mode (Fang, X. et al., 2012):

$$f_{ac} \approx 2 \cdot D \cdot \rho_b \frac{d}{dL}\left(\frac{1}{\rho_b}\right) = \frac{-8q}{G C_p}\left(\frac{\beta}{}\right)_b, \tag{4.6}$$

where ρ_b – fluid density at fluid bulk temperature, kg/m^3;

q – heat flux from fluid to wall, W/m^2;

β – thermal expansion coefficient at fluid bulk temperature, 1/K;

C_p – specific heat at constant pressure, J/(kg·K).

As the procedure of pressure drop calculation is complicated for long pipelines with a large number of segments, computational methods are applied. The associations established for the liquid retention and frictional pressure declines can be categorized as either empirical or mechanistic. Empirical methods are based only on experimental data (Beggs&Brill, Orkiszewski). Typically, established terms are employed which involve prevalent unitless figures, like the Reynolds number. Due to their development in specific experimental conditions, it is advisable to avoid using them for varied flow situations. Alternatively, mechanistic methods have an analytical basis on first principles (Tulsa Unified Model, OLGAS, HTFS). Accordingly, they are often more successful with a wide range of data. However, there

are often closure relationships that are based on experimental results so care still needs to be used when applying mechanistic models where they have not been validated. One potential issue with both empirical and mechanistic formulations that use flow regime predictions is that if the model is not continuous across the flow regime boundaries, then convergence issues can arise when using numerical methods to solve for the flow characteristics in pipelines (Aspen HYSYS, 2023). The study utilizes the mechanistic approach as its method.

One of the limiting criteria for operating pipelines is velocity of fluid. API-RP-14E specifies the avoidance of swift erosion on the interior pipeline surface and reduction of high-pressure drops as its primary demand. For a continuous flow the following formula for erosional velocity is applied (Peletiri, P.S et al., 2017):

$$\vartheta_e = 0{,}82\frac{100}{\sqrt{\rho}}. \tag{4.7}$$

Another equation suggested by API standard to define the maximum velocity (Peletiri, P.S et al., 2017):

$$\vartheta_{max} = \frac{122}{\sqrt{\rho}}. \tag{4.8}$$

As it can be seen, the second equation provides higher values. Assuming calculated mass flow actual planned velocity are calculated by the formula (Peletiri, P.S et al., 2017):

$$\vartheta = \frac{4G}{\pi\rho d^2}. \tag{4.9}$$

For a proper calculation of temperature drop the full heat exchange coefficient should be known. Considering the actual number of layers of the pipeline the equation can be written in the following form (Molchanova R.A. et al., 2009):

$$K = \left(\sum_{i=1}^{5} R_i\right)^{-1} = (R_{in} + R_w + R_c + R_{is} + R_{amb})^{-1}. \tag{4.10}$$

Components represent thermal resistance values of layers and can be defined by the following equations:

$$R_{in} = \frac{1}{\alpha_1}, \tag{4.11}$$

$$R_w = \frac{D_{in}}{2 \cdot \lambda_t} ln\frac{D_{out}}{D_{in}}, \tag{4.12}$$

$$R_{is} = \frac{D_{in}}{2 \cdot \lambda_{is}} ln \frac{D_{out.i}}{D_{out}}, \quad (4.13)$$

$$R_c = \frac{D_{in}}{2 \cdot \lambda_c} ln \frac{D_{out.c}}{D_{out.i}}, \quad (4.14)$$

$$R_{amb} = \frac{D_{in}}{\alpha_2 \cdot D_{out.c}}, \quad (4.15)$$

where α_1, α_2 – heat transfer from fluid to wall and from the pipeline last layer to the soil respectively, W/(m^2· K);

λ_w, λ_{is}, λ_c – thermal conductivity of carbon steel, bitumen isolation and concrete respectively, W/(m· K);

D_{in}, D_{out}, $D_{out.i}$, $D_{out.c}$ – inner diameter, outer diameter, isolated pipe diameter, diameter of the pipe with concrete layer respectively, m.

If the pipeline is buried and the criteria of H/$D_{out.c}$ < 3 is met, the value of α_2 should be calculated by Arons-Kutateladze equation (Molchanova R.A. et al., 2009):

$$\alpha_2 = \frac{2\lambda_{soil}}{\frac{4H}{D_{out.c}} \cdot ln\left(\frac{\lambda_{soil}}{D_{out.c}} + \alpha_0 \cdot D_{out.c}\right)}, \quad (4.16)$$

where λ_{soil} – thermal conductivity of soil, W/(m· K);

H – burial depth, m;

α_0 – heat transfer from soil to water, W/(m^2· K).

Heat transfer coefficient from soil to water may be calculated by the given criterial equation of free convection process in relatively infinite volume (Molchanova R.A. et al., 2009):

$$Nu_{s-w} = 0{,}7 \cdot c \cdot (Gr \cdot Pr)^n, \quad (4.17)$$

where c, n – constants that depend on $(Gr \cdot Pr)$ value.

The Nusselt parameter describes the proportion of convective and conductive heat transfer per unit area.

The included criterial numbers are calculated by following equations:

$$Pr = \frac{Cp_{sw} \cdot \rho_{sw} \cdot \nu_{sw}}{\lambda_{sw}}, \quad (4.18)$$

$$Gr = \frac{g \cdot \beta \cdot \Delta t \cdot H^3}{\nu_{sw}^2}, \quad (4.19)$$

where Cp_{sw} – heat capacity of salted water, J/(kg·K);

ρ_{sw} – density of salted water, kg/ m^3;

ν_{sw} – kinematic viscosity of salted water, m^2/s;

λ_{sw} – heat conductivity, W/(m· K);

β – thermal expansion coefficient, 1/K;

Δt – temperature difference between water and inner layer, K.

Empirical equations for calculation of water properties are used considering the mean salinity value (Shepelev A.V. et al., 2020):

$$\rho_{sw} = \frac{1009 + 0{,}733 \cdot (K_{sw} - 10)}{1 - 3 \cdot 10^{-4} \cdot (t - 10)}, \tag{4.20}$$

$$Cp_{sw} = \frac{4194 - 1{,}115 \cdot t + 0{,}015 \cdot t^2}{[0{,}987 - 0{,}0013 \cdot (K_{sw} - 10)]^{-1}}, \tag{4.21}$$

$$\lambda_{sw} = 0{,}553 \cdot (1 + 0{,}003 \cdot t), \tag{4.22}$$

$$\nu_{sw} = 10^{-6} \cdot [0{,}602 + 0{,}0009 \cdot (K_{sw} - 10) \cdot (\frac{50}{t})^{0{,}56}], \tag{4.23}$$

where K_{sw} – salinity of the water, %;

t – temperature of the water, ºC.

Therefore, the α_0 is calculated (Molchanova R.A. et al., 2009):

$$\alpha_0 = \frac{Nu_{s-w} \cdot \lambda_{sw}}{H}. \tag{4.24}$$

Accurately determining the inner heat transfer coefficient α_1 for supercritical flows is a difficult task because of the scarceness of data regarding these conditions and the irregular fluctuations in fluid parameters. Various authors described barometric fluctuations of SCF flows and provided related equations (Kurganov, V., Isaev, G., Protopopov, V., 1977). Criterial equations for Nu depend on the direction of fluid flow: up, down or horizontal. Considered marine pipeline imposes all of them. The main criteria for choosing the proper equation is Gr number for a SCF flow:

$$Gr = \frac{g \cdot (\rho_f - \rho_w) \cdot \rho_f \cdot {D_{in}}^3}{{\mu_f}^2}, \tag{4.25}$$

where ρ_f, ρ_w – density at temperature of fluid and wall respectively, kg/m^3;

μ_f – dynamic viscosity at temperature of fluid, Pa· s.

Grashof number represents ratio between buoyancy forces and restraining forces. The SCF flow omits the thermal expansion as apparent from the observation.

If Gr > 10^5, the Nu number is defined by the following equation (Kurganov V. et al., 1977):

$$Nu_{f-w} = 0{,}405 \cdot Re^{0{,}5} \cdot Pr^{0{,}43} \cdot (Gr \cdot 10^{-5})^{1{,}15} \cdot \left(\frac{D_{in}}{x}\right)^{0{,}4}, \quad (4.26)$$

where the x represents the distance measured from the start point of the pipeline., m.

The determining parameter in that case is $\frac{D^{in}}{x}$, so the local values of Re, Pr and Gr are recommended to calculate. However, this equation can only be applied to short pipelines.

Assuming turbulent thermogravitational convection with heat transfer, the following equation can be applied to long pipelines (Borodkin, S. et al., 2021):

$$Nu_{f-w} = 0{,}15 \cdot (Gr \cdot Pr)^{0{,}33}. \quad (4.27)$$

The variation in temperature caused by particular pumping techniques results in elevated temperature strains in the wall, which can be expressed through the subsequent equation (Code of Practice 36.13330.2012, 2012):

$$\sigma_t = \alpha \cdot E \cdot \Delta t, \quad (4.28)$$

where α – the coefficient of linear expansion, 1/K;

E – Young's modulus or the coefficient of the elasticity in tension, Pa;

Δt – temperature difference between values at pipeline welding and actual operational value, K.

4.2 Strength analysis

The durability and reliability of the pipeline are crucial factors that determine its functionality and secure functioning. In simple terms, strength refers to a material's capacity to withstand both internal and external forces without succumbing to damage or destruction. One of the main goals in performing these calculations is to determine the optimal wall thickness, however, in this project the pipeline has already been constructed and all thicknesses have been set, so only a comparative analysis of the actual loads during pumping of oil, gas and carbon dioxide was performed. It is imperative that the original shape and structure of the pipeline are not compromised when switching to different fluids to prevent the occurrence of an unsafe incident involving loss of stability, both on a general and local scale. For this purpose, stability calculations were performed in the most dangerous sections of the offshore pipeline.

Most often, when checking the strength of offshore pipelines, the probability of crumpling of the pipeline wall when critical pressure is reached, local crumpling and avalanche crumpling

are investigated. In the future, the wall thickness values are used in the strength verification calculation, taking into account the potential corrosion wear by the time of pipeline conversion. The designed corrosion allowance for oil and gas pipelines are 3 mm and 1 mm respectively. The calculation is based on the requirements given by various standards (DNV, 2007, № 2-020301-004, 2016).

The calculated pressure in marine pipelines is determined by the following formula (DNV, 2007, № 2-020301-004, 2016):

$$P_0 = (P_i - P_{g\,min}) + \Delta P, \tag{4.29}$$

where P_i– operated pressure in the pipeline, MPa;

$P_{g\,min}$ – ambient pressure component, MPa;

ΔP – extra pressure component due to hydraulic hammer, MPa.

Ambient pressure component is defined by the following equation (DNV, 2007, № 2-020301-004, 2016):

$$P_{g\,min} = \rho_{sw} \cdot g \cdot (d_{min} - h_w/2) \cdot 10^{-6}, \tag{4.30}$$

where d_{min} – minimum level of still water along the pipeline route, taking into account tidal phenomena and surges with the expected occurrence of 10^{-2} 1/year;

h_w – calculated wave height at designed pipeline route with the expected occurrence of 10^{-2} 1/year.

Extra pressure component due to hydraulic hammer and transition processes is defined by the following equation (DNV, 2007, № 2-020301-004, 2016):

$$\Delta P = \upsilon \cdot \sqrt{\frac{\rho \cdot E \cdot \delta \cdot K}{E \cdot \delta + D_{in} \cdot K}} \cdot 10^{-3}, \tag{4.31}$$

where υ – operated velocity of the fluid, m/s;

K – coefficient of volumetric elasticity of the fluid, MPa.

The named extra pressure is only considered for resulting converted CO_2 pipelines due to general instability of SCF flows. For oil pipelines it is not taken into consideration because precise control of valves opening time and velocity is assumed.

The calculation of mechanical stresses in the pipeline is carried out for compliance with the maximum permissible equivalent and longitudinal mechanical stresses with the calculated safety factor following the recommendations presented by Borodavkin, P., Volmir, A., Ilgamov, M. et al. (Borodavkin P. et al., 2002):

$$\begin{cases} \sigma_{eq} \leq \eta \cdot R_e \\ \sigma_l \leq \eta_u \cdot R_{\square} \end{cases}, \tag{4.32}$$

where equivalent stresses are calculated by the following equation (Borodavkin P. et al., 2002):

$$\sigma_{eq} = \sqrt{\sigma_{cir}{}^2 + \sigma_l{}^2 - \sigma_{circ} \cdot \sigma_l + 3\tau^2}, \tag{4.33}$$

where σ_{cir} – total circumferential stresses in the wall, MPa;

τ – total shear stresses, MPa.

As shear stresses are negligible in comparison with the circumferential and longitudinal ones, the formula may be imposed in the following way (Borodavkin P. et al., 2002):

$$\sigma_{eq} = \sqrt{\sigma_{cir}{}^2 + \sigma_l{}^2 - \sigma_{circ} \cdot \sigma_l}. \tag{4.34}$$

Total longitudinal and circumferential stresses may be evaluated in the following way (Borodavkin P. et al., 2002):

$$\sigma_l = -\alpha \cdot E \cdot (T_0 - T_a) + \mu \cdot \sigma_{circ}; \tag{4.35}$$

$$\sigma_{circ} = \frac{P_0 \cdot D_{in}}{2 \cdot \delta}, \tag{4.36}$$

where μ stands for the Poisson's ratio (assuming μ =0,3);

T_0 – the operational temperature of the fluid within the pipeline., °C;

T_a –the ambient construction temperature, °C.

When calculating the longitudinal stresses, the possible operating temperature of the product is taken into account, which ensures the maximum temperature difference.

4.3 Stability analysis

Since offshore pipelines are often laid in severe climatic and seismic conditions, all possible negative factors are considered when designing, taking into account their period of repeatability. However, under certain conditions, it is possible to exceed the loads laid down in the project. The potential for instability arises if permafrost soils thaw or if the soil layer on which the pipeline is placed liquefies.

Dilution of the soil under the influence of the mass of the pipeline is possible if the specific weight of the pipeline with the transported product significantly exceeds the specific weight of the soil itself. In this case, the possibility of this process considering seismic activity is calculated by the following formula (Gaythwaite, J., 1981):

$$E = 1 - (1 - \frac{1}{T})^{L}, \tag{4.37}$$

where T – period of repeatability of earthquakes, years;

L – total period of time since the pipeline construction, years.

4.3.1 Simplified calculation scheme

The case is considered when the soil has a partial erosion on the section with a length of L, and the ends of the pipeline are rigidly pinched by stable soil to the left and right of the considered section. It is assumed that at the initial moment of time the pipe was located in a horizontal position, and after a certain period of time, due to soil deformation the pipeline descended (Akhtyamov, A., 2015, Korobkov, G., et al., 2009). Since in this section pipe elongation is possible only when it is stretched, a tensile longitudinal force S_x appears in the pipes and the section begins to work as a rigid line (Figure 11).

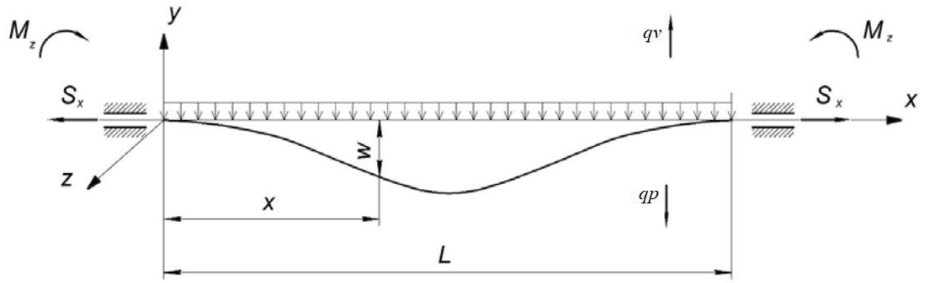

Figure 11 – The design scheme of the modeling the stress-strain state of the pipeline, the ends of which are pinched by the ground (Akhtyamov, A., 2015, Korobkov, G., et al., 2009)

In that case the pipeline is assumed as rigid line with no pipeline-soil interaction. The differential equation of the longitudinal-transverse bending of the elastic beam line has the form (Akhtyamov, A., 2015):

$$\frac{d^4w}{dx^4} - S_x \cdot \frac{d^2w}{dx^2} = \frac{q_y}{EI'} \tag{4.38}$$

where w – pipeline displacement;

I – the moment of inertia of the cross section of the pipe;

$q_y = q_v - q_p$ – average distributed load acting on the pipeline considering weight of the pipeline and water force.

Tensile longitudinal force may be evaluated by the following equation:

$$S_x = P_0 \cdot F - N_x, \tag{4.39}$$

where F – cross section of inner area of the pipeline;

N_x – axial longitudinal force that occurs in the pipeline wall from strain-compression deformations of the axial line of the line.

The last component is defined by the designing standards (SNiP 2.05.06-85, 2000*)*:

$$N_x = 100 \cdot [(0{,}5 - \mu) \cdot \sigma_{\text{circ}} + \alpha \cdot E \cdot \Delta T] \cdot F. \tag{4.40}$$

The moment of inertia of the cross section of the pipe with concrete coating is calculated by the following formula:

$$I = \frac{\pi}{64} (D^4_{out.c} - D^4_{in}). \tag{4.41}$$

The differential equation provided can be reformulated in the following manner:

$$w^{IV} - \beta^2 w^{II} = \frac{q_y}{EI}, \tag{4.42}$$

where $\beta^2 = \frac{S_x}{EI}$.

The solution for the equation, which is a linear one and has constant coefficients, is a combination of both general and partial components:

$$w(x) = w_0(x) + w^*(x). \tag{4.43}$$

Taking derivatives of the function to the fourth grade the characteristic equation is obtained:

$$r^4 - \beta^2 r^2 = 0. \tag{4.44}$$

The solutions of the equation are:

$$r_{1,2} = 0; \tag{4.45}$$

$$r_{3,4} = \pm\beta. \tag{4.46}$$

Therefore, the general solution that matches the routes of the equation:

$$w_0(x) = C_1 + C_2 x + C_3 \operatorname{ch} \beta x + C_4 \operatorname{sh} \beta x. \tag{4.47}$$

As the right part is constant, the partial component:

$$w^*(x) = -\frac{q_y}{2S_x} x^2. \tag{4.48}$$

Taking into account the results, the common solution:

$$w(x) = C_1 + C_2 x + C_3 \operatorname{ch} \beta x + C_4 \operatorname{sh} \beta x - \frac{q_y}{2S_x} x^2. \tag{4.49}$$

The boundary conditions due to fixed supports are the following:

$$w\left(\pm\frac{L}{2}\right)=0; \tag{4.50}$$

$$\frac{dw}{dx}\left(\pm\frac{L}{2}\right)=0. \tag{4.51}$$

Since symmetrical loading and fixing of the pipe relative to the middle of the pipeline is assumed, it is sufficient to leave only even functions in the general form of the equation:

$$w(x)=C_1+C_3\,\mathrm{ch}\,\beta x-\frac{q_y}{2S_x}x^2. \tag{4.52}$$

For the named boundary conditions the following system may be formed:

$$\begin{cases} C_1+C_3\,\mathrm{ch}\,\beta\dfrac{L}{2}=\dfrac{q_y}{8S_x}L^2; \\ C_3\,\mathrm{sh}\,\beta\dfrac{L}{2}=\dfrac{q_y}{2S_x}L. \end{cases} \tag{4.53}$$

It has certain solutions for C_1 and C_3 if $S_x\neq 0, \beta\neq 0$ and $sh\left(\beta\frac{L}{2}\right)\neq 0$:

$$C_1=\frac{q_yL}{2S_x}\left[\frac{L}{4}-\frac{1}{\beta}cth\left(\beta\frac{L}{2}\right)\right]; \tag{4.54}$$

$$C_3=\frac{q_yL}{2S_x\beta sh\left(\beta\frac{L}{2}\right)}. \tag{4.55}$$

Substituting values in the initial equation the resulting formula for pipeline displacement is obtained:

$$w(x)=\frac{q_y}{2S_x}\left(\frac{L^2}{4}-\frac{L}{\beta}cth\frac{\beta L}{2}+\frac{Lch\beta x}{\beta sh\beta\frac{L}{2}}-x^2\right). \tag{4.56}$$

For this case tensile longitudinal force is defined only by first component of inner pressure in the pipe. Load from own weight of the pipeline is the sum of loads of its components (Akhtyamov, A., 2015):

$$q_p=q_m+q_{pr}+q_{is}+q_c, \tag{4.57}$$

where q_m, q_{pr}, q_{is}, q_c – loads from metal of the pipe, product, isolation and concrete layers respectively.

The loads may be calculated using the following formulas:

$$q_{oil} = \rho_{oil} \cdot g \cdot 10^{-4} \cdot \pi \cdot \frac{(100 \cdot D_{in})^2}{4}; \quad (4.58)$$

$$q_{CO_2} \approx \rho_{CO_2} \cdot g \cdot 10^{-4} \cdot \pi \cdot \frac{(100 \cdot D_{in})^2}{4}; \quad (4.59)$$

$$q_{gas} \approx P_0 \cdot 10^{-2} \cdot \pi \cdot \frac{(100 \cdot D_{in})^2}{4}; \quad (4.60)$$

$$q_m = n \cdot \rho_m \cdot g \cdot \frac{\pi}{4} \cdot (D_{at}^2 - D_{in}^2); \quad (4.61)$$

$$q_{is} = n \cdot \rho_{is} \cdot g \cdot \frac{\pi}{4} \cdot (D_{outis}^2 - D_{out}^2); \quad (4.62)$$

$$q_c = n \cdot \rho_c \cdot g \cdot \frac{\pi}{4} \cdot (D_{outc}^2 - D_{out.is}^2), \quad (4.63)$$

where ρ – density of the substance, kg/m^3;

P_0 – inner pressure in the gas pipeline, MPa;

n – safety margin coefficient for pipeline loads (assuming n = 0,95 when checking stability).

The buoyant force of water:

$$q_v = 1{,}05 \cdot \frac{\pi \cdot D_{out.c}^2}{4} \cdot \gamma_w, \quad (4.64)$$

where γ_w – specific weight of salt water, N/m^3.

It is practical to investigate the stability of the pipeline when experiencing critical longitudinal force and length while undergoing bending. The critical length of an underwater conduit is the highest acceptable hanging length that prevents oscillations and maintains the pipe material's resistance capacity against stress.

Given the inflexible uniformly distributed pillars that uphold the pipeline, it is feasible to establish a criterion for the midpoint of the pipeline:

$$\sin\beta \frac{L}{2} = 0; \quad (4.65)$$

When substituting values, the following solution of this equation may be written:

$$S_{cr} = \frac{4 \cdot \pi^2 \cdot k^2 \cdot EI}{L^2}, \quad (4.66)$$

where k – the coefficient that depends on a wave type (for real systems k=1 is considered).

Solving this equation for L the following formula is obtained:

$$L_{cr} = 2\pi\sqrt{\frac{\overline{EI}}{S_{cr}}}. \quad (4.67)$$

4.3.2 Advanced calculation scheme

The case is considered when the soil has a partial erosion on the section with a length of 2L, and the ends of the pipeline are rigidly pinched by stable soil to the left and right of the considered section. It is assumed that at the initial moment of time the pipe was located in a horizontal position, and after a certain period of time, due to soil deformation the pipeline descended. Since in this section (–L; +L) pipe elongation is possible only due to when it is stretched, a tensile longitudinal force N appears in the pipes and the section begins to work as a rigid line (Figure 12).

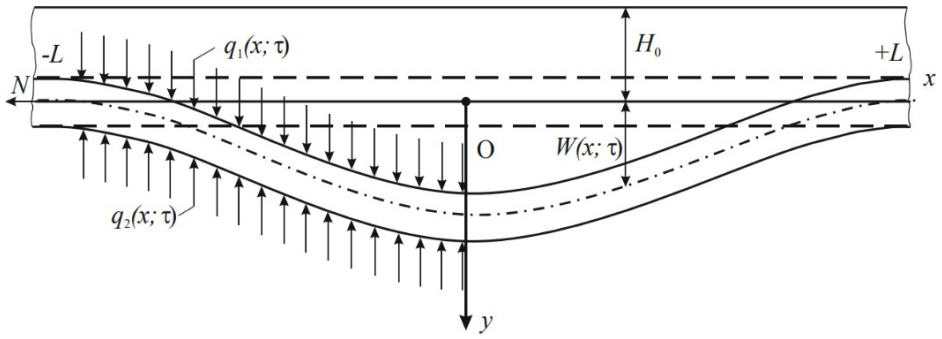

$q_1(x;\tau)$ – the average distributed load acting on the pipeline down; $q_2(x;\tau)$ – the mean burden that is dispersed and affecting the pipeline (considering the load's symmetrical nature. $q_1(x;\tau)$ and $q_2(x;\tau)$ are shown in the left part of the figure); H_0 – the distance between the pipeline's axis and the undisturbed surface of the seabed at the start, where the axis of oxygen aligns with the elastic axis of the pipeline.

Figure 12 – The scheme of interaction of the pipeline with the ground during its subsidence (Lapteva, T., 2019)

The elastic beam's longitudinal-transverse bending on a Winkler type base can be represented by the differential equation (Lapteva, T., 2019):

$$EI \cdot \frac{d^4w}{dx^4} - N \cdot \frac{d^2w}{dx^2} + k \cdot w = q_1 - q_2, \quad (4.68)$$

where w – pipeline displacement;

I – the moment of inertia of the cross section of the pipe;

k – the coefficient of the base bed or the coefficient of normal soil resistance.

In the given equation w, q_1 and q_2 are the functions of distance and time while N is the function of distance only. The named model based on a principle of elastic base. The model under consideration involves two noteworthy suppositions. Firstly, it assumes that the precipitation w(x, y) at a given point on the base surface is in direct proportion to the pressure p(x, y) at said point. Secondly, the model postulates that precipitation solely occurs at the site where the load is applied, with no precipitation occurring outside the loading area, where W(x, y) = 0. The k coefficient represents proportionality.

If the effective width of the beam is assumed to be equal to the diameter of the pipe, then the coefficient of the base bed can be represented as follows (Aybinder, A., 1988,1981):

$$k = C_{y0} \cdot D_{out.c}, \tag{4.69}$$

where C_{y0} – the generalized coefficient of normal soil resistance, MPa/cm:

$$C_{y0} = \frac{0{,}12 \cdot E_s \cdot \eta_s}{(1-\mu_s^2)\sqrt{l_0 D_{out.c}}}\left[1 - e^{\frac{-2 \cdot H_0}{D_{out.c}}}\right], \tag{4.70}$$

where E_s – the soil deformation modulus of undisturbed structure, MPa;

η_s – the coefficient of reduction of the modulus of deformation of the soil;

μ_s – the Poisson's coefficient of the soil;

l_0 – unit length of pipe equal to 100 cm.

The load q_1 consists of two components: the load from the action of the soil q_{1s} and the load from the action of the pipeline itself q_{1p}. The load from the action of the soil is defined as follows:

$$q_{1s} = \gamma_s \cdot [H_0 + w] \cdot D_{out.c}. \tag{4.71}$$

The load q_2 is determined by two components. The first of them is related to the normal reaction of the soil:

$$q_{2n} = R(T) \cdot D_{out.c}, \tag{4.72}$$

where R(T) – bearing capacity of the soil (function of temperature).

The second component is the viscosity force that occurs when the pipeline flows around the ground:

$$q_{2v} = 10{,}53 \cdot \eta(T) \cdot \frac{\partial w}{\partial \tau}, \tag{4.73}$$

where $\eta(T)$ – dynamic viscosity (function of temperature);

$\frac{\partial w}{\partial \tau}$ – pipeline precipitation rate.

Functions of temperature are calculated by empirical equations as follows (Khabibullin, P., 2001):

$$R(T) = (54{,}7 - 0{,}48 \cdot (T - 275)) \cdot 10^3; \tag{4.74}$$

$$\eta(T) = 3{,}74 \cdot 10^9 \cdot e^{-0{,}22 \cdot (T-275)}. \tag{4.75}$$

Summarizing the formulas, the final equations for loads are obtained:

$$q_1 = q_{1s} + q_{1p} = \gamma_s \cdot [H_0 + w] \cdot D_{out.c} + q_{1p}; \tag{4.76}$$

$$q_2 = q_{2n} + q_{2v} = R(T) \cdot D_{out.c} + 10{,}53 \cdot \eta(T) \cdot \frac{\partial w}{\partial \tau}. \tag{4.77}$$

Final form of the initial equation:

$$EI \cdot \frac{d^4w}{dx^4} - N \cdot \frac{d^2w}{dx^2} + 10{,}53 \cdot \eta(T) \cdot \frac{\partial w}{\partial \tau} + \\ + (C_{y0} - \gamma_s) \cdot D_{out.c} \cdot w = q_{1p} + D_{out.c} \cdot [\gamma_s \cdot H_0 - R(T)]. \tag{4.78}$$

Let's make the following substitution of variables:

$$a = \frac{N}{EI}; \tag{4.79}$$

$$b = \frac{10{,}53 \cdot \eta(T)}{EI}; \tag{4.80}$$

$$c = \frac{(C_{y0} - \gamma_s) \cdot D_{out.c}}{EI}; \tag{4.81}$$

$$h = \frac{q_{1p} + D_{out.c} \cdot [\gamma_s \cdot H_0 - R(T)]}{EI}. \tag{4.82}$$

The differential equation then can be rewritten:

$$\frac{d^4w}{dx^4} - a \cdot \frac{d^2w}{dx^2} + b \cdot \frac{\partial w}{\partial \tau} + c \cdot w = h. \tag{4.83}$$

The most useful solution is the type of the limiting curve of the pipeline corresponding to a large period of precipitation time (formally, for $\tau \to \infty$). In this case, the result can be obtained in a closed form as a stationary solution of the problem:

$$\frac{d^4w}{dx^4} - a \cdot \frac{d^2w}{dx^2} + c \cdot w = h. \tag{4.84}$$

The above-mentioned equation is equivalent to the homogeneous equation that follows:

$$\frac{d^4w}{dx^4} - a \cdot \frac{d^2w}{dx^2} + c \cdot w = 0 \tag{4.85}$$

The characteristic equation for this case:

$$r^4 - a \cdot r^2 + c = 0 \tag{4.86}$$

Solutions of the biquadratic equation are the following:

$$r_{1,2} = \pm\sqrt{\frac{a}{2} + d}, \tag{4.87}$$

$$r_{3,4} = \pm\sqrt{\frac{a}{2} - d}, \tag{4.88}$$

where $d = \sqrt{\left(\frac{a}{2}\right)^2 - c}$.

As $\frac{a}{2} < c$ for all the cases, then the complex solutions of the given biquadratic equation are the following:

$$r_{1,2} = \pm\sqrt{\frac{a}{2} + \beta_o i}, \tag{4.89}$$

$$r_{3,4} = \pm\sqrt{\frac{a}{2} - \beta_o i}, \tag{4.90}$$

where $\beta_o{}^2 = -\left(\frac{a}{2}\right)^2 + c$.

To find the proper complex solution trigonometric form should be applied and parameters are found:

$$\rho = \sqrt{c}; \tag{4.91}$$

$$\varphi = arctg\frac{\beta_0}{\alpha_0}, \tag{4.92}$$

where $\alpha_0 = \sqrt{\frac{a}{2}}$

Then applying Moivre's equation complex routes are defined:

$$r_{1,2} = \sqrt[4]{c}\left(cos\frac{\varphi}{2} + isin\frac{\varphi}{2}\right); \tag{4.93}$$

$$r_{3.4} = \sqrt[4]{c}\left(cos\frac{\varphi}{2} - isin\frac{\varphi}{2}\right). \tag{4.94}$$

To get the certain solution trigonometric form should be transformed into algebraic one:

$$\varphi = arctg\frac{\beta_0}{\alpha_0} = arccos\frac{1}{\sqrt{1+\left(\frac{\beta_0}{\alpha_0}\right)^2}}; \quad (4.95)$$

$$cos\frac{\varphi}{2} = \pm\sqrt{\frac{1+cos\varphi}{2}}; \quad (4.96)$$

$$sin\frac{\varphi}{2} = \pm\sqrt{\frac{1-cos\varphi}{2}}. \quad (4.97)$$

Substituting φ into the given equations:

$$cos\frac{\varphi}{2} = \pm\sqrt{\frac{1+cos\left(arccos\frac{1}{\sqrt{1+\left(\frac{\beta_0}{\alpha_0}\right)^2}}\right)}{2}} = \pm\sqrt{\frac{1+\frac{1}{\sqrt{1+\left(\frac{\beta_0}{\alpha_0}\right)^2}}}{2}}; \quad (4.98)$$

$$sin\frac{\varphi}{2} = \pm\sqrt{\frac{1-cos\left(arccos\frac{1}{\sqrt{1+\left(\frac{\beta_0}{\alpha_0}\right)^2}}\right)}{2}} = \pm\sqrt{\frac{1-\frac{1}{\sqrt{1+\left(\frac{\beta_0}{\alpha_0}\right)^2}}}{2}}. \quad (4.99)$$

Through the utilization of the acquired expressions, the distinct real and imaginary components of the expression can be effectively determined:

$$\alpha = \sqrt[4]{\cdot}\frac{\sqrt{1+\frac{1}{\sqrt{1+\left(\frac{\beta_0}{\alpha_0}\right)^2}}}}{\sqrt{2}}; \quad (4.100)$$

$$\beta = \sqrt[4]{\cdot}\frac{\sqrt{1-\frac{1}{\sqrt{1+\left(\frac{\beta_0}{\alpha_0}\right)^2}}}}{\sqrt{2}}. \quad (4.101)$$

$$4\sqrt{\quad}\quad 2$$

$$-$$

The following general solution of the homogeneous differential equation corresponds with the given routes:

$$w_0(x) = C_1 \operatorname{ch} \alpha x \cdot cos\beta x + C_2 \operatorname{ch} \alpha x \cdot sin\beta x + C_3 \operatorname{sh} \alpha x \cdot cos\beta x + \\ + C_4 \operatorname{sh} \alpha x \cdot sin\beta x. \tag{4.102}$$

The partial solution is the following:

$$w^*(x) = \frac{h}{c}. \tag{4.103}$$

The total solution:

$$w(x) = C_1 \operatorname{ch} \alpha x \cdot cos\beta x + C_2 \operatorname{ch} \alpha x \cdot sin\beta x + C_3 \operatorname{sh} \alpha x \cdot cos\beta x + \\ + C_4 \operatorname{sh} \alpha x \cdot sin\beta x + \frac{h}{c}. \tag{4.104}$$

The boundary conditions due to fixed supports are the following:

$$w\left(\pm\frac{L}{2}\right) = 0; \tag{4.105}$$

$$\frac{dw}{dx}\left(\pm\frac{L}{2}\right) = 0. \tag{4.106}$$

Since symmetrical loading and fixing of the pipe relative to the middle of the pipeline is assumed, it is sufficient to leave only even functions in the general form of the equation:

$$w(x) = C_1 \operatorname{ch} \alpha x \cdot cos\beta x + C_4 \operatorname{sh} \alpha x \cdot sin\beta x + \frac{h}{c}. \tag{4.107}$$

The constants are defined taking into consideration the boundary conditions and resulting equation for the pipeline-soil displacement is obtained:

$$w(x) = \frac{2h}{c} \cdot \frac{-\left(\alpha ch\alpha \frac{L}{2} sin\beta \frac{L}{2} + \beta sh\alpha \frac{L}{2} cos\beta \frac{L}{2}\right) ch\alpha x cos\beta x}{\alpha sin\beta L + \beta sh\alpha L} + \\ + \frac{2h}{c} \cdot \frac{\left(\alpha sh\alpha \frac{L}{2} cos\beta \frac{L}{2} - \beta ch\alpha \frac{L}{2} sin\beta \frac{L}{2}\right) sh\alpha x sin\beta x}{\alpha sin\beta L + \beta sh\alpha L} + \frac{h}{c}. \tag{4.108}$$

The aforementioned expression is a modified iteration of the deflection equation applicable to a beam situated on an elastic Winkler base, considered by Korobkov, G. et al (Korobkov, G., Zaripov, 2009). The difference lies in the calculation of the reaction of the soil, taking into account the change in its bearing capacity, which is used in the analytical solution by Lapteva, T. The difference in the form of the final expression is due to the solution method. In the named work, the decomposition of the differential equation into a Fourier series using harmonics is used, while in this work, the direct solution of the differential equation is considered.

Like the preceding scenario, it behooves one to assess the robustness of the pipeline through an appraisal of its critical strength and length. To do this, we investigate the following case (Akhtyamov, A., 2015):

$$\alpha sin\beta L + \beta sh\alpha L = 0. \tag{4.109}$$

The solutions of the aforementioned equation are indicative of a scenario wherein the rod undergoes an infinite deflection leading to an eventual loss of stability. It is rational to solve it graphically by the point of intersection of functions. During the course of the solution, it was ascertained that the equation exhibits an absence of any real roots apart from the value of zero. This does not make physical sense, and therefore it is not possible to accurately assess the stability

4.4 Corrosion control

As noted earlier, the control of the corrosion process in pipelines pumping carbon dioxide is extremely important. The dependence of the corrosion rate on pressure and temperature is discussed in detail by authors mentioned in previous chapters. However, an important parameter is not only the thermobaric component, but also the phenomenon of water solubility in pure CO_2 and the flow with impurities. For a reliable assessment of the interaction of components, it is necessary to choose the right EOS when modeling the fluid. Basic equations (Peng-Robinson, CPA, CERG-2008) can often be applied, but with modified BIPs (Sabirzyanov, A., 2002). So, the modified equation of state was used in this paper earlier when calculating phase envelopes. It is worth noting that according to DNVGL-RP-J202 it is Peng- Robinson that should be used for modeling.

As in the case of technological calculation of supercritical flow, it is recommended to use a mechanistic approach rather than an empirical one. At the same time, traditional electrochemical methods for assessing corrosion in SCF do not agree well with experimental data, while weight loss measurements showed underestimated values (Wei, L. et al., 2015).

The risk of an active corrosion process can be assessed by the operating parameters of the pipeline, as well as by the water content in the product. Since in this paper it is proposed to pump CO_2 in the supercritical zone of the phase diagram, then all the water will be dissolved in carbon dioxide, i.e. there will be no free liquid phase of water (Figures 6-8). And in the absence of free water, the corrosion rate is negligible. Moreover, in the fluids considered, the molar water content does not exceed 10 ppm, which allows us to consider the mixture dry

(Table 4). According to DNVGL-RP-J202, the critical value at which a detailed calculation of carbon dioxide corrosion should be performed is 500 ppm.

In addition to carbon dioxide itself, other aggressive impurities (SO_2, H_2S) are present in the medium under consideration. However, due to the complete dissolution of water, there is also no risk of corrosion.

Nevertheless, the aforementioned provisions hold validity solely in instances of standard pipeline operations. The present analysis concerns the scenario in which the integrity of the pipeline is compromised. In this case, the process of active pressure reduction along the curve on the phase diagram will begin before the appearance of the liquid phase of CO_2. In the case of extremely rapid depressurization of the system, a case is possible in which all the water cannot be dissolved and a rapid corrosion process begins. In addition, the pipeline under consideration is marine, which only aggravates the situation. The corrosion process then can be described by the following equation for the Top-Of-The Line corrosion model (Wei, L. et al., 2015):

$$\frac{d(V \cdot [Fe^{2+}])}{dt} = \Phi_c \cdot A_c - \Phi_p \cdot A_p - m \cdot A_{cond} \cdot [Fe^{2+}], \tag{4.110}$$

where V – the volume of condensed water, m^3;

$[Fe^{2+}]$ – the total quantity of iron ions present within a given solution, $kmol/m^3$;

Φ_c – the corrosion rate, $kmol/s/m^2$;

Φ_p – the precipitation rate, $kmol/s/m^2$;

A_c – the area where corrosion takes place, m^2;

A_p – the area where precipitation takes place, m^2;

A_{cond} – the area where condensation takes place, m^2;

m – the condensation rate, $m^3/s/m^2$.

When considering the impact of the buildup of iron carbonate scale, the equation can be expressed in the following manner:

$$\frac{d(V \cdot [Fe^{2+}])}{dt} = K \cdot \Phi_c \cdot A_c - (1 - K) \cdot \Phi_p \cdot A_p - m \cdot A_{cond} \cdot [Fe^{2+}], \tag{4.111}$$

or if the condensed film thickness δ is known and equal areas are assumed:

$$\frac{d(V \cdot [Fe^{2+}])}{dt} = \frac{1}{\delta} \cdot [K \cdot \Phi_c - (1 - K) \cdot \Phi_p - m \cdot A_{cond} \cdot [Fe^{2+}]], \tag{4.112}$$

where K – percentage of the covered corroding surface.

The film thickness is defined as follows:

$$\delta = \sqrt{\frac{\sigma}{g \cdot (\rho_l - \rho_g)}}, \tag{4.113}$$

where σ – the surface tension coefficient;

g – the gravity constant;

ρ_l, ρ_g – the liquid and gas density respectively.

Chapter 5

Environmental aspects and strategic analysis

5.1 Environmental analysis

As in the case of transportation of hydrocarbon raw materials, pipeline transportation of carbon dioxide requires an assessment of possible risks during operation and possible emergency situations. In the case of CO_2, there are a number of works on the development of such a technique (McGillivray, A. et al., 2014). So, it is possible to use integral consequence modeling (Figure 13).

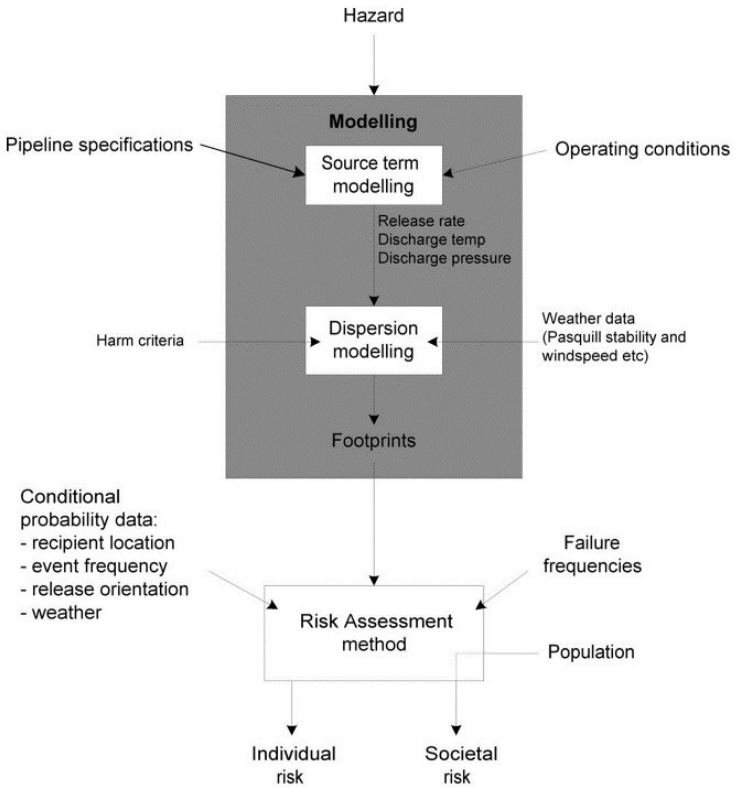

Figure 13 – Risk assessment outline (McGillivray, A. et al., 2014)

The approach introduced herein is specifically designed for the CO2 pipeline utilized in the CO2Pipehaz initiative, and its application may not be suitable for other forms of CO2 discharge,

such as vessel malfunction. It is also not applicable to cases where other fluids are implied to be pumped. Nevertheless, the underlying assumptions and the derived event tree can be corrected as appropriate for other purposes of hazard identification and risk assessment. Another significant assumption is that marine pipelines are not the main object of the study, albeit some points can be applied for them as well. The event tree for full-bore rupture or guillotine failure is presented at Figure 14.

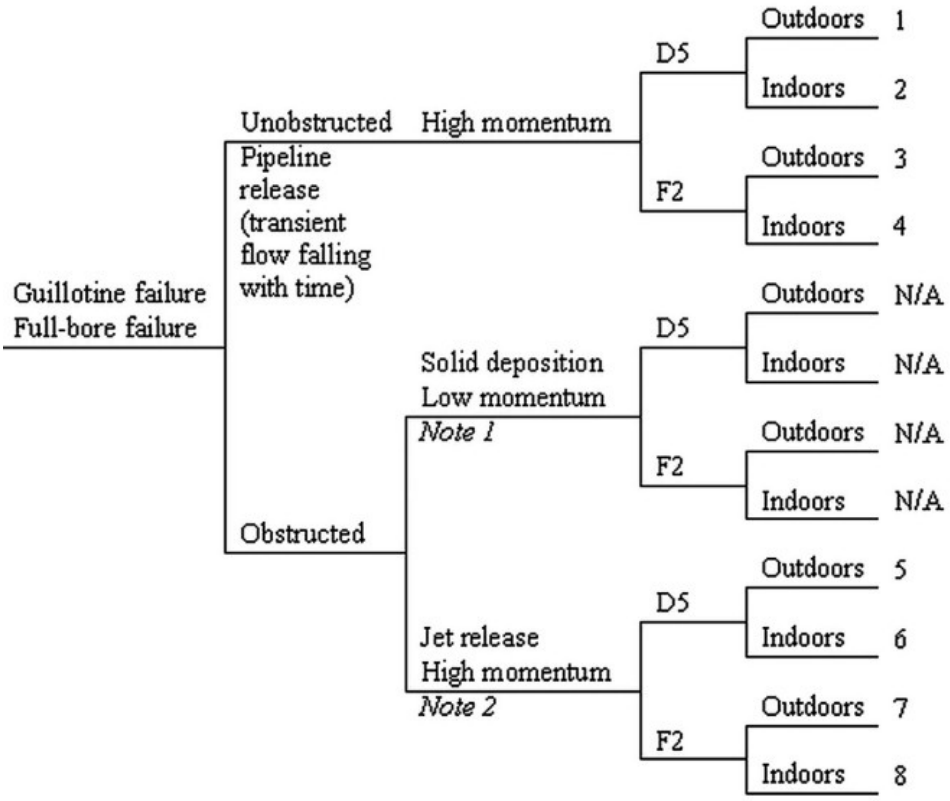

Figure 14 – Guillotine failure or full-bore rupture event tree (McGillivray, A. et al., 2014)

The following notes should be mentioned. The percentage of CO_2 deposited as a solid need to be estimated. The sublimation rate should also have to be estimated. The flow rate should consider the solid particles that have been deposited. Numerical simulation results and real-world measurements suggest that the jet experiences a minor loss of impetus as it strikes the crater sides. The low pulse release should perhaps be considered if there are other associated topographic/local entities. The flux rate ought to take into consideration the settled hard substance. The leakage is probably sufficiently minor that hitting the crater/cave walls would deflect substantial impetus. A tentative best estimation technique is to model the vent as a descent shock jet.

The solid deposition resulting from a minor leakage is expected to be minimal, Therefore, it is possible that its significance may not meet the appropriate threshold for inclusion in the event

tree. The unrestricted discharges are appropriate for instances when the stream is aimed upwards, slanted from the horizontal, or makes contact with the ground, whereas the impeded ejections represents emissions aimed straight down into the soil or where a crater shock takes place. D5 and F2 stand for two different ambient conditions.

Figure 15 – Holes in the pipeline event tree (McGillivray, A. et al., 2014)

The event tree displayed in Figure 15 was developed specifically for big and small openings found in a CO_2 pipeline. Transport pipelines used in CCUS are expected to be concealed beneath the ground. In case of extensive ruptures or piercing breaches, the aggressive impact of the malfunction may result in an indentation forming around the discharge location. Although there is limited understanding of the plume's interaction with the volcanic crater, computational fluid dynamics (CFD) suggests that the jet's speed remains mostly unaltered. Moreover, it is confirmed that in the case of punctures occurring in clay soil, the force generated during the initial release is of considerable intensity to hoist and disintegrate the soil, albeit

insufficient to propel it away. Alternatively, subterranean chambers develop near the point of emission, featuring ample fissures that enable the CO_2 to disperse upward, albeit with less force than in cases where a discernible crater occurs. Thus, the named event trees may be used for a certain project and design conditions. For the studied pipeline «OPF-Molikpaq» the following factors may be set. As the main type of the soil along the route is marine clay one and the operating pressure is high enough to transport supercritical fluid, the possible leak in the wall may eventually lead to release in the water. In previous chapters, it was noted that strong currents are established in the pipeline laying zone at the bottom of the sea, which significantly accelerates the process of pollution of the surrounding environment (Ji, H. et al., 2020). One way to determine the efficacy of diffusion transfer is by solving the equations of energy conservation and continuity. Since an analytical solution is not possible, CFD methods are used, including RANS averaging methods and various turbulence models. However, the modelling of leakages is not a part of this study. The flow pattern of the product flowing out of the pipe depends on the CO_2 stream and salted water properties and the ratio between leakage and current velocities.

Since the pipeline is offshore, the possible impact on marine life shall be considered. The main problem in the case of CO_2 leakage into the water body is a sharp change in the previously established pH level.

Since 1998, several specialized investigations have been conducted to examine the benthic species makeup on the coastal shelf of the Piltun location, particularly in the proximity of the Molikpak platform (PA-A) and the surrounding area. The results of these studies have shown that annual benthic perturbation at depths up to 20 m as a result of plowing by drifting ice (January–April), as well as under the influence of storm waves that lead to changes in the physical characteristics of soils can lead to the predominance of such opportunistic species as cumulus crustaceans (a group of small crustaceans living in bottom sediments) Diastylis bidentata. Henceforth, it is justifiable to assume that the underwater organisms at the bottom adjust to physical alterations on a yearly basis.

The average benthic biomass for the shelf zone (up to a depth of 100 m) is 500 g/m^2. This value may vary depending on the type of bottom sediments and the presence or absence of some key species (e.g. E. parma). A relatively high biomass index was recorded at depths up to 100 m on the northern and central shelves. Koblikov et al. presented the value of the average benthic biomass at the level of 428,6 g/m^2 for the shelf area between Cape Schmidt in the north and Cape Lunsky Bay in the south (Koblikov, V., 1982). This value it is consistent with the data of the report by Kusakin, O. et al., which indicates a range from 200 to 500 g/m^2 for this area,

where sea urchins accounted for 58% of the biomass, crustaceans — 12.3%, bivalves — 7.4% and polychaete worms - 4.9% (Kusakin, O. et al., 2001).

According to Auerbach, D. et al. there is enough information about the effects of variable pH on organisms living at relatively shallow depths (Auerbach, D.I. et al., 1997). Considering the maximum depth of 30-35 m along the route of the pipeline, named analysis results may be applied to this case. Then population and diffusivity equation can be applied considering Richardson's density concept (Caulfield, J.A. et al., 1997). Other models that can be used are average path, average experience and non-diffusive transport. All of them impose various values of mortality and mortality flux. Mortality is defined as a function of pH and exposure time. It has been posited that an abrupt escalation in acidic levels is observed. in the oceanic area could have negative consequences for the benthic organisms inhabiting the zone, and may also have an impact on the population of fish (Figure 16).

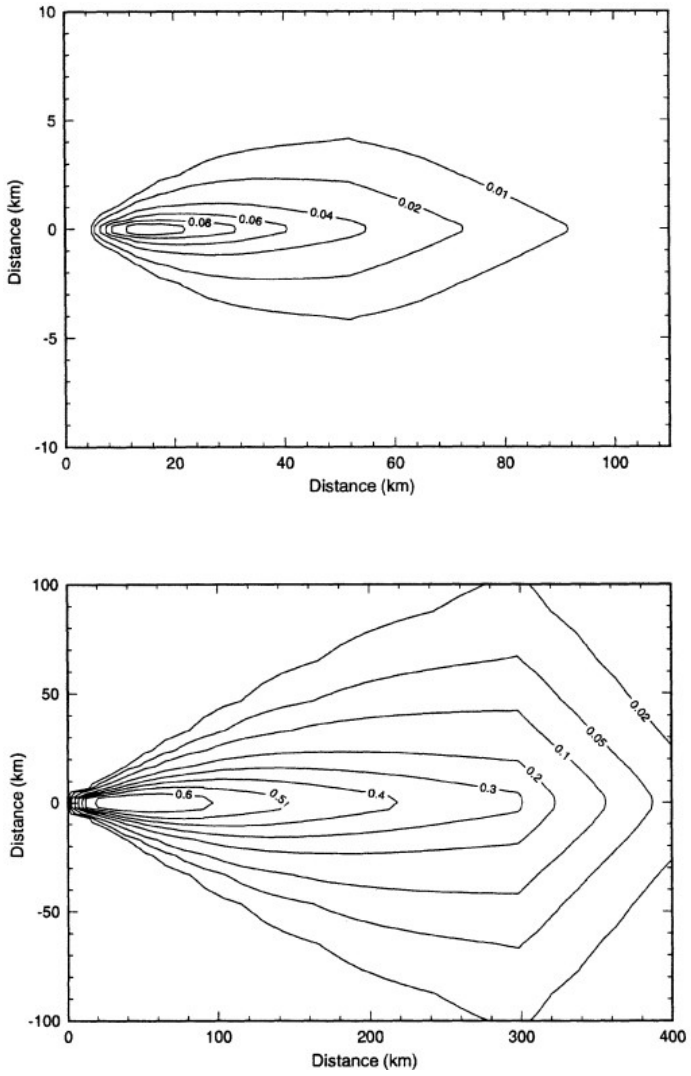

Figure 16 – Deficit of zooplankton caused by CO_2 injection (Caulfield, J.A. et al., 1997)

However, after the leak in the pipeline is eliminated, the sea currents will return the pH to its original values and restore the balance. Thereupon, comparing the possible consequences of

accidents on offshore oil pipelines, gas pipelines and converted ones, it is clear that in the latter case the damage is minimal.

5.2 Strategic analysis

For a preliminary assessment of the attractiveness of the project for investors and stakeholders, SWOT analysis is implemented (Table 7).

Table 7 – SWOT analysis of the project

Criteria	Option
Strengths	S1. Utilization of CO_2 emissions, reduction of the total carbon footprint
	S2. Use of existing marine pipeline infrastructure
	S3. Use of depleted deposits for storage
	S4. Cleaning of the inner cavity of the oil pipeline in case of conversion
	S5. Gradual implementation of the project starting from the IV stage of field development using EOR
	S6. Reduced risk of negative environmental impact in comparison with oil and gas facilities
Weaknesses	W1. Lack of sufficient theoretical basis for accurate preliminary calculations
	W2. Lack of previous experience in implementing similar projects
	W3. Weak regulatory framework for monitoring the operation of converted pipelines
Opportunities	O1. Development of methods for calculating converted pipelines
	O2. Expanding the existing regulatory framework
	O3. Possibility of registration of new technologies, intellectual property
Threats	T1. Reduction of investor interest and financing of the project
	T2. Development of other methods of CO_2 transportation
	T3. Development of other renewable energy resources, reduction of hydrogen production

	T4. High corrosion activity in case of violation of the preparation technology
	T5. Accidents on pipelines due to preliminary wear

Inasmuch as the total number of strengths and opportunities prevails over the negative aspects of the project, it can be asserted that the potential effectiveness and attractiveness of the project.

Chapter 6

Requalification regulation

At the moment, the regulatory documentation for the conversion of existing pipelines for pumping carbon dioxide is based on a special standard DNV-RP-J202: Design and Operation of CO_2 Pipelines (DNV-RP-J202,2017). This document reflects the basic requirements for conversion facilities from the standpoint of safe operation, and also defines a systematic approach to project implementation (Figure 17). So, 9 main stages are defined.

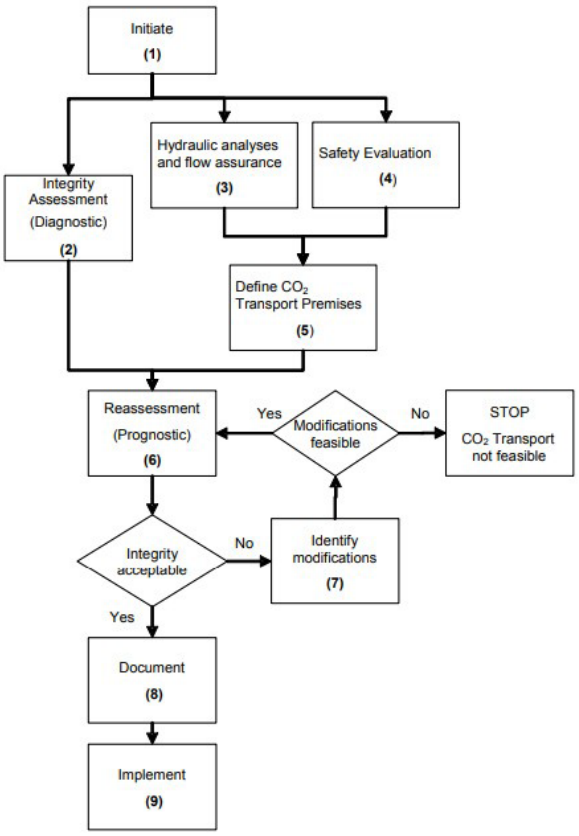

Figure 17 – Re-qualification process (DNV-RP-J202,2017)

Step 1 – Initiation. It has been decided to assess a current pipeline infrastructure for the primary objective of transporting CO_2. It is crucial to determine the initial design principles and subsequent updates, operational details, and key components within the pipeline, including material selection and pressure ratings. Additionally, assessing the battery limits is an important step in this process. It is essential to examine this critical data as part of the re-evaluation process. A foundation on which to conduct a gap analysis pertaining to the prerequisites for running on CO_2. A risk analysis needs to be undertaken and a project risk register established, indicating the dangers posed by modifying the type of conveyed product from existing to either dense-phase or gaseous-phase. The baseline expectations for the re-qualified pipeline have to be defined. The transportation of CO2 is influenced by various factors like the amount to be transported, the pressure required for delivery, the state and composition of the CO2. These factors are essential in determining the integrity and safety of the transportation process. From recent studies, often seen gaps related to this step is lack of original design basis and material certificates.

Step 2 – Integrity assessment. First and foremost, it is crucial to assess the state of the pipeline system before transitioning to CO2 operation, ensuring its integrity and technical soundness are intact. Evaluating and documenting of the historical data pertaining to the operation techniques used in the system and comparing them with the necessary requirements for efficient functionality are crucial tasks. While the data obtained from an integrity management program can be helpful, it may not necessarily encompass all the required information. It is crucial to examine the material choices, pressure levels, and overall condition of the pipeline system during integrity evaluations.

Step 3 – Hydraulic analysis and flow assurance. Changing existing product to CO_2 may have implications for the pipeline transport capacity and load conditions. The performance of a flow analysis is imperative to ascertain the feasibility in terms of transport capacity, pressure, and temperature distribution along the designated route. A thorough hydraulic analysis at an advanced level will be conducted to compare important operational parameters while using the current product versus CO_2, which will be utilized to determine pipeline load conditions. To ensure pressure and temperature profiles are properly established, it is necessary to cover a representative range of operating conditions, including both steady state and transient situations. It is important to identify and assess any necessary alterations to the pipeline system.

Step 4 – Conducting safety assessments is crucial. It is important to assess the system's compliance with the safety standards applicable to CO2 pipelines. It is important to analyze and assess potential changes to the pipeline system, such as identifying areas that require improvement. Improvements such as the installation of more block valves and the enhancement of the leak detection system will be made. It is important to assess whether valves and gaskets

that are incompatible with carbon dioxide are appropriate replacements or components. Accidental release situations and their impact on the extent of consequences should be carefully considered, particularly when the product in question is altered.

Step 5 – Define CO_2 transport premises. It is important to establish the specifications for carrying CO_2, taking into account both the findings from hydraulic scrutiny and safety assessment. These factors will determine the operational and structural needs that could differ from the initial design specifications. It is essential to determine the system requirements and incorporate them into the overall plan for re-qualification. This includes stating design, incidental pressure, receiving pressure etc.

Step 6 – Reassessment. The evaluation of integrity of novel premises ought to be predicated upon the data acquired from the evaluation of integrity. and CO_2 transport facilities. If any aspects of the system are found to not meet the integrity standards, they will need to undergo design changes and be re-evaluated through an iterative process. There are situations where making the necessary changes may not be possible, such as. Based on analysis of the pros and cons, it has been determined that the re-qualification process should be terminated.

Step 7 – Variable alternatives to retrofits should be appraised in regard to practicability, safety and integrity. A reassessment of the modification alternative will be performed through documenting the integrity status. This task will involve recognizing and explaining effective solutions or alterations to ensure safe use of CO_2, taking into account acceptable impurity levels, operational boundaries, and other measures for enhancing pipeline load conditions. Additionally, material testing will be conducted to establish original material properties in cases where information is absent, and any tasks related to product change and initial filling will be commissioned and confirmed as ready for operation.

Step 8 – To ensure safe and efficient operation of the repurposed pipeline, it is essential to document the re-qualification process and update system documentation, drawings, equipment lists, and operating procedures.

Step 9 – Before the revised operational regime for CO_2 comes into effect, it is imperative to carry out the necessary system adjustments.

The main safety requirements include the following.

Internal corrosion: If there is any trace of water in the CO_2 stream, it could potentially cause corrosion at a high rate, and simply selecting a corrosion allowance as a preventive measure might not be effective enough. Hence, it is imperative to exercise meticulous supervision over the impurities in the flow and to ensure adequate drying of the flow during CO_2 transportation to evade any potential risks of internal erosion. Opting for corrosion-resistant alloys for new

pipelines entails a higher financial investment but isn't a viable choice for retrofitting carbon steel pipelines. Sequestration wells or valves may face the problem of corrosion material ingress or obstruction caused by rust buildup. If corrosion is expected, then filtration before the CO_2 goes subsurface could e.g. be needed.

Running ductile fracture: Tests conducted on preventing fractures have shown that pipelines transporting CO_2 are more susceptible to ductile fractures compared to pipelines carrying natural gas. The design methods utilized for natural gas pipelines are not suitable for conservative C pipelines. Therefore, it is anticipated that a pipeline that carries CO_2 will need increased resistance to fractures, achieved either through thicker walls or higher fracture toughness, or by imposing constraints on the CO_2 composition and temperature to regulate the saturation pressure that governs the energy required to propagate a viscous fracture. It is not possible to increase the fracture toughness or wall thickness for re-qualification, so in case of insufficient performance the alternative is to control the CO_2 composition and temperature to achieve an adequate saturation pressure, or to attenuate the fracture stop by using arresters, where required and applicable.

Brittle fracture: If a minor leak is present in a CO2 pipeline and combined with considerable tension in the region, it could result in brittle fracture initiation. Comprehensive assessment of this topic is complicated at present. Valuable information would be provided if the present certification of materials indicates high quality.

Based on the above assessment algorithm and generalized recommendations, a refined algorithm for qualitative analysis of the possibility of using the existing offshore pipeline infrastructure for carbon dioxide pumping was developed and compiled. This text provides valuable insights into the accurate evaluation of technological and operational risks using specific calculation models that take into account the behavior of the pumped medium under certain pressure and temperature conditions. By applying these models, one can obtain the most reliable information about potential risks with the current technology and knowledge. A schematic representation of the algorithm is shown in Figure 18.

The modified algorithm includes following steps:

1. The process commences from the initial concept of repurposing a pipeline to transfer carbon dioxide. At this stage, a preliminary request for evaluation to an expert organization (request for proposal) is formed.

2. An initial strategic analysis of the project by means of risk assessment tools (SWOT, risk matrices) is performed by a respective party. An initial determination regarding the practicality of the project, its advantages and disadvantages, and possible obstacles that may hinder its successful execution is produced.

3. After preliminary approval by risk management team the detailed analysis of carbon dioxide source is carried out with determination of the following data: source nature (capture or other), mass consumption of raw materials as well as full component composition of raw materials.

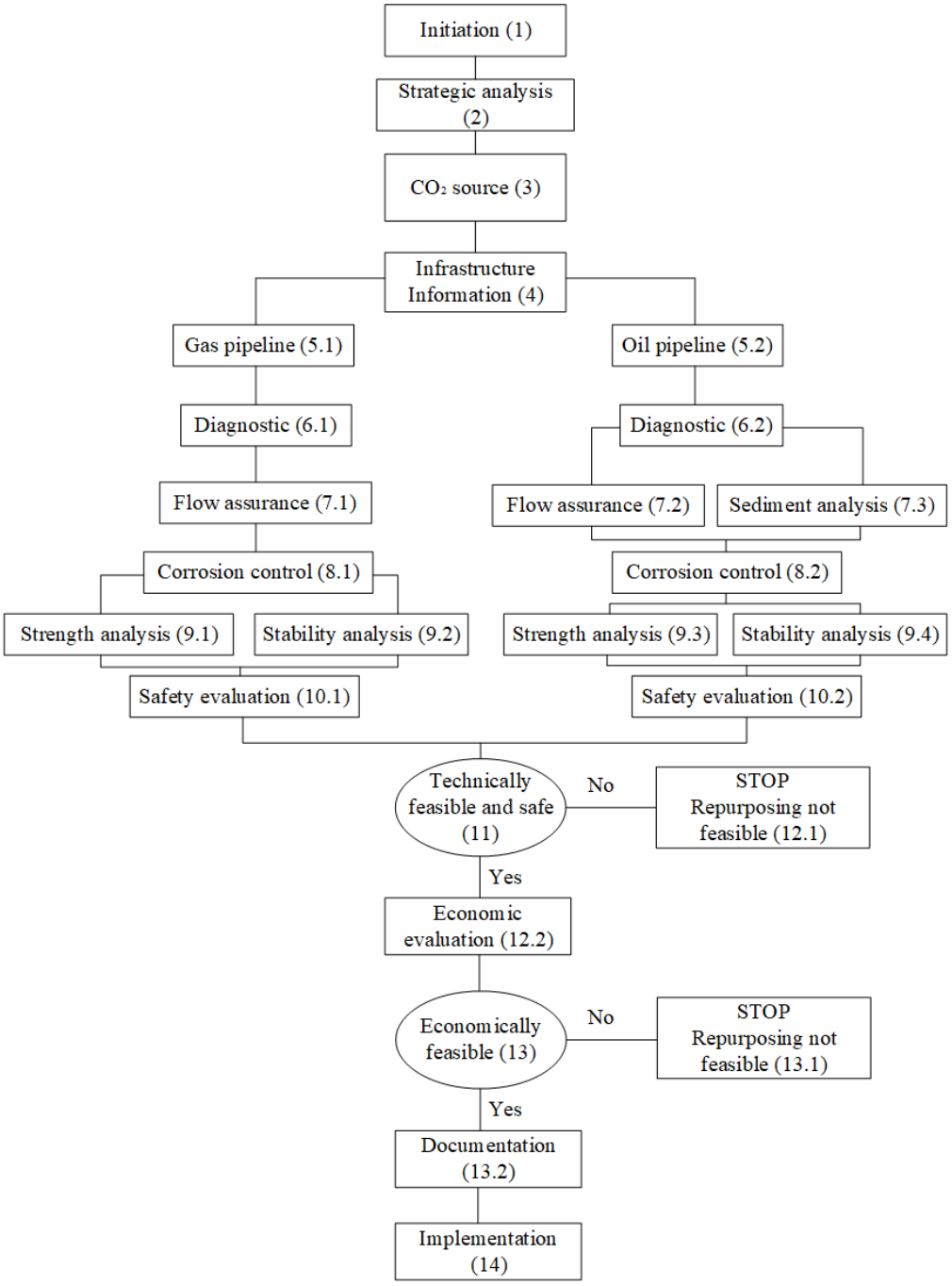

Figure 18 – Modified marine pipelines repurposing algorithm

Phase diagrams are made to determine the working environment of the zone from the condition of ensuring a stable supercritical state. The recommended model for studying carbon dioxide with impurities is a modification of the Peng-Robinson formula with modified binary interaction coefficients based on the laboratory data on the competent VLE points. The level of the most problematic impurities in the resulting carbon dioxide stream is determined, as well as possible methods of reducing their impact on the behavior of the fluid during technological operations.

4. The next stage is the collection of necessary information about the pipeline and pumping infrastructure of the object of implementation. At this stage the initial report on structure of the technological complex is formed, the profile of occurrence of the offshore pipeline, and also a way of its lining is defined.

5. A direct continuation of the previous stage is the division of the algorithm into two directions, depending on the type of pipeline. The division is necessary because of the different composition of the following studies.

6. At the stage of diagnostics, we gather detailed information about the pipeline condition from the moment of its putting into operation up to the present moment. In addition, the pipeline must be inspected for corrosion and erosion damage in order to obtain up-to-date information about its technical condition. In the case of gas pipelines, an additional inspection for hydrates is possible (6.1). For oil pipelines, inspection for asphalt-resin-paraffin deposits is relevant (6.2).

7. On the basis of information from diagnostic services, technological calculations with definition of pressure and temperature distribution profiles along the pipeline route are performed. The main purpose of this stage is to determine necessary and sufficient conditions of carbon dioxide injection into the pipeline at the coastal point, at which the fluid is in supercritical zone along the whole pipeline route. For realization of the set task various program complexes and calculation models, as well as experimental methods can be used. A necessary criterion in choosing a model is a good predictive estimation of the state both in vertical downward movement and in horizontal sections of the route. An example of such a relationship is the Beggs&Brill version, OLGAS. In addition to static analysis with verification of stability of the obtained solution in time, it is also recommended to conduct various dynamic studies (simulation of increase/decrease in flow rate when changing the incoming product volume, when using shut-off valves and emergency leakage variants). It is advisable to carry out laboratory-based experimentation if feasible. However, it should be noted that application of the known scaling method using pi-theorem is not possible due to pressure and temperature boundary conditions. An additional stage of research for oil pipelines is the calculation of the

solubility of carbon dioxide in the presence of significant deposits on the inner wall (7.3). Conducting empirical investigation is strongly advisable in this scenario.

8. Estimation of the calculated corrosion rate should be performed from the position of manifestation of both carbon dioxide and sulfur impacts (in the presence of appropriate impurities). The Top-Of-The Line model shows good agreement with experimental data. In addition to normal pumping conditions, a pressure and temperature drop with a shift of the operating point to the two-phase zone should also be considered. Calculation should be performed even for cases of maximum dissolution of water in carbon dioxide. Particular attention should be paid to pipeline sections with significant negative drop in elevation as well as sections of complex geometry (bends, tee-joints, coils). The result is the calculated corrosion rates and residual life of the pipeline wall and fittings.

9. Strength analysis is performed to prevent the occurrence of stresses that exceed the allowable values for the given characteristics of the pipeline material and operating conditions (9.1, 9.3). Both original pipelines and versions of already converted pipelines are considered. Stress calculations are recommended to be carried out using 4.29-4.36 equations. The stability calculation should be carried out for the most vulnerable areas, such as areas with increased risk of subsidence or liquefaction of soils when laying in a trench, in the case of free sag of the pipeline, the occurrence of increased lateral perpendicular flow of water masses is dangerous (9.2, 9.4). When laying in a trench, the analysis is carried out taking into account the impact of the backfill soil according to the equation 4.108. Winkler's dependence or multi-parameter computational complexes can be used as a model.

10. Although there is no critical impact of CO_2 leaks on the water masses, an assessment of the potential areola of altered pH should be performed in the case of direct carbon dioxide ingress into the surrounding volumes. The most dangerous are the streams in which the content of toxic impurities can be considered significant. The analysis should be performed with hazard identify / hazard and operability study tools.

11. Using data collected from stages 1-10, an initial determination is made regarding the potential success of the project in terms of technical feasibility and adherence to health, safety, and environmental standards. In case of a negative decision of the expert committee, further consideration of the project is terminated due to failure to meet the necessary safety requirements.

12. Economic assessment includes the calculation of the cost of a set of works to re-equip the facility for the transportation of carbon dioxide. It is recommended to apply an estimate by aggregate indicators to assess the profitability of future capital investments.

13. The economic analysis serves as the basis for determining the feasibility of the project, leading to a conclusive judgment. If the project is approved, the required project documentation is developed (13.2).

14. The final stage is the implementation of the developed and approved project in the form of reprofiling the offshore pipeline for CO_2 re-injection to the production platform.

Upon analyzing the proposed plan for replacing products in the pipeline alongside the concerns presented in this paper, it can be inferred that all the crucial aspects have been thoroughly examined and the project is adequately supported.

Chapter 7

Results and Discussion

7.1 Results Section

7.1.1 Technological calculation

The operating «PA-A/Molikpaq–OPF(Piltun-Astokhskoye)» marine oil and gas pipelines are considered as an example (Table 2). According to Nadein, V. the part connecting the OPF and J-type steel catenary riser has the following geometry (Figure 19). The pipelines have the wall thickness of 14,5 mm and two extra layers: 6 mm of bitumen to cover the steel and 71 mm of concrete to stabilize the position. The objects are positioned in the lowermost portion of the trench, with a parallel line spacing of five meters and an average depth of one meter for each object's burial. The 1:0 slope and cofferdam wall construction method are used (Nadein, V. et al., 2010).

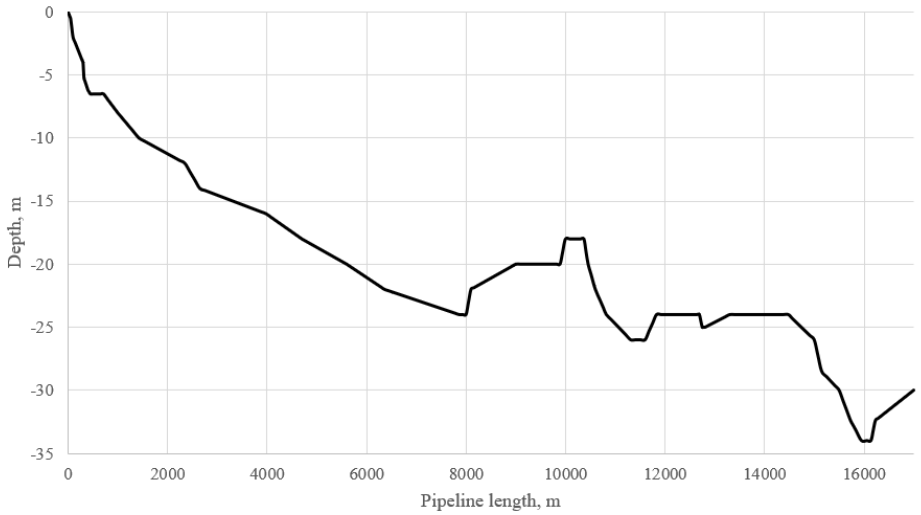

Figure 19 – OPF-Molikpaq pipeline geometry (Nadein, V. et al., 2010)

The results of velocity calculation considering density at critical point with equations 4.7 and 4.8 are presented at Table 8. Assuming calculated mass flow actual planned velocity are calculated with the equation 4.9 (Table 9).

Table 8 – Density of the fluids at critical point

Capture type	Density, kg/ m^3	Erosional velocity, m/s	Maximum velocity, m/s
Post-combustion	398,239	4,1091	6,1135
Oxy-fuel combustion	398,358	4,1084	6,1126
Pre-combustion	400,293	4,0985	6,0978

Table 9 – Calculated velocities of the flow

Capture type	Planned velocity, m/s
Post-combustion	0,5414
Oxy-fuel combustion	0,5418
Pre-combustion	0,5421

Calculated mean water properties of water are given at Table 10.

Table 10 – Mean water properties

Salinity, %	Temperature, °C	λ_{sw}, Wt/(m·K)	Cp_{sw}, J/(kg·K)	ρ_{sw}, kg/m^3	ν_{sw}, m^2/s
3,185	2,95	0,5579	4173,489	1001,886	$5{,}721 \cdot 10^{-7}$

As the temperature difference between water and inner layer is unknown, for the first iteration assumption is made that the full heat exchange coefficient is equal to recommended value of 3,22 W/(m^2· *K*) for marine soils. The temperature distribution along all layers assuming SCF oxy-fuel flow at initial temperature of 65 °C was calculated using software (Figure 20).

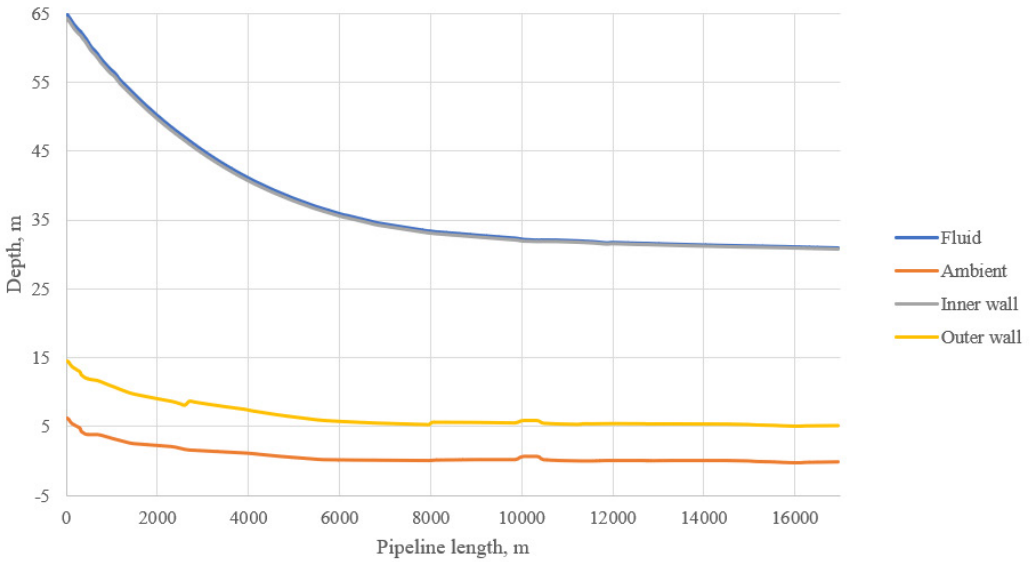

Figure 20 – Preliminary temperature distribution along the pipeline

The average temperature difference between water and outer layer of the pipeline is 6,041 °C. The determining temperature in that case is defined as mean between water and concrete layer and equals to 3,939 °C. Therefore, the Pr at determining temperature is 4,3087. To calculate Gr the thermal expansion should be evaluated. According to experimental data array, the β ranges from 0,000014 to 0,000015 at the water level and the bottom respectively. So, the average 0,0000145 1/K is assumed. In that case Gr equals to $2{,}625 \cdot 10^{-9}$ and (Gr·Pr) is $11{,}312 \cdot 10^{-9}$. The resulting criterial equation 4.17 is the following:

$$Nu_{s-w} = 0{,}7 \cdot 0{,}135 \cdot (Gr \cdot Pr)^{0{,}33} = 0{,}7 \cdot 0{,}135 \cdot (11{,}312 \cdot 10^{-9})^{0{,}33} = 196{,}38.$$

Therefore, the α_0 is calculated with 4.24:

$$\alpha_0 = \frac{196{,}38 \cdot 0{,}5579}{1} = 109{,}56\ \mathrm{W/(m^2 \cdot K)}.$$

As the heat transfer coefficient from soil to water is known, the α_2 can be evaluated with 4.16:

$$\alpha_2 = \frac{2 \cdot 1{,}866}{0{,}51 \cdot ln\left(\frac{4}{0{,}51} + \frac{1{,}866}{109{,}56 \cdot 0{,}51}\right)} = 3{,}546\ \mathrm{W/(m^2 \cdot K)}.$$

Assuming mean values along the pipeline, Gr is calculated with 4.19:

$$Gr = \frac{9{,}81 \cdot (513{,}71 - 400) \cdot 400 \cdot 0{,}331^3}{(2{,}645 \cdot 10^{-5})^2} = 2{,}23 \cdot 10^{13}.$$

Due to the significant effect of correct inner heat transfer coefficient 10 discrete points were considered along the pipeline (Table 11).

Table 11 – Nu parameter along the pipeline

№	x, m	Temperature, °C	Re	Gr, $\cdot 10^{11}$	Pr	Nu	α_1, W/(m^2·K)
1	1700	51,48	1546237,5	1,75626	1,184	888,72724	89,6011
2	3400	43,18	1713219,8	2,83389	1,546	1139,3252	118,5978
3	5100	37,79	1858801,1	5,15404	2,218	1568,4268	170,3014
4	6800	34,56	1982341,3	9,96425	3,559	2287,4599	260,9103
5	8500	33,02	2059223,7	17,8539	5,5718	3226,0174	382,288
6	10200	32,03	2128107,6	39,313	9,719	5052,2318	621,0228
7	11900	31,61	2221040,6	161,678	24,061	10950,11	1408,111
8	13600	31,38	2331790,1	153,543	63,1856	14849,356	1959,479
9	15300	31,14	1721060,3	27,9774	27,0694	6346,2921	1182,7
10	17000	30,88	1716729,5	21,4977	17,9527	5069,1077	986,9382

From the obtained data, a graph was created to demonstrate the correlation between the Nu parameter and the length of the pipeline (Figure 21).

As all the heat transfer coefficients are known, the total one can be calculated using information about materials. The summary data about thermal resistances is represented at Table 12.

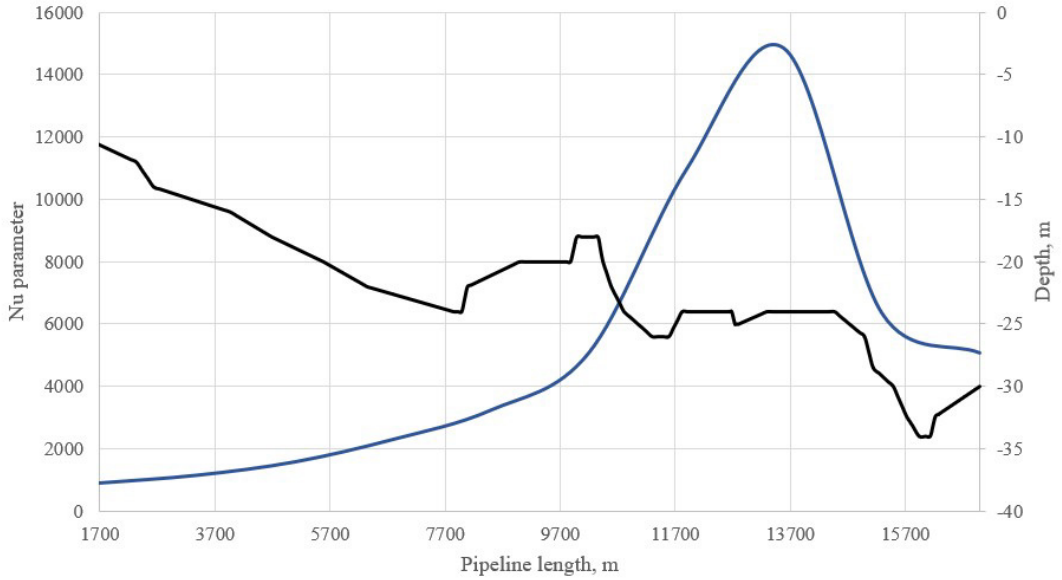

Figure 21 – Nu parameter distribution along the pipeline

Table 12 – Total heat transfer coefficient

№	x, m	R_{in}, (m·K)/W	R_w , (m·K)/W	R_{is}, (m·K)/W	R_c, (m·K)/W	R_{amb}, (m·K)/W	K, W/(m²·K)
1	1700	0,0112	0,0003	0,0077	0,0296	0,282	3,0224
2	3400	0,0084	0,0003	0,0077	0,0296	0,282	3,0475
3	5100	0,0059	0,0003	0,0077	0,0296	0,282	3,0715
4	6800	0,0038	0,0003	0,0077	0,0296	0,282	3,0909
5	8500	0,0026	0,0003	0,0077	0,0296	0,282	3,1025
6	10200	0,0016	0,0003	0,0077	0,0296	0,282	3,1122
7	11900	0,0007	0,0003	0,0077	0,0296	0,282	3,121
8	13600	0,0005	0,0003	0,0077	0,0296	0,282	3,1229
9	15300	0,0008	0,0003	0,0077	0,0296	0,282	3,1197
10	17000	0,001	0,0003	0,0077	0,0296	0,282	3,1180

As the initial assumption about K and temperature differences was made, the calculation error should be defined. Comparing assumed 3,22 and resulting average 3,093 the inaccuracy is calculated:

$$\Delta K = \left|\frac{K_0 - K}{K_0}\right| \cdot 100\% = \left|\frac{3{,}22 - 3{,}093}{3{,}22}\right| \cdot 100\% = 3{,}94\ \%.$$

The assumption was deemed appropriate given that the error margin was below the threshold of 5%.

A mechanistic approach was employed to calculate the pressure and temperature distributions in a steady state. The objective was to determine the suitable temperature and pressure values at the entrance, given that the corresponding values at the exit were already known, and present the SCF state. To ensure the highest critical value was covered, the outlet pressure was adjusted to 7,64 MPa while maintaining a temperature of 32 °C (Figures 22-25). The outlet temperature for pre-combustion stream was set at 33 °C due to convergence limitations. Two distinct correlations were utilized to analyze and contrast the outcomes: HYSYS Beggs&Brill (model 1) and OLGAS (model 2).

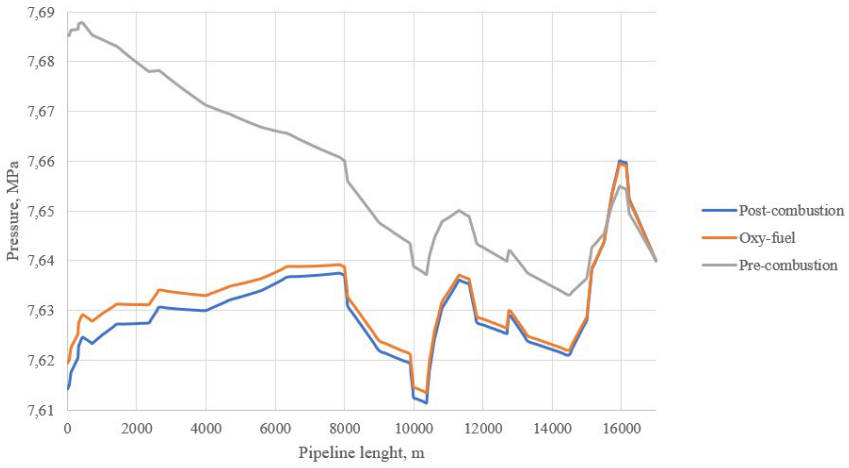

Figure 22 – Pressure distribution along the pipeline at τ=0 (model 1)

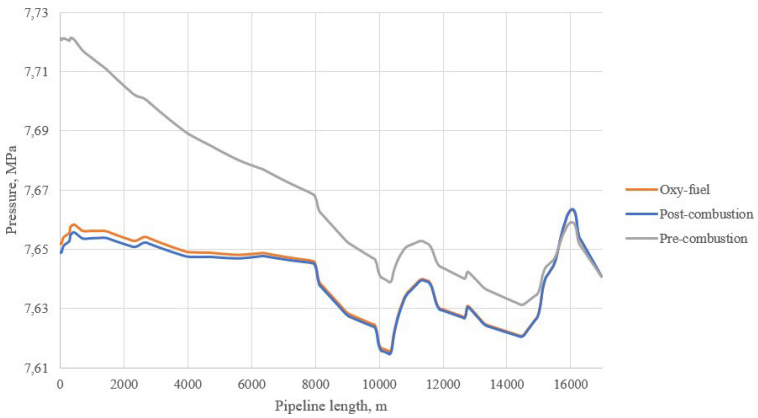

Figure 23 – Pressure distribution along the pipeline at τ=0 (model 2)

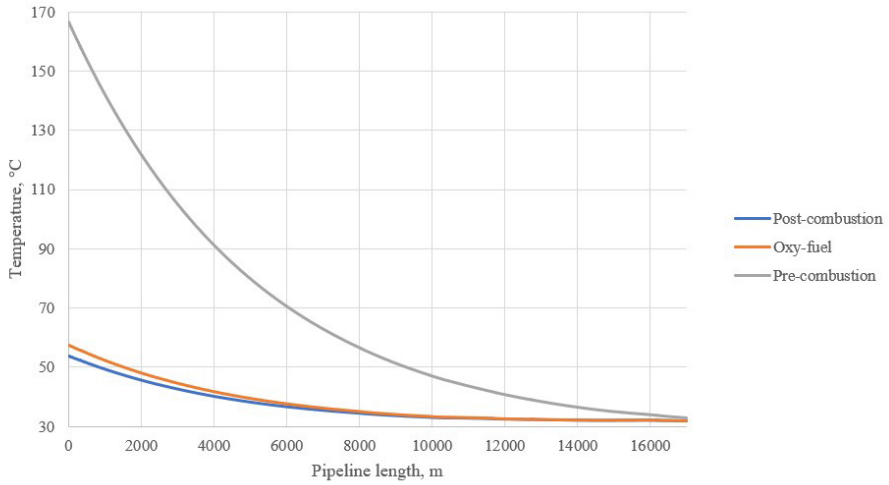

Figure 24 – Temperature distribution along the pipeline at τ=0 (model 1)

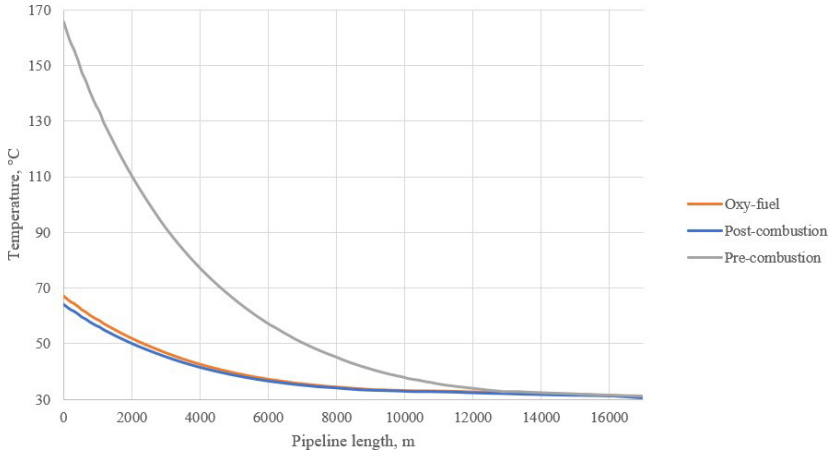

Figure 25 – Temperature distribution along the pipeline at τ=0 (model 2)

The graphs generated at the starting point (τ=0) distinctly indicate variations in the conduct of streams with diverse sources. Due to the comparatively elevated level of pollution, the pre-combustion flow experiences much greater levels of pressure and temperature than those observed in oxy-fuel and post-combustion situations. (Table 13). Although the aspect in question is specified, it is possible to carry out all instances as long as the maximum operating pressure (MOP) and maximum allowable operating pressure (MAOP) levels are not surpassed. Reference values are 9,1/9,8 MPa and 10 MPa respectively. Nevertheless, the temperature recorded for the pre-combustion stream is considerably higher than the typical operational temperature for oil or gas. Reference values are 12,5 °C and 5 °C respectively.

Upon examination of the outcomes, it can be deduced that the second computational model presents greater figures. Nonetheless, the correlation results in a marginally reduced inlet temperature for pre-combustion. If the changes in parameters over time are taken into account, the SCF flows become unstable. In order to monitor alterations in the system's condition over a period of time, the utilization of the second model was deemed favorable owing to its notable

proficiency in handling dynamic tasks. The problem was solved for a period of 72 hours to check solution stability. The outcomes of the model at specific temporal instances are exhibited through the visual representation of Figures 26-31.

Table 13 – Modelling results at τ=0

Capture type	Inlet pressure, MPa		Inlet temperature, °C	
	Model 1	Model 2	Model 1	Model 2
Post-combustion	7,614	7,649	53,78	63,92
Oxy-fuel combustion	7,619	7,652	57,57	66,92
Pre-combustion	7,685	7,721	166,84	165,68

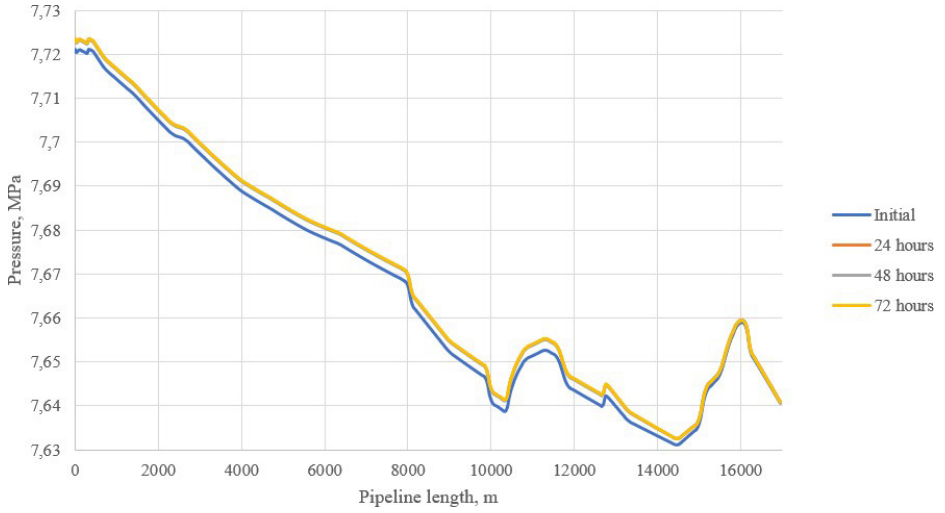

Figure 26 – Pressure distribution for the pre-combustion flow

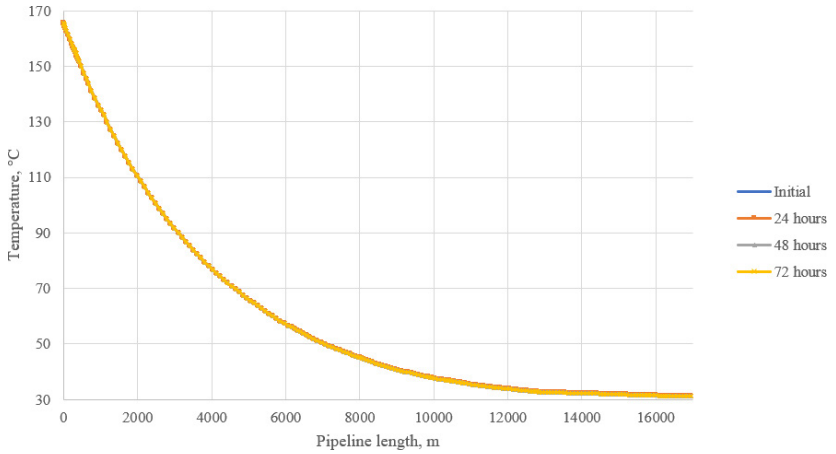

Figure 27 – Temperature distribution for the pre-combustion flow

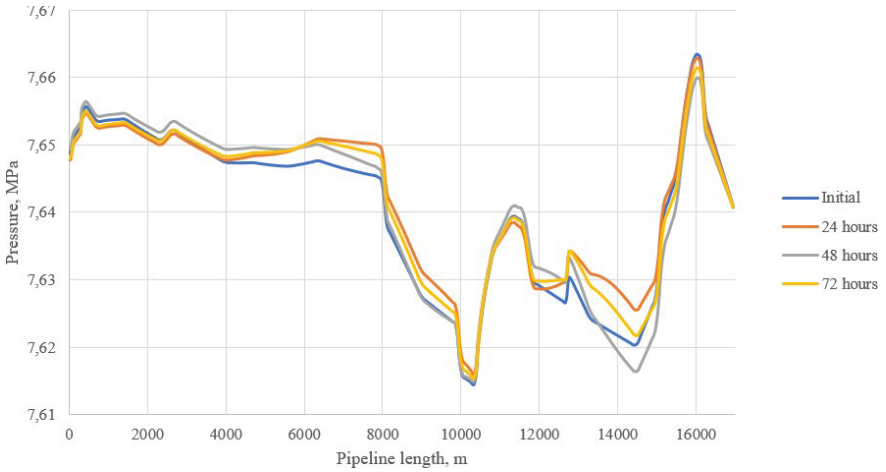

Figure 28 – Pressure distribution for the post-combustion flow

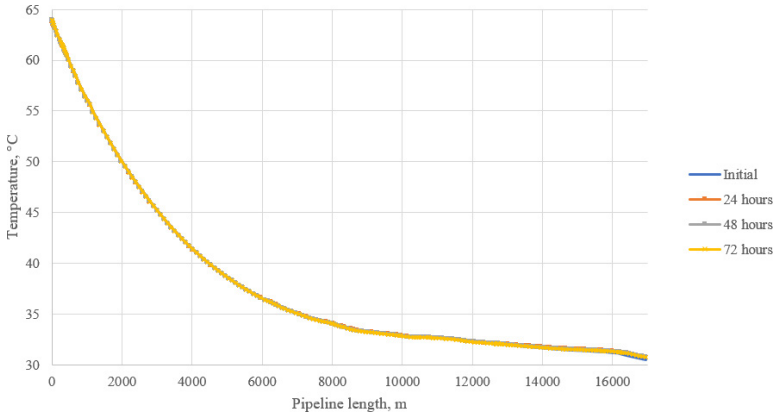

Figure 29 – Temperature distribution for the post-combustion flow

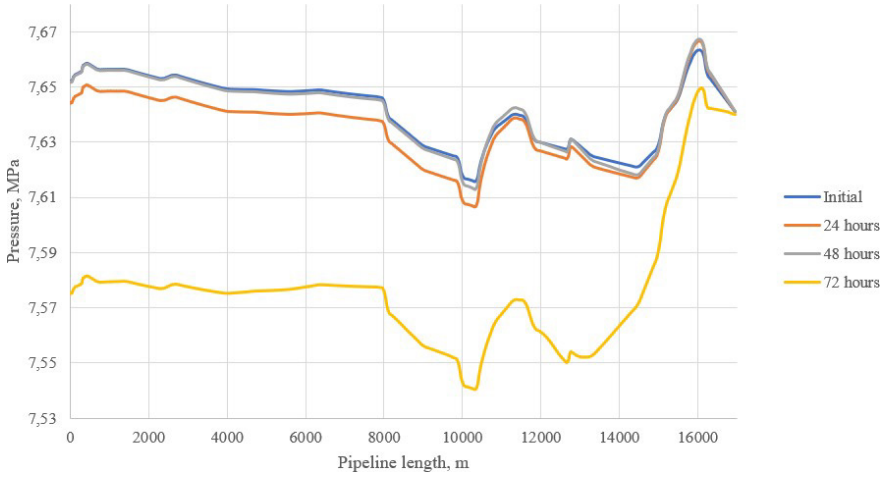

Figure 30 – Pressure distribution for the oxy-fuel flow

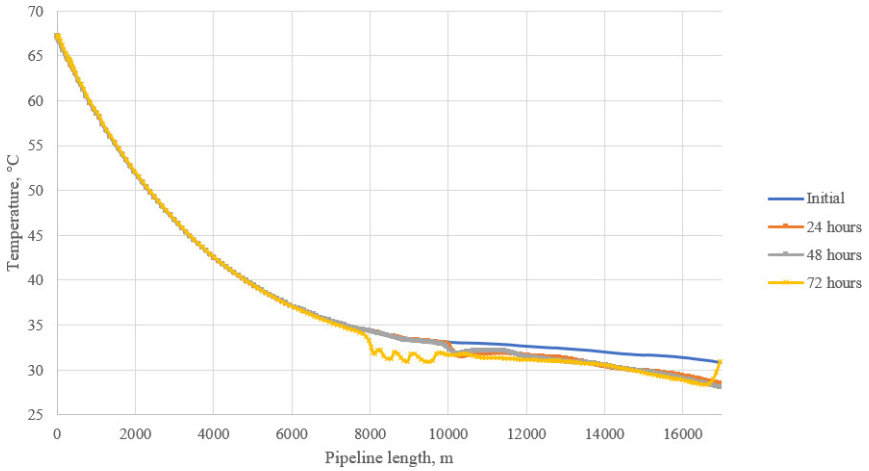

Figure 31 – Temperature distribution for the oxy-fuel flow

One plausible methodology for stabilizing fluid flow is to elevate the pumping rate to the prescribed threshold of 2 meters per second. Increasing the mass flow of air from nearby industrial facilities can solve the problem. In that case, the flow rate would be 66,876 kg/s. For example, consider the most unstable option – oxy-fuel stream (Figures 32,33).

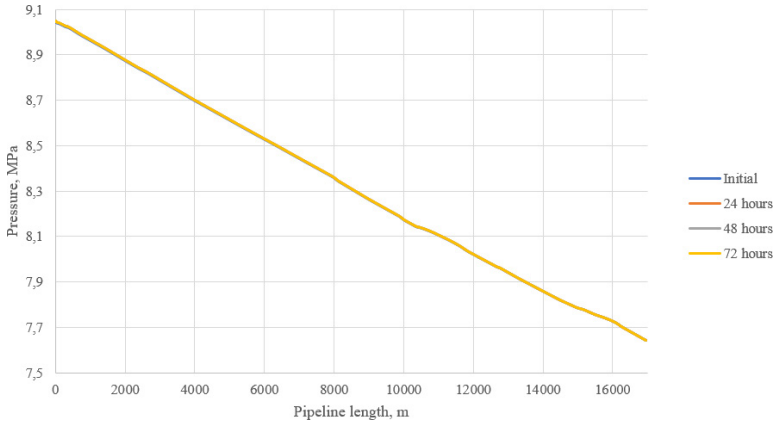

Figure 32 – Modified pressure distribution for the oxy-fuel flow

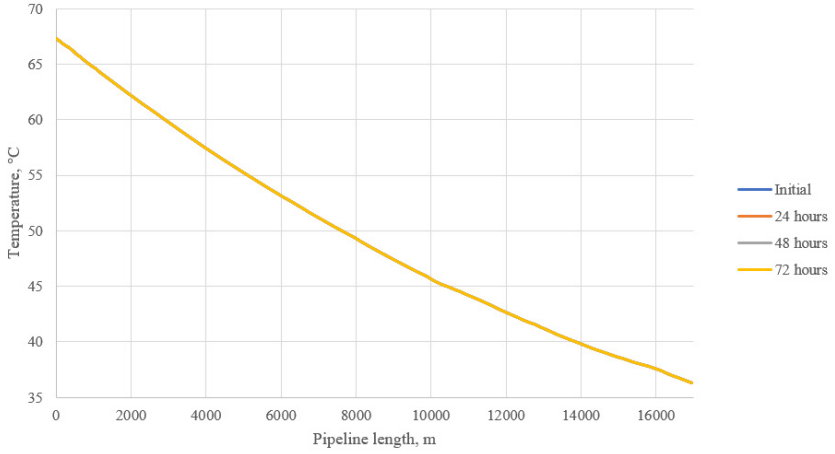

Figure 33 – Modified temperature distribution for the oxy-fuel flow

The required initial pressure increased to 9 MPa, while the temperature remained at the same level. To further assess the strength and stability of the converted pipeline, fluid properties and operating parameters corresponding to the post-combustion stream were applied due to lower initial required parameters and lower contamination at same solution stability level.

In order to investigate the dynamic behavior of the flow, simulations were performed with a gradual increase in the mass flow rate of fluid at the inlet to the system from the initial calculated 18,1 kg/s to 80 kg/s. The real interpretation of this increase is related to a possible build-up of hydrogen production in the region and a corresponding increase in the total volume of captured carbon dioxide. The boundary value of 80 kg/s corresponds to the option at which the recommended pumping rate above 2 m/s is achieved. Figures 34 and 35 depict pressure distribution curves for different flow rates. Temperature distribution is depicted at Figure 36.

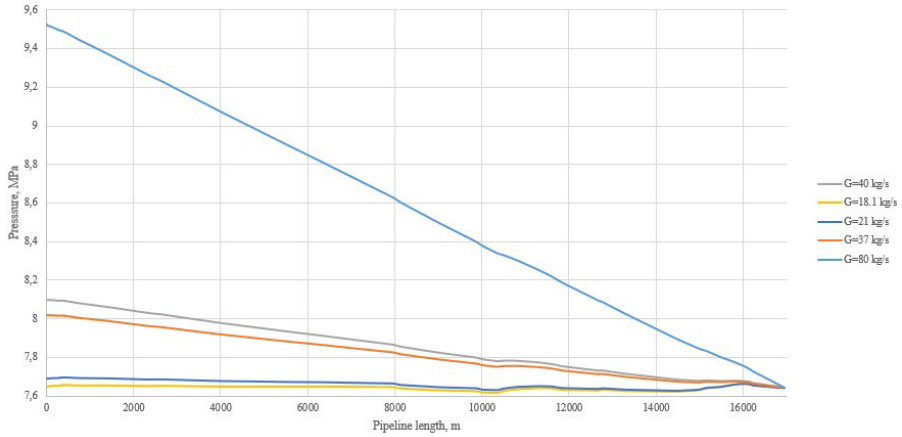

Figure 34 – Pressure distribution curves for various mass flow values (general view)

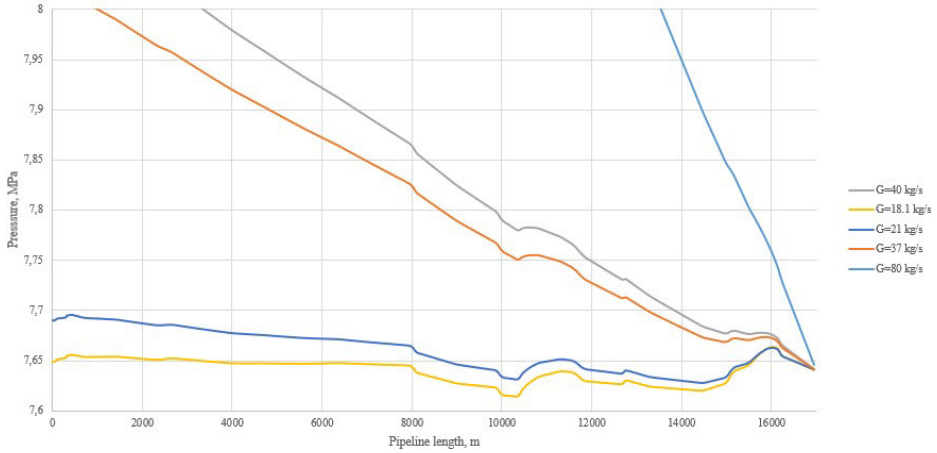

Figure 35 – Pressure distribution curves for various mass flow values (close view)

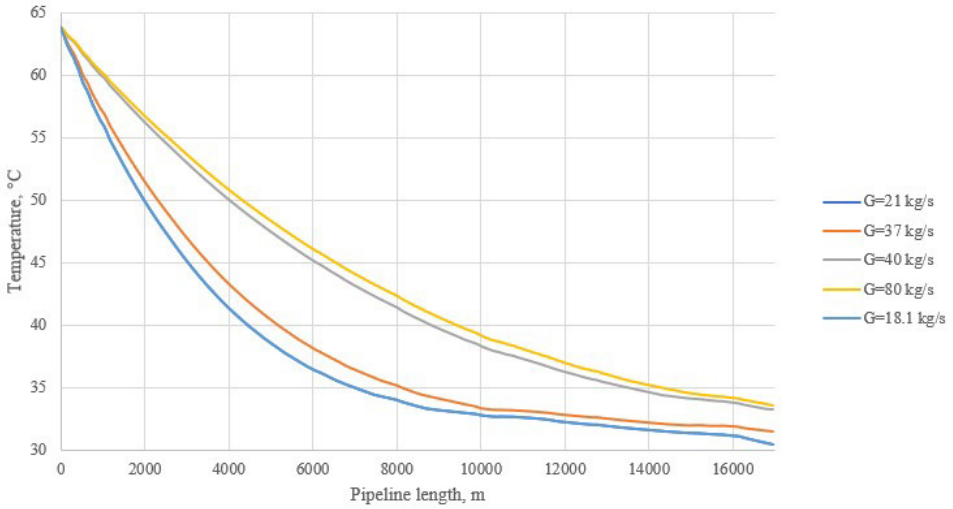

Figure 36 – Temperature distribution curves for various mass flow values

7.1.2 Stress analysis

For the considered OPF-Molikpaq pipeline the following values are obtained with 4.30–4.31:

$$P_{g\,min} = 1001{,}886 \cdot 9{,}81 \cdot (8 - 4/2) \cdot 10^{-6} = 0{,}0589\ MPa;$$

$$K = \left[\frac{\Delta\rho}{\rho \cdot \Delta P}\right]^{-1} = \left[\frac{90{,}713}{398{,}24 \cdot 0{,}099}\right]^{-1} = 0{,}4346\ MPa;$$

$$\Delta P_{gas} = 0{,}542 \cdot \sqrt{\frac{398{,}239 \cdot 2{,}1 \cdot 10^5 \cdot 13{,}5 \cdot 0{,}4346}{2{,}1 \cdot 10^5 \cdot 13{,}5 + 327{,}5 \cdot 0{,}4346}} \cdot 10^{-3} = 0{,}0071303\ MPa.$$

$$\Delta P_{oil} = 0{,}542 \cdot \sqrt{\frac{398{,}239 \cdot 2{,}1 \cdot 10^5 \cdot 11{,}5 \cdot 0{,}4346}{2{,}1 \cdot 10^5 \cdot 11{,}5 + 328{,}5 \cdot 0{,}4346}} \cdot 10^{-3} = 0{,}0071302\ MPa.$$

Thus, two values of inner pressure are calculated for gas and oil pipelines with 4.29:

$$P_{0(gas)} = (9{,}8 - 0{,}0589) = 9{,}741\ \text{MPa};$$

$$P_{0(CO2-gas)} = (7{,}67 - 0{,}0589) + 0{,}0071303 = 7{,}6182303\ \text{MPa};$$

$$P_{0(CO2-oil)} = (7{,}67 - 0{,}0589) + 0{,}0071302 = 7{,}6182302\ \text{MPa};$$

$$P_{0(oil)} = (9{,}1 - 0{,}0589) = 9{,}041\ \text{MPa}.$$

The average water temperature at the bottom in the summer period of 1,5 °C is taken as the ambient construction temperature (Sakhalin Energy, 2002). Results of the stress calculation are presented at Table 14.

Table 14 – Total stress verification

Case	Maximum operated product temperature, °C	Total longitudinal stresses σ_l, MPa	Total circumferential stresses σ_{circ}, MPa	Total equivalent stresses σ_{eq}, MPa
Oil pipeline	45	-70,351	130,898	176,896
Gas pipeline	30	-36,211	118,696	140,349
CO_2 converted oil pipeline	64	-124,410	110,299	203,387
CO_2 converted gas pipeline	64	-129,651	92,829	193,552

The maximum permissible values of the safety factor for operating conditions is 0,77 and 0,9 for the longitudinal and circumferential stresses respectively give the following limiting values:

$$\eta \cdot R_e = 0{,}9 \cdot 485 = 436{,}5 \text{ MPa};$$

$$\eta_u \cdot R_e = 0{,}77 \cdot 485 = 373{,}45 \text{ MPa}.$$

To confirm the assumption that it is impossible to transport pre-combustion flow due to relatively high temperature stresses the same equivalent and longitudinal stresses were evaluated with equations 4.34–4.36 (Table 15).

Table 15 – Total stress verification for the pre-combustion flow

Case	Maximum operated product temperature, °C	Total longitudinal stresses σ_l, MPa	Total circumferential stresses σ_{circ}, MPa	Total equivalent stresses σ_{eq}, MPa
CO_2 converted oil pipeline	167	-383,970	110,299	449,389
CO_2 converted gas pipeline	167	-389,211	92,829	442,982

7.1.3 Stability analysis

The pipeline construction zone considered in this work is characterized by the active movement of water masses in the bottom layers, which contributes to increased sedimentation and erosion of marine soils. Based on local statistics average period of repeatability of earthquakes with the magnitude of M >7,5 for the given region is 30 years (Sakhalin Energy, 2002). That gives the value of E equal to 0,64 if the magnitude of 7,5 is considered critical.

According to the geological and seismic survey, another problem in this area is small-scale gas (Sakhalin Energy, 2002, Geomar, 2002). The continuous movement of gas from gas reservoirs results in a considerable reduction in the capacity of the ground foundation of the pipeline. Active development of new horizons of the oil and gas field increases the possibility of gas output.

Taking into account all these factors, consider the option of partial erosion of the soil under the pipeline. In this investigation, the final segment of the pipeline is being examined in light of its maximum pressure levels along the route and its physical proximity to the platform.

For the given oil and gas pipelines the movement of inertia with 4.41:

$$I_g = \frac{\pi}{64}(0{,}51^4 - 0{,}329^4) = 0{,}002744\ m^4;$$

$$I_o = \frac{\pi}{64}(0{,}51^4 - 0{,}333^4) = 0{,}002716\ m^4.$$

In this study the pipeline section of 100 m is considered. Results of calculation with the equations 4.56–4.64 are presented at Table 16 and Figure 37.

Table 16 – Total pipeline displacement (simplified scheme)

Distance, m	Displacement w, m			
	Gas pipeline	Oil pipeline	CO_2 converted gas pipeline	CO_2 converted oil pipeline
-50	0	0	0	0
-40	-0,0427	-0,0666	-0,0568	-0,0500
-30	-0,1308	-0,2044	-0,1751	-0,1542
-20	-0,2206	-0,3448	-0,2965	-0,2609
-10	-0,2844	-0,4447	-0,3832	-0,3372
0	-0,3073	-0,4806	-0,4144	-0,3646
10	-0,2844	-0,4447	-0,3832	-0,3372

20	-0,2206	-0,3448	-0,2965	-0,2609
30	-0,1308	-0,2044	-0,1751	-0,1542
40	-0,0427	-0,0666	-0,0568	-0,0500
50	0	0	0	0

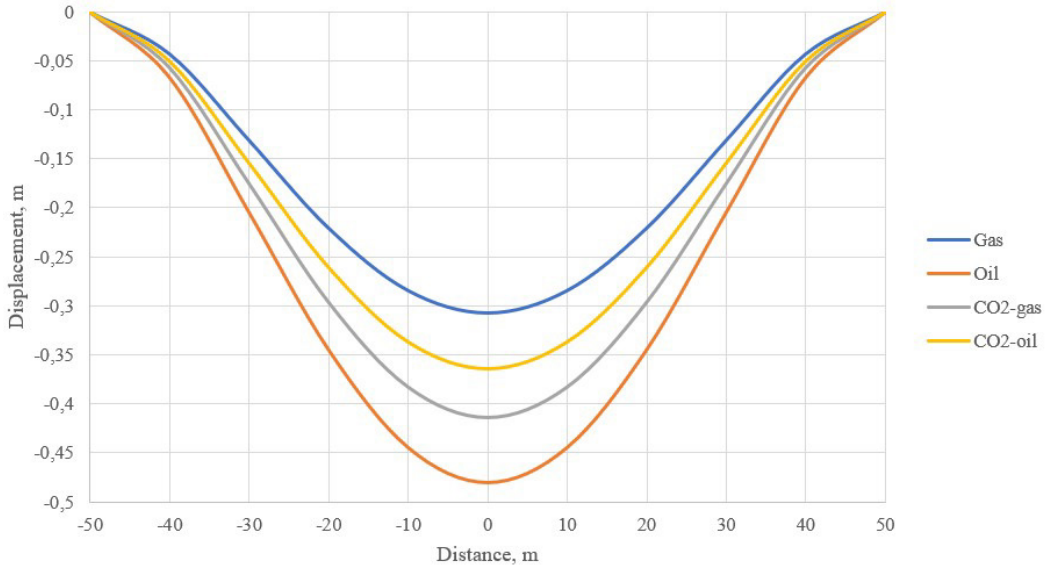

Figure 37 – Total pipeline displacement (simplified scheme)

Assuming $S_{cr} = S_x$ the critical length was defined for all the cases with 4.67 (Table 17).

Table 17 – Critical length

Case	Critical length, m
Gas pipeline	93,517
Oil pipeline	95,405
CO_2 converted gas pipeline	105,747
CO_2 converted oil pipeline	103,933

For the advanced scheme the following results are provided by equations 4.70–4.108. According to Mashtakov et al. the maximum value of reduction coefficient is 30% (Mashtakov A., 2013):

$$C_{y0} = \frac{0{,}12 \cdot 12 \cdot 0{,}7}{1 - 0{,}43\sqrt{100 \cdot 51}}\left[1 - e^{\frac{-2\cdot(100+51/2)}{51}}\right] = 0{,}01719\ MPa/cm.$$

The average temperature of soil of 1,5 °C was considered. Results of calculation for all the cases are presented at Table 18 and Figure 38.

Table 18 – Total pipeline displacement (pipeline-soil interaction)

Distance, m	Displacement w, m			
	Gas pipeline	Oil pipeline	CO_2 converted gas pipeline	CO_2 converted oil pipeline
-50	0	0	0	0
-40	-0,1485	-0,1444	-0,1458	-0,1487
-30	-0,4541	-0,4417	-0,4459	-0,4545
-20	-0,7640	-0,7430	-0,7501	-0,7646
-10	-0,9838	-0,9566	-0,9659	-0,9845
0	-1,0624	-1,0331	-1,0431	-1,0632
10	-0,9838	-0,9566	-0,9659	-0,9845
20	-0,7640	-0,7430	-0,7501	-0,7646
30	-0,4541	-0,4417	-0,4459	-0,4545
40	-0,1485	-0,1444	-0,1458	-0,1487
50	0	0	0	0

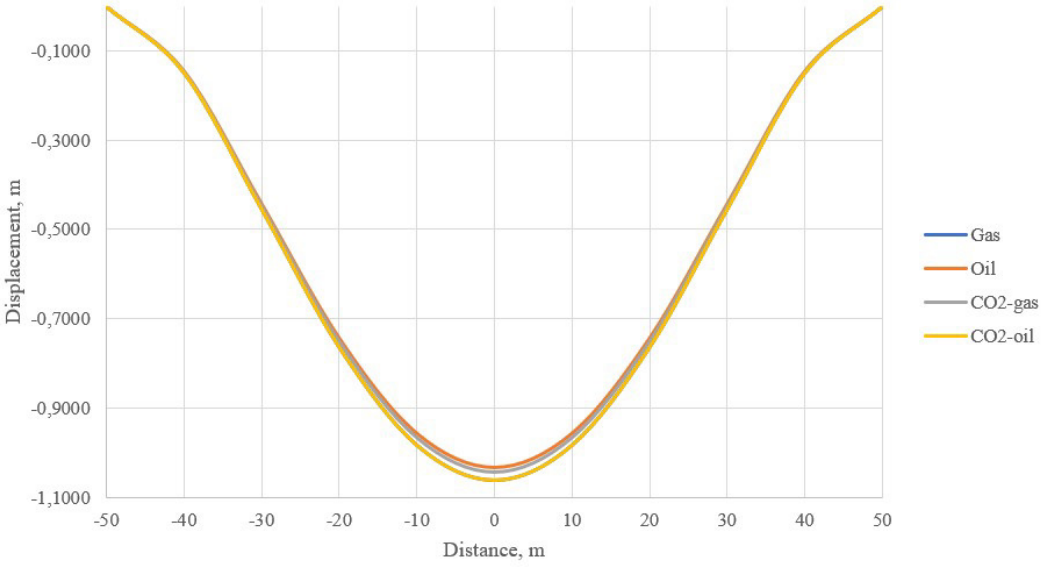

Figure 38 – Total pipeline displacement (advanced scheme)

In addition, the absolute difference in determining the maximum deflection value was estimated using the two schemes considered. Summary information is given in the Table 19.

Table 19 – Comparative analysis of calculation scheme

Case	Results difference, %
Gas pipeline	71,075
Oil pipeline	53,479
CO_2 converted gas pipeline	60,272
CO_2 converted oil pipeline	65,707

7.1.4 Corrosion analysis

Comparative analysis for both normal operation and case of pipeline temperature and pressure decrease to 6 MPa and 20 °C modelling emergency depressurization was provided (Figure 39).

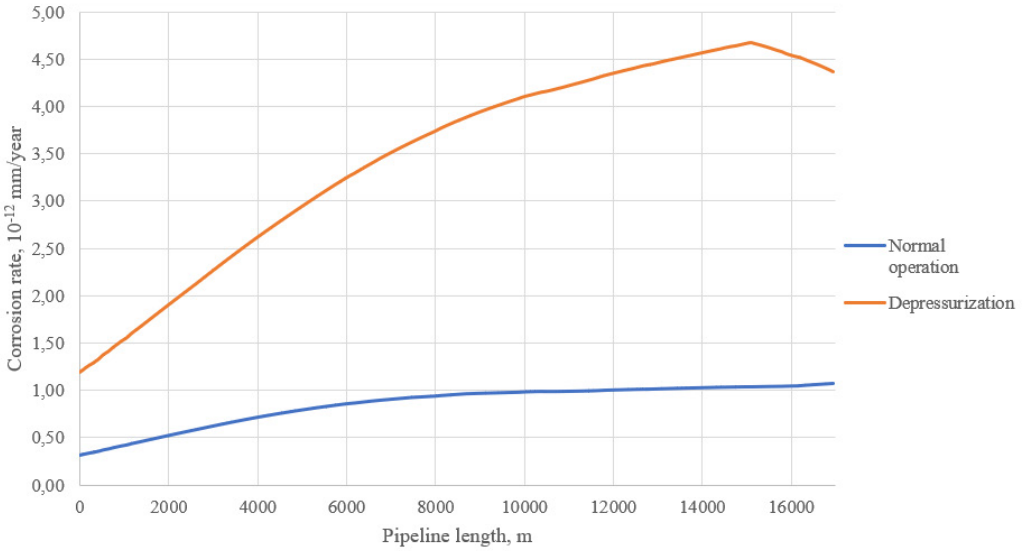

Figure 39 – Corrosion rate calculation

7.1.5 Peculiarities of oil pipeline conversion

The conversion of a pipeline pumping oil to carbon dioxide in a supercritical state, unlike a gas pipeline, has a distinctive feature. It consists in the ability of CO_2 to dissolve asphaltene-resin-wax deposits on the wall.

The pipeline «Molikpaq-OPF» pumps oil with an average wax content of 1.2%. At the design temperature values, this leads to the gradual deposition of hydrocarbons on the walls, significantly increasing the hydraulic resistance. According to the analysis of the results of in-line diagnostics and cleaning of pipelines with scrapers, it was found that the average thickness of the paraffin layer along the pipeline route is 5 mm (Kosyak, D. et al., 2011). To combat this

phenomenon, the Nalco FX2407 inhibitor is regularly injected, which allowed increasing the effective protection against deposits by 70-80%.

In the case of replacing oil with carbon dioxide in the liquid phase, preliminary cleaning of the inner cavity of the pipe will be required, because otherwise irregularities can cause excessive pressure pulsations and a general decrease in throughput. In the case of SCF of CO_2, the fluid itself will perform the function of a solvent due to its ability to penetrate, which will greatly decrease the expenses involved in the project.

Currently, there is a deficiency in recognized approaches for determining the efficacy of the solvent in question, thereby precluding any prior estimations. To accurately predict the interaction of substances, an experimental base is needed, obtained by conducting a series of experiments at different values of diameters, product flow rates, thermobaric parameters and configurations of the geometry of the pipeline route.

7.2 Discussion Section

Results of preliminary calculation assured the fact that no significant erosion is to be occurred in the considered pipeline system due to the level of resulting velocities being much lower than the maximum allowed (Tables 8,9). However, these values of velocities are also far away from the average used of 2,0 m/s, so the flow may be unstable under certain circumstances. And this can manifest itself in pressure surges in areas of complex geometry and where the route rises considerably. In such a case it must be ensured that the full cross-section of the pipeline is being pumped. The solution is to increase the liquid flow rate, which provides a stable flow pattern in the pipeline

The heat transfer was calculated taking into account the properties of seawater throughout the depth, but the variation in the external heat transfer coefficient is negligible, allowing an average value to be applied. It is noteworthy that the internal heat transfer coefficient from the liquid to the pipe wall exhibits significant variability along the entire length, contingent upon the altitude profile (Table 11). This is how the range of values relates to both forced liquid and gas flow processes. Thermodynamic analysis indicated that the Nu criteria curve aspires to its maximum at approximately 13450 m of the pipeline (Figure 21). The aforementioned phenomenon can be elucidated by reference to the descending terrain, which causes a predominance of the downward current, thereby leading to a substantial enhancement in the transfer of heat. In general, the question of precisely defining characteristic equations to describe the flow of supercritical carbon dioxide in a complex geometry with alternating descending and ascending sections is relevant. Despite this, however, the overall heat transfer

coefficient varies slightly from 3,0224 W/m·K to 3,1229 W/m·K (Table 12). This is due to the considerable thermal insulation of the system.

According to the received schedules of changes of the technological analysis with two models, the following conclusions can be drawn. The steady-state solution showed a significant difference in the pressure and temperature profiles: thus, the values for oxy-fuel and post-combustion are approximately equal, but the curves for pre-combustion are significantly higher, which is due to the large amount of impurities in the fluid (Figures 22-31). The variability of oxy-fuel flow is most prominent in the solution, with the most significant changes occurring around the 72-hour mark of the simulation. At this juncture, there is a significant decrease in the pressure within the pipeline throughout its entirety, and the temperature curve exhibits wave-like behavior where the route encounters localized elevation. In the second scenario, a reduction in the operational temperature below the critical threshold results in the emergence of a liquid phase. Regarding the flow after combustion, pressure irregularities were observed, particularly in the pipeline routes located at shallower depths. The pre-combustion one turned out to be the most stable flow, probably due to the comparatively high temperature values. The removal of instability through an elevation in mass flow has induced a distinctive shift in the distribution of pressure and temperature along the length, specifically a consistent reduction in values. This particular trend contrasts significantly with the curves that were previously obtained. With an increased flow rate, absolute stability is shown for 72 hours, which is shown on the graph in the complete overlap of lines (Figures 32-33).

Taking into account all the technological data obtained, the following points should be noted. Out of three distinct streams, the most efficient option for utilization would be post-combustion. The pre-combustion flow necessitates exceedingly elevated temperatures, which the current pipelines were not initially intended to endure. The Oxy-fuel alternative is the most unstable option, as minor adjustments to its operating parameters can result in modifications to the pipeline's flow pattern. After selecting the priority flow, a dynamic analysis with a change in mass flow value showed that increasing this value significantly changes the character of the pressure curve along the pipeline route. Consequently, a gradual diminishing in curvature can be observed as the flow rate reaches 80 kg/s, ultimately resulting in a near-linear profile. (Figures 34,35). Thus, the dynamic component of the forced movement far exceeds the potential components caused by altitude. The temperature curves have the same character, but with larger values, respectively (Figure 36).

Apart from the technological analysis, the solid mechanics test indicated that all the considered pipelines passed the strength verification with significant safety zone (Table 14). When considering a subsea pipeline, the impact of gravitational and Archimedean forces on the fluid

flow within the pipe represents a crucial aspect of the calculations, particularly with regards to supercritical fluids that exhibit dual-phase behavior. It can be stated, that taking into account the maximum corrosion effect and thinning of the pipeline wall over 30 years of operation at the specified pumping parameters, the current and converted pipelines are not subjected to critical damage from internal and external loads showing significant strength margin. It was found that in the case of gas pipeline conversion, total equivalent stresses decrease by 37,91%, while replacing oil with carbon dioxide reduces this parameter by 14,98%.

The stress-strain state was calculated when the soil was eroded under the pipeline using a simplified model (Table 16). It was found that in the case of gas pipeline conversion, the deflection increases by an average of 34,09%, while replacing oil with carbon dioxide reduces this parameter by an average of 24,34% along the length of the section. Converted pipelines also show better stability in case of ground erosion processes (Figure 37). Since the obtained values of critical lengths for oil and gas are less than the 100 m long section under consideration, in these cases a loss of stability will occur. However, for converted pipelines this risk does not exist due to the difference in product weight and internal pressure values (Table 17).

The derived expression used for the advanced scheme is a modified version of the deflection equation of a beam on an elastic Winkler base, considered by Korobkov, G. et al. The difference lies in the calculation of the reaction of the soil, taking into account the change in its bearing capacity, which is used in the analytical solution by Lapteva, T. The difference in the form of the final expression is due to the solution method. In the named work, the decomposition of the differential equation into a Fourier series using harmonics is used, while in this work, the direct solution of the differential equation is considered.

The evidence implies that there has been an increase in deflection due to the additional weight of the ground filling above the pipeline (Table 18). In addition, the order of increasing the maximum deflection among the considered cases has changed. So, the maximum deflection when calculating according to this model is at the converted oil pipeline, then at the gas pipeline itself (Figure 38). The minimum value in this case is for the oil pipeline.

This means that if the product is replaced from gas to CO_2, the deflection will decrease, and when oil is converted to CO_2, the deflection will increase. Nevertheless, in this particular instance, the contrast is significantly diminished: 1,82% for gas and 2,91% for oil (Table 19). The values described above may be attributed to the sophisticated calculation methodology that takes the elastic base into consideration. This scheme reveals that the component responsible for the impact of the soil on the pipeline is several times more substantial than the impact of the pipeline and the product contained therein. In addition, the backfill layer exceeds. The presented summary strongly indicates that the consideration of the simultaneous interaction

between the pipeline and the soil results in significant occurrences of deflection values. Hence, it is imperative to account for the volumetric stress state not only of the rod but also of the surroundings.

Corrosion analysis results confirmed that in the case of the transition of the working point from the supercritical zone to the gas zone, the corrosion rate in the pipeline increases sharply by an average of 75,14%. Notwithstanding the aforementioned scenario, it is imperative to note that the data derived from the experiment indicate values that are considerably inferior to the projected corrosion rates of 0,033 and 0,1 mm/year for the gas and oil pipelines, respectively. Consequently, various types of corrosion are not a significant hazard when repurposing existing pipelines with the use of products of the considered composition.

An environmental assessment has shown that a spill can affect the surrounding water masses by changing the balance of hydrogen and oxygen ions. The rate of propagation in such an instance is positively correlated with the governing operational factors of the pipeline and the velocity of subaqueous flow (Figure 16). However, as the average burial below the fill is 1 m, instantaneous release of carbon dioxide into the water is difficult. Even in the case of contamination, regeneration of the biological balance takes a short time. It is worth noting that the flow considered consists of 99,8% carbon dioxide, which reduces its contamination, but in the case of pumping a more contaminated product with sulphur and heavy metal admixtures the system must be operated with extreme care to minimize the possibility of even the smallest reductions.

Based on a comprehensive evaluation algorithm that incorporates technical, environmental, and strategic considerations, specifically demonstrated by a project analysis in the Sakhalin Region, it has been determined that the project is deemed practicable across all criteria with the exception of its economic assessment (Figure 18). The latter is explained by the fact that at the moment the corresponding calculation method is not presented. It can be concluded that pipeline conversion is potentially feasible for both oil and gas.

Chapter 8

Conclusion

8.1 Summary

The primary aim of this study was to evaluate the practicality or achievability of repurposing offshore pipelines for conveying supercritical carbon dioxide, as part of the broader initiative towards decarbonization. For this purpose, a set of calculations and estimates was carried out: from determining the properties of fluids obtained by trapping from a hydrogen production plant, to calculations of strength loads and deflections of pipeline spans during soil destruction. The global result was the development of a refined algorithm for reprofiling the system with two important criteria: technical feasibility and safety of the operation, as well as strategic and economic feasibility.

Using the named algorithm, specific offshore pipelines on Sakhalin Island were considered. The results showed the technical safety of re-equipment: the replacement of transported raw materials will reduce the pressure in the system, reduce the corrosive effect, and also avoid destruction and loss of stability even with significant subsidence of the soil, which is critical for the original oil and gas pipelines. The environmental assessment showed complete safety for the environment even in case of emergency situations in the form of leaks. Following the criteria of the algorithm, the primary possibility of implementing the project is determined, while full approval is possible after an economic calculation that was not included in the scope of this work. In the future, it is recommended to use the data obtained for calculations of similar projects, which will greatly simplify and speed up the work.

8.2 Evaluation

Within the framework of these objectives, it can be indicated that the study has been carried out in its entirety, from the definition of raw material baselines to the strategic analysis. Moreover, it is advisable to assess the requisite expenditures to attain complete adherence to the formulated algorithm.

8.3 Future Work

The principal constraint of the investigation is the deficiency of tangible empirical foundations attained through experimental assessments. Difficulties in organizing experiments are related both to the risks of supercritical carbon dioxide operations and to the lack of access to blower units capable of providing the necessary operating flow point. The scale-up experiments are therefore a logical extension of the pipeline repurposing study.

Furthermore, the present study delineates prospective domains that warrant thorough investigation within this particular topic. This mainly relates to the study of the effects of supercritical carbon dioxide on high-molecular-weight formations in the form of paraffins and asphaltenes on the walls of the pipelines in question. A detailed consideration and evaluation of the solubility of this substance is of practical interest. At the moment, there is no publicly available information about the studies carried out in this direction.

References

Adams, R., Miller, H. (Ed.) (2014). *A tutorial.*

Afanasiev, V. (2021). Gazprom and Rosatom announce Blue Hydrogen Project for Sakhalin. *Upstream News*. https://www.upstreamonline.com/energy-transition/gazprom-and-rosatom-announce-blue-hydrogen-project-for-sakhalin/2-1-1063311

Akhtyamov, A., Zaripov, R. (2015). Mathematical modelling of the stress-strain state of an offshore pipeline. https://www.elibrary.ru/

Aminu, M. D., Nabavi, S. A., Rochelle, C. A., & Manovic, V [Vasilije] (2017). A review of developments in carbon dioxide storage. *Applied Energy*, *208*, 1389–1419. https://doi.org/10.1016/j.apenergy.2017.09.015

Anderson, M. (Ed.) (2011). *Pressure drop & critical flow of SCF*. ICTP-IAEA. https://indico.ictp.it/event/a10196/session/21/contribution/15/material/0/0.pdf

Andre, L. e. a. (2007). Control of supercririca CO2 injectivity in the deep Dogger aquifer of the Paris basin from different injection scenarios.

ASPEN HYSYS. (2023). *Multiphase Pipe Flow Modeling in ASPEN HYSYS*. https://www.aspentech.com/en/resources/white-papers/multiphase-pipe-flow-modeling-in-aspen-hysys

Auerbach, D. I., Caulfield, J. A., Adams, E. E., & Herzog, H. J. (1997). Environmental Modeling and Assessment. *Environmental Modeling and Assessment*, *2*(4), 333–343. https://doi.org/10.1023/a:1019029931755

Aybinder, A. (1988). *Calculation of main pipelines for strength and stability*. Nedra.

Aybinder, A. (1991). *Calculation of main and field pipelines for strength and stability*. Nedra.

Bachu, S. (1970). *Carbon dioxide sequestration in salt caverns : Capacity and Long Term Fate, Carbon Dioxide Sequestration in Salt Caverns : Capacity and Long Term Fate*. https://www.semanticscholar.org/paper/Carbon-Dioxide-Sequestration-in-Salt-Caverns-%3A-and-Bachu/04fd6f7a72e06d7c0b2c2be5ae24f2d118549874

Bachu, S., & SHAW, J. CO2 storage in oil and gas reservoirs in western CanadaEffect of aquifers, potential for CO2-flood enhanced oil recovery and practical capacity. In https://doi.org/10.1016/b978-008044704-9/50037-9

Barbir, F., Basile, A. and Veziroğlu T. Nejat. (2016). *Compendium of hydrogen energyn3*. *Woodhead publishing series in energy: Vol. 85*. Elsevier, Woodhead.

Bielinski, A., Kopp, A., Schutt, H., & Class, H. (2008). Monitoring of CO2 plumes during storage in geological formations using temperature signals: Numerical investigation. *International Journal of Greenhouse Gas Control*, *2*(3), 319–328. https://doi.org/10.1016/j.ijggc.2008.02.008

Bloomberg. (2020). *Hydrogen Economy Outlook [*Press release]. https://data.bloomberglp.com/professional/sites/24/BNEF-Hydrogen-Economy-Outlook-Key-Messages-30-Mar-2020.pdf

Borodavkin, P. (1982). *Underground trunk pipelines (design and construction)*. http://elib.gubkin.ru/en/content/13578

Borodavkin, P. and Sinuykov, A. (2002). *Strength of main pipelines.* https://search.rsl.ru/ru/record/01001193784

Borodkin, S. V., Bataronov, I. L., Ivanov, A. V., & Ryazhskikh, V. I. (2021). One-Dimensional Model of Heat and Mass Transfer in Closed-Type Cryogenic Gasifiers. *Journal of Siberian Federal University. Engineering & Technologies*, 714–730. https://doi.org/10.17516/1999-494X-0315

Busch, A., Alles, S., Gensterblum, Y., Prinz, D., Dewhurst, D. N., Raven, M. D., Stanjek, H., & Krooss, B. M. (2008). Carbon dioxide storage potential of shales. *International Journal of Greenhouse Gas Control*, *2*(3), 297–308. https://doi.org/10.1016/j.ijggc.2008.03.003

Caulfield, J. A., Adams, E. E., Auerbach, D. I., & Herzog, H. J. (1997). Environmental Modeling and Assessment. *Environmental Modeling and Assessment*, *2*(4), 345–353. https://doi.org/10.1023/a:1019081915826

(2013). *Code of Practice 36.13330.2012 Trunk pipelines*. https://docs.cntd.ru/document/1200103173

Davletbaev, A. and Ilyaeva, M. (Ed.) (2021). *Analysis of carbon dioxide utilisation potential in the Sakhalin Oblast*.

Davletbaev, A. and Ilyaeva, M. (Ed.) (2022). *Justification for the choice of equation of state for modelling the carbon dioxide transport process with impurities*.

Derkatszayan, A., Shpotakvskiy, M. and Volkov, B. (2011). *Handbook for the design of trunk pipelines*. Nedra. https://search.rsl.ru/ru/record/01007722991

(2017). *Design and operation of carbon dioxide pipelines*. DNV. https://www.dnv.com/oilgas/download/dnv-rp-f104-design-and-operation-of-carbon-dioxide-pipelines.html

Dmitrievski, A. e. a. (2016). Sokrashhenie obemov bufernogo gaza pri sozdanii gazohranilishh v mestorozhdenijah uglekislogo gaza. https://www.elibrary.ru/

DNV (2007). *Submarine Pipeline Systems*. Det norske Veritas. Høvik.

Dorokhin, V. (2017a). *Metodika ispol'zovanija uglekislogo gaza v razlichnyh agregatnyh sostojanijah na podzemnyh hranilishhah gaza*. https://vniigaz.gazprom.ru/d/textpage/43/67/avtoreferat_dorokhinvg.pdf

Dorokhin, V. (2017b). *Opyt "Gaz de Frans" po zameshheniju chasti bufernogo gaza PHG vyhlopnymi gazami*. https://vniigaz.gazprom.ru/d/textpage/fb/251/dissertatsiya_dorokhinvg.pdf

Dunn, R. J. H., Aldred, F., Gobron, N., Miller, J. B., Willett, K. M., Ades, M., Adler, R., Allan, R. P., Allan, R., Anderson, J., Argüez, A., Arosio, C., Augustine, J. A., Azorin-Molina, C., Barichivich, J., Beck, H. E., Becker, A., Bellouin, N., Benedetti, A., . . . Zotta, R. M. (2021). Global Climate. *Bulletin of the American Meteorological Society*, *102*(8), S11-S142. https://doi.org/10.1175/bams-d-21-0098.1

Fang, X., Xu, Y., Su, X., & Shi, R. (2012). Pressure drop and friction factor correlations of supercritical flow. *Nuclear Engineering and Design*, *242*, 323–330. https://doi.org/10.1016/j.nucengdes.2011.10.041

Gaythwaite, J. (1981). *The Marine Environment and Structural Design. New York.* Van Nostrand Reinhold Co.

GEOMAR. (2002). *Geomar Helmholtz Zentrum für Ozeanforschung Kiel - Geomar - Helmholtz-Zentrum für Ozeanforschung Kiel*. https://www.geomar.de/

The Government of the Russian Federation (Ed.). *Koncepcija razvitija vodorodnoj jenergetiki v Rossijskoj Federacii*. The Government of the Russian Federation.

Gupta, R. B. (2009). *Hydrogen fuel: Production, transport, and storage*. CRC Press.

Harrison, S. (2016). GCE moles, formulae and equations edexcel advanced GCE in Chemistry (9080) edexcel advanced GCE in Chemistry. https://www.academia.edu/28209847/GCE_Moles_Formulae_and_Equations_Edexcel_Advanced_GCE_in_Chemistry_9080_Edexcel_Advanced_GCE_in_Chemistry_Nuffield_9086

Hendriks, C., Graus, W. and Van Bergen, F. (2004). Global carbon dioxide storage potential and costs. https://inis.iaea.org/search/search.aspx?orig_q=RN%3A35053050

Hickem, T. and Siew, S. (2019). Carbon capture utilisation and storage. https://www.researchgate.net/publication/337621313_Carbon_Capture_Utilisation_and_Storage

HighExpert.RU. (2020). *Physical properties of seawater, Physical properties of seawater*. https://www.highexpert.ru/content/liquids/seawater.html

Howarth, R. W., & Jacobson, M. Z. (2021). How green is blue hydrogen? *Energy Science & Engineering*, *9*(10), 1676–1687. https://doi.org/10.1002/ese3.956

Huang, H. P., Shi, Y., Li, W., & Chang, S. G. (2001). Dual Alkali Approaches for the Capture and Separation of CO 2. *Energy & Fuels*, *15*(2), 263–268. https://doi.org/10.1021/ef0002400

Ilgamov, M. (1994). Static hydroelasticity problems. Institute of Mechanics and Mechanical Engineering, Russian Academy of Science.

Isaev, G. (2006). Convective Heat Exchange in Downward Moving Liquid under Conditions of Over-Critical Pressures. *ENERGETIKA*. https://energy.bntu.by/jour/article/view/674/668

Isaev, G. (2009). Heat transfer in supercritical fluid flow in a horizontal pipe. *Education and Science*. http://www.rusnauka.com/1_NIO_2012/Tecnic/5_98196.doc.html

Ji, H., Xu, M., Huang, W., & Yang, K. (2020). The Influence of Oil leaking rate and Ocean Current Velocity on the Migration and Diffusion of Underwater Oil Spill. *Scientific Reports*, *10*(1), 9226. https://doi.org/10.1038/s41598-020-66046-1

Joint Communication to the European Parliament and the Council the EU.

Kang, K., Huh, C., Kang, S.-G., Baek, J.-H., & Noh, H. J. (2014). Estimation of CO2 Pipeline Transport Cost in South Korea Based on the Scenarios. *Energy Procedia*, *63*, 2475–2480. https://doi.org/10.1016/j.egypro.2014.11.270

Khabibullin, P. (2001). Influence of the temperature factor on the operational reliability of pipelines in weakly bearing soils.

Khan, S. and Garajshin, A. (2016). Issledovanie vozmozhnosti chastichnogo zameshhenija bufernogo obema gaza na dioksid ugleroda na PHG. https://www.elibrary.ru/

Khan, S., Dorokhin, V. and Bondarenko, N. (2016). Ispol'zovanie osobennostej agregatnyh sostojanij dvuokisi ugleroda dlja zameshhenija chasti bufernogo ob#ema podzemnyh hranilishh gaz. https://www.elibrary.ru/item.asp?id=27252693

Khan, S., Dorokhin, V. and Khvostova, V. (2015). Disposal method of CO2 (options)(RU2583029C1). https://patents.google.com/patent/RU2583029C1/ru

Knoope, M., Ramírez, A., & Faaij, A. (2013a). Economic Optimization of CO2 Pipeline Configurations. *Energy Procedia*, *37*, 3105–3112. https://doi.org/10.1016/j.egypro.2013.06.196

Knoope, M., Ramírez, A., & Faaij, A. (2013b). A state-of-the-art review of techno-economic models predicting the costs of CO2 pipeline transport. *International Journal of Greenhouse Gas Control*, *16*, 241–270. https://doi.org/10.1016/j.ijggc.2013.01.005

Koblikov, V. (1982). Composition and quantitative distribution of macrobenthos on the Sakhalin shelf in the Sea of Okhotsk. *Izvestia of the Primorsky Federal District*, *106*, 90–96.

Korobkov, G., Zaripov, R. and Shammazov, I. (2009). *Numerical modelling of the stress-strain state and stability of pipelines and tanks under difficult operating conditions*. Nedra.

Kosowski, P., & Kuk, M. (2016). Cost analysis of geological sequestration of CO_2. *AGH Drilling, Oil, Gas*, *33*(1), 105. https://doi.org/10.7494/drill.2016.33.1.105

Kosyak, D. and Markin, A. (2011). Control of wax deposition in subsea pipelinesof Sakhalin-II project. *Territoriya Neftegaz*, *5*, 78–86.

KSB (2021). KSB CO2 capture report. *Sphere Oil and Gas*, *4*(1). https://xn--80aaigboe2bzaiqsf7i.xn--p1ai/

Kurganov, V. (2006). Heat transfer in pipes at supercritical pressures coolant: some results of scientific research: Institute of High Temperatures. http://rnhtc.ru/year/2006/lib/1-74.pdf

Kusakin, O., Sobolevskiy, Y. and Blockhin, S. (2001). Overview of a benthic survey on the north-eastern Sakhalin shelf.

Lapteva, T. (2019). *Developing methods to ensure the operability of offshore oil and gas pipelines in the challenging engineering and geological conditions of the Arctic shelf*. https://vniigaz.gazprom.ru/d/textpage/3a/570/1-tekst-avtoreferata.pdf

Li, H., & Yan, J [J.] (2009). Impacts of equations of state (EOS) and impurities on the volume calculation of CO2 mixtures in the applications of CO2 capture and storage (CCS) processes. *Applied Energy*, *86*(12), 2760–2770. https://doi.org/10.1016/j.apenergy.2009.04.013

Markin, A., Kalashnikov, V. and Sukhoverkhov, S. (2011). Protection of multiphase pipelines of the Sakhalin-2 project with a corrosion inhibitor. *Territorija Neftegaz*(12). https://neftegas.info/tng/vypusk-12-2011-g/

Mashtakov, A. (2013). Evaluation of integrated influence on bearing resistance of heat cycling and shallow free gas. *International Scientific Journal for Alternative Energy and Ecology (ISJAEE)*. https://ruslan.library.spbstu.ru/pwb/detail?db=ANALITS2005&id=RU%5CSPSTU%5Canalits2005%5C396142

Mazzoccoli M., e. a. (2013). CO2-mixture properties for pipeline transportation in the CCS Process, CO2-mixture Properties for Pipeline Transportation. *Chemical Engineering Transactions*, *32*(1). https://www.semanticscholar.org/paper/CO2-mixture-Properties-for-Pipeline-Transportation-Cal-Tran/8e4ebe28cbe5364ae84eeb7f4aee36de52febcd1

McCollum, D.L. and Ogden, J.M. (2010). Techno-economic models for carbon dioxide compression, transport, and storage & correlations for estimating carbon dioxide density and viscosity. *EScholarship*. https://escholarship.org/uc/item/1zg00532

McGillivray, A., Saw, J. L., Lisbona, D., Wardman, M., & Bilio, M. (2014). A risk assessment methodology for high pressure CO2 pipelines using integral consequence modelling. *Process Safety and Environmental Protection*, *92*(1), 17–26. https://doi.org/10.1016/j.psep.2013.09.002

Mikhailovskij, A., Khan, S. and Isaeva, N. (2014). Sovershenstvovanie tehnologij chastichnoj zameny bufernogo metanovogo gaza PHG neuglevodorodnymi gazami. https://www.elibrary.ru/item.asp?id=21183775

Molchanova, R., Telyasheva, G. and Novoselov, I. (2009). *Zadachnik po teplotehnike. Chast' II. Teploobmen.*

Nadein, V., Putilov, M. and Kuzmin, Y. (2010). Opyt reshenija geodinamicheskih problem sahalinskih neftegazovyh proektov. https://www.elibrary.ru/item.asp?id=21771164

NCEI (Ed.). *Annual 2019 Global Climate Report: NCEI.Monitoring.Info@noaa.gov*. National Centers for Environmental Information (NCEI).

NORSOK (2006). *P-001 Process Design* (5). NORSOK. https://www.standard.no/en/sectors/energi-og-klima/petroleum/norsok-standard-categories/p-process/p-0012/

(2016). *№ 2-020301-004 Rules classification and construction of sea submarine pipelines*.

Onyebuchi, V. E., Kolios, A., Hanak, D. P., Biliyok, C., & Manovic, V [V.] (2018). A systematic review of key challenges of CO2 transport via pipelines. *Renewable and Sustainable Energy Reviews*, *81*, 2563–2583. https://doi.org/10.1016/j.rser.2017.06.064

(2000a). *Seabed intervention works, engineering geology, geotechnical surveys, crossings in Piltun-Astokh area.: H00027/05.* Pacific Engineering Company (PECO).

(2000b). *Seabed intervention works, engineering geology, geotechnical surveys, PA-B to PA-A pipeline route in Piltun-Astokh area: H00027/04.* Pacific Engineering Company (PECO).

Parker, N. (1970). Using Natural Gas Transmission Pipeline Costs to Estimate Hydrogen Pipeline Costs.

Peletiri, P.S., Rahmanian, N. and Mujtaba, I.M. (2017). Effect of Impurities on CO2 Pipeline Perfomance. *Directory of Open Access Journals, Chemical Engineering Transactions*. https://doaj.org/article/19dc39a515c746c89bccda213127d8d5

Protopopov, V. (1977). Generalised dependencies for local heat transfer coefficients for turbulent flow of water and supercritical carbon dioxide in uniformly heated circular pipes. *High Temperature*. http://energy.ihed.ras.ru/arhive/article/7146

Riding, J. B., & Rochelle, C. A. (2009). Subsurface characterization and geological monitoring of the CO 2 injection operation at Weyburn, Saskatchewan, Canada.

Geological Society, London, Special Publications, *313*(1), 227–256. https://doi.org/10.1144/sp313.14

Sabirzyanov, A. (2002). Water solubility in supercritical carbon dioxide. *High Temperature*. http://energy.ihed.ras.ru/arhive/article/1770

Safonov, M. and Lisichkin, G. (1970). Mozhno li umen'shit' koncentraciju uglekislogo gaza v atmosfere. https://www.semanticscholar.org/paperBD/6c0643c13a21f6e9a1c004232f02183dbd95e95a

Sakhalin Energy. (2023). *Sakhalin Energy assets*. https://www.sakhalinenergy.ru/en/company/assets/

(2002a). *TEOC, Chapter 1: 2002a, Volume 7* (Book 1-EIA). Sakhalin Energy investment company ltd. http://www.sakhalinenergy.ru/en/

(2002b). *TEOC, Chapter 5: 2002a, Volume 2B.* Sakhalin Energy investment company ltd. http://www.sakhalinenergy.ru/en/

(2010). *3D seismic survey programme environmental impact assessment on the Piltun-Astokhskoye field.* Sakhalin Energy investment company ltd. https://www.sakhalinenergy.ru/en/

Savin, V. e. a. (2021). *Prospects for hydrogen production on Sakhalin Island*. Moscow. KPMG.

Shogenova, A., Sliaupa, S., Vaher, R., Shogenov, K., & Pomeranceva, R. (2009). The Baltic Basin: structure, properties of reservoir rocks, and capacity for geological storage of CO 2. *Estonian Journal of Earth Sciences*, *58*(4), 259. https://doi.org/10.3176/earth.2009.4.04

SNiP (1997). *2.05.06-85 Main pipelines*. Moscow. Ministry of Oil and Gas Construction.

Stevens, S. H., Spector, D., & Riemer, P. Enhanced Coalbed Methane Recovery Using CO2 Injection: Worldwide Resource and CO2 Sequestration Potential. In https://doi.org/10.2118/48881-ms

van der Meer, B. (2005). Carbon Dioxide Storage in Natural Gas Reservoir. *Oil & Gas Science and Technology*, *60*(3), 527–536. https://doi.org/10.2516/ogst:2005035

Vitse, F., Nešić, S., Gunaltun, Y., Torreben, D. L. de, & Duchet-Suchaux, P. (2003). Mechanistic Model for the Prediction of Top-of-the-Line Corrosion Risk. *CORROSION*, *59*(12), 1075–1084. https://doi.org/10.5006/1.3277527

Volmir, A. (1963). Stability of elastic systems. https://pnu.edu.ru/media/filer_public/2013/04/10/4-7_volmir_1967.pdf

Wei, L., Zhang, Y., Pang, X., & Gao, K. (2015). Corrosion behaviors of steels under supercritical CO2 conditions. *Corrosion Reviews*, *33*(3-4), 151–174. https://doi.org/10.1515/corrrev-2014-0067

White, V., Wright, A., Tappe, S., & Yan, J [Jinying] (2013). The Air Products Vattenfall Oxyfuel CO2 Compression and Purification Pilot Plant at Schwarze Pumpe. *Energy Procedia*, *37*, 1490–1499. https://doi.org/10.1016/j.egypro.2013.06.024

Wintershall DEA. (2021). *Wintershall DEA investigates conversion of North Sea natural gas pipelines for CO2 transport* [Press release]. https://wintershalldea.com/sites/default/files/media/files/210930_PI_Erdgas%20Pipelines_EN.pdf

Yasin, E. (1967). *Stability of underground pipelines*. Nedra. https://www.geokniga.org/books/11426

Zhao, Q., & Li, Y.-X. (2014). The influence of impurities on the transportation safety of an anthropogenic CO2 pipeline. *Process Safety and Environmental Protection*, *92*(1), 80–92. https://doi.org/10.1016/j.psep.2013.10.007

Zinnatullin, A. e. a. (2007). Summary of mathematical models used to calculate the rates of carbon dioxide corrosion. https://www.elibrary.ru/

Appendix A

Sakhalin Infrastructure scheme

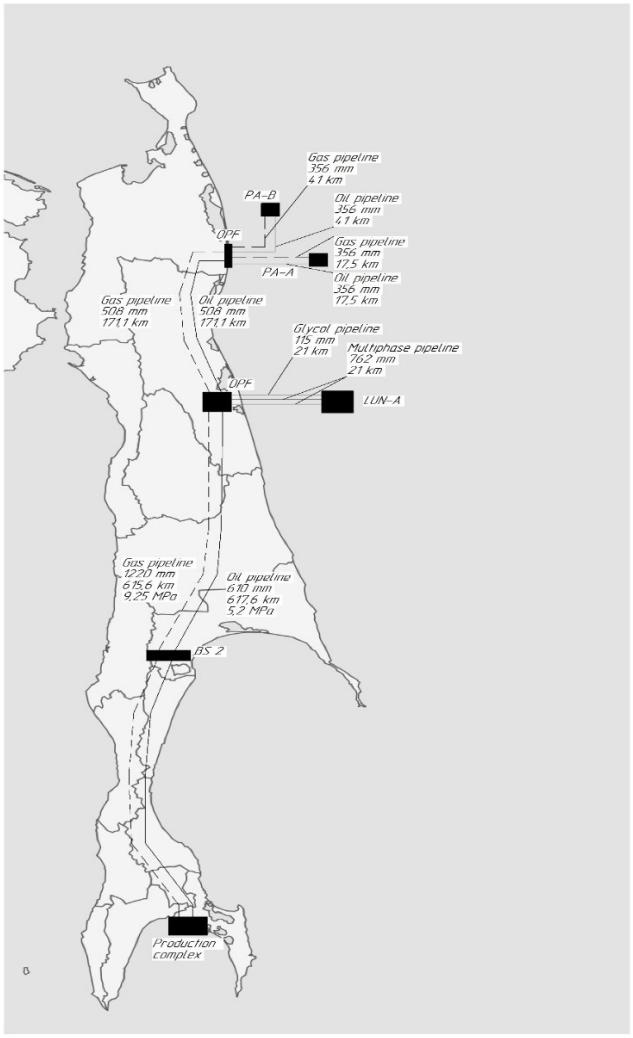

Figure 40 - Sakhalin marine oil and gas pipeline infrastructure

List of Figures

List of Tables

Nomenclature

m	mass	[kg]
$[Fe^{2+}]$	iron ions concentration	[kmol/m^3]
h_w	wave height	[m]
Φ_c	corrosion rate	[kmol/s/m^2]
Φ_p	precipitation rate	[kmol/s/m^2]
A_c	corrosion area	[m^2]
A_{cond}	condensation area	[m^2]
A_p	precipitation area	[m^2]
C_p	specific isobaric heat	[J/(kg·K)]
C_{y0}	coefficient of normal soil resistance	[MPa/cm]
E_s	soil deformation modulus	[MPa]
K_{sw}	water salinity	[%]
L_t	perioid	[years]
N_x	axial force	[N]
S_x	force	[N]
T_y	period of repeatability	[years]
l_0	unit length	[m]
m_r	condensation rate	[m^3/s/m^2]
η_s	reduction coefficient	
Δt	temperature difference	[K]
μ_s	Poisson's coefficient	
D	outer diameter	[m]

E	Young's modulus	[Pa]
F	cross section	[m^2]
G	mass flux	[kg/(m^2· s)]
H	depth	[m]
I	moment of inertia	[m^4]
K	volumetric elasticity	[MPa]
L	length	[m]
M	molar mass	[g/mol]
P	pressure	[MPa]
V	volume	[m^3]
d	inner diameter	[m]
q	heat flux	[W/m^2]
q	distributed load	[N/m]
t	temperature	[ºC]
w	displacement	[m]
x	distance	[m]
α	heat transfer coefficient	[W/(m^2· K)]
α	linear expansion coefficient	[1/K]
β	thermal expansion	[1/K]
γ	specific wight	[N/m^3]
δ	wall thickness	[mm]
θ	angle	[rad]
λ	thermal conductivity	[W/(m· K)]
μ	dynamic viscosity	[Pa· s]
ν	amount	[mol]

ρ	density	[kg/m^3]
σ	normal stress	[MPa]
τ	shear stress	[MPa]
ϑ	velocity	[m/s]

Abbreviations

ANSI	American National Standards Institute
API	American Petroleum Institute
BIP	Binary interaction coefficient
BS	Booster station
CAPEX	Capital Expenditure
CCS	Carbon Capture and Storage
CCUS	Carbon Capture and Utilization and Storage
CFD	Computational Fluid Dynamics
DNV	Det Norske Veritas
DTS	Distributed temperature sensing
ECBM	Enhanced coal bed methane
EOR	Enhanced oil recovery
EOS	Equations of state
FGCC	Flue gas cooler condenser
ISO	International Organization for Standardization
LCOH	Levelized cost of hydrogen
LNG	Liquid natural gas
MAOP	Maximum allowable operating pressure
MOP	Maximum operating pressure
NCEI	National Centers for Environmental Information
NOAA	National Oceanic and Atmospheric Administration
NPS	Nominal Pipe Size
NPSH	Net positive suction head
OOIP	Original oil in place
OPF	Onshore production facility

RANS	Reynolds-averaged Navier–Stokes
SCF	Supercritical flow
SMR	Steam methane reforming
SWOT	Strengths-Weaknesses-Opportunities-Threats
TSA	Temperature Swing Adsorption
VLE	Vapor-liquid equilibrium